UNIVERSITÀ
DI SIENA
1240

Department of Information Engineering and Mathematics

PhD in Information Engineering and Science
-XXXIII Cycle-

Control Techniques for Optimal Management of Microgrids in the Presence of Uncertainty

Advisor:
Prof. Antonio Vicino
Co-advisor:
Prof. Marco Casini

PhD Candidate:
Giovanni Gino Zanvettor

February 2021

Contents

Nomenclature **vii**

1 Introduction **1**

1.1 Thesis Contribution 3

1.2 Thesis Organization 3

1.3 List of Publications 4

2 Peak Shaving Strategies for an EV Charging Station Under Vehicle Uncertainty **7**

2.1 Introduction 7

2.2 Problem Description 10

2.3 Problem Formulation 12

2.4 EV Charging Policy without a-Priori Information 14

2.5 EV Charging Policy with a-Priori Information 21

2.6 EV Charging Policy with Chance Constrained Optimization . . 22

3 Energy Pricing of an EV Parking Lot Under Vehicle Demand Uncertainty **27**

3.1 Introduction 27

3.2 Problem Formulation 29

3.3 Selling Price Optimization 33

3.3.1 Optimal selling price algorithm 39

3.4 Optimal ESS operation 41

4 Robust Energy Management of an IMG Under EV Arrival Uncertainty **43**

4.1 Introduction . . . 43

4.2 Formulation of the Optimal Control of an IMG . . . 46

4.2.1 Objective Function . . . 46

4.2.2 Physical and Security Constraints . . . 47

4.2.3 Operational Constraints . . . 50

4.3 Optimal Control Implementation . . . 50

4.3.1 Uncertainty Modeling . . . 51

4.3.2 Optimization Problem Formulation . . . 52

4.3.3 Chance Constraint Approximation . . . 54

4.3.4 Receding Horizon Implementation . . . 55

5 Smart Buildings Energy Management Under Environmental Uncertainty and DR **57**

5.1 Introduction . . . 57

5.2 System Architecture Overview . . . 60

5.3 System Modeling . . . 61

5.3.1 Zone Thermal Model . . . 62

5.3.2 HVAC System Model . . . 63

5.3.3 Electrical Storage Model . . . 66

5.3.4 PV Generation Model . . . 67

5.3.5 Energy Consumption and Demand-Response Model . . . 68

5.4 Optimal HVAC and Storage Operation Problem . . . 70

5.4.1 Heating Mode Operation with Thermal Storage . . . 70

5.4.2 Cooling Mode Operation . . . 71

5.4.3 Managing Constraint Violations and Uncertainty . . . 71

5.4.4 MPC Algorithm . . . 72

6 Numerical Simulations **75**

6.1 EV Peak Power Minimization . . . 75

6.1.1 Simulation Setup 75
6.1.2 Simulation Results 77
6.2 Energy Pricing Optimization 82
6.2.1 Simulation Setup 82
6.2.2 Simulation Results 83
6.2.3 Discussion 86
6.3 Industrial Microgrid Management 88
6.3.1 Simulation Setup 88
6.3.2 Simulation Results 91
6.4 Building Energy Management 95
6.4.1 Simulation Setup 95
6.4.2 Winter Season Simulation - Heating Operation Results . 97
6.4.3 Summer Season Simulation - Cooling Operation Results 102
6.4.4 Performance Analysis Under Uncertainties 104
6.4.5 Discussion 108

7 Conclusions **111**

Bibliography **115**

Nomenclature and Notation

Nomenclature	
Name	**Description**
Acronyms	
BCVTB	Building Controls Virtual Test Bed
CHP	Combined Heat and Power
CPO	Car Park Owner
CVaR	Conditional Value at Risk
DEC	Desired Energy to be Charged
DG	Distributed Generation
DOPF	Dynamic Optimal Power Flow
DR	Demand-Response
ESS	Electrical energy Storage System
EV	Electric Vehicle
FIT	Best FIT index
FU	Factory Unit
HP	Heat Pump
HVAC	Heating, Ventilation and Air Conditioning
ICP	Ideal Charging Policy
IMG	Industrial Micro-Grid
LOC	Level Of Charge
LP	Linear Program
MILP	Mixed Integer Linear Program
MPC	Model Predictive Control
NCP	Nominal Charging Policy
PV	PhotoVoltaic
PVUSA	PhotoVoltaics for Utility Systems Applications
RHCC	Receding Horizon policy with Chance Constraint
RHP	Receding Horizon Policy
RHPP	Receding Horizon Policy with Prior information
TES	Thermal Energy storage System

Nomenclature	
Name	**Description**
Mathematical notation	
$\mathbb{N}$	Set of natural numbers
$\mathbb{R}^m$	Real space of dimension m
$\mathbb{S}^m$	Space of symmetric $(m \times m)$ matrices
$k \in \mathbb{N}$	Generic time index
$\mathcal{I}(k, \lambda) = [k, k + \lambda) \subseteq \mathbb{N}$	Generic time interval
$x \in \mathbb{R}$	Real variable
$\underline{x}$	Lower bound of variable x
$\overline{x}$	Upper bound of variable x
x^*	Optimal value of x
$x(k)$	Value of variable x at time k
$\mathbf{x} = [x_1 x_2 \dots x_m]'$	$m-$dimensional real vector
$\mathbf{X} = \{x_{i,j}\}$	Real matrix with entries $x_{i,j}$
$\mathbf{X}'$	Transpose of $\mathbf{X}$
$Tr(\mathbf{X})$	Trace of matrix X.
$\mathcal{X}$	Generic set
$\mathcal{X}^m$	Cartesian product of m sets identical to $\mathcal{X}$
$\mathcal{X} \backslash \{x\}$	Set $\mathcal{X}$ without its element x
$\mathcal{P}(e)$	Probability that event e occurs
$\mathcal{P}(e\|e')$	Probability that event e occurs given event e'
$\mathbb{E}[x]$	Expected value of random variable x
$\mathcal{B} = \{0, 1\}$	Binary set
$\mathbf{U}(k, \lambda) = [\mathbf{u}(k) \dots \mathbf{u}(k + \lambda - 1)]'$	Matrix grouping $\mathbf{u}(l)$ for $l \in \mathcal{I}(k, \lambda)$
Time notation	
t	Present time step
Δ	Sampling time
λ	Horizon length (number of time steps inside the horizon)
General notation	
E^G	Energy drawn from the grid
C^G	Cost of electricity from the main grid
p	Unit electricity price

Nomenclature

Name	Description
Electric vehicle notation	
P_0^{EV}	Nominal EV charging power
τ_v^f	Number of time slots needed to fulfill vehicle v
t_v^f	Fulfillment time of vehicle v
E_v^f	Desired energy to be charged for vehicle v
$E_{*,v}^{EV}$	Level of charge of the v-th EV
$P_{*,v}^{EV}$	Charge power of the v-th EV
$\eta_{*,v}^{EV}$	Charging efficiency fir vehicle v
$t_{*,v}^a$	Arrival time (starting charging time) of the v-th EV
$t_{*,v}^d$	Departure time (stopping charging time) of the v-th EV
N_{V_*}	Total number of vehicles
$\mathcal{V}_*(k)$	Set of vehicles which are charging at time k
$\mathcal{H}(k)$	Number of vehicles which are charging at time k
r_v	Customer satisfaction profile
$\widehat{\gamma}$	Daily peak power till the present time
$\widetilde{\gamma}$	Power for charging parked vehicles at maximum rate
γ_p	Predicted peak power
α_v	Weights for cost function
$\mathcal{A}$	Vector collecting all the α_v
N_m	Average number of incoming vehicles at each time step
E_m	Mean value of the charged energy for each vehicle
P_a	Estimate of power consumption
ρ	Gain on daily profit with respect to daily cost
s	Daily selling price
$\mathcal{V}_i(k,\lambda)$	Set of indices of vehicles connected to bus i whose minimum arrival time belongs to $\mathcal{I}(k,\lambda+1)$
$\mathcal{H}(t,k)$	Number of vehicles which are still charging at time $k > t$
ϵ	Failure tolerance level
$\gamma_{i,v}(k)$	Binary random variable denoting if vehicle v connected to bus i is charging at time k
$\Gamma_{i,v}$	Random vector containing $\gamma_{i,v}(k)$
$\Xi_{i,v}$	Support of random vector $\Gamma_{i,v}$
$\pi_{i,v}^{k^a}$	Vector of charging powers related to v-th vehicle connected to bus i during $[\underline{t}_{i,v}^a, \overline{t}_{i,v}^a]$
$*$ subscript	$* = i$ if present, is referring to vehicles connected at bus i

Nomenclature	
Name	**Description**
Electrical energy storage system model	
E^{ESS}	Battery level of charge
P_*^{ESS+}, P_*^{ESS-}	Battery charge/discharge signal
P_*^{ESS}	Net power exchanged into the battery
η_*^{ESS}	Battery charging/discharging efficiency
$\mathcal{C}^{ESS}$	Set of constraints of ESS
$*$ subscript	$* = i$ if present is referring to ESS connected at bus i
PV notation	
$\widehat{P}_*^{PV}$	Power absorbed from the PV plant
P_*^{PV}	Maximum power production of the PV plant
I	Global solar irradiance
T^A	Outside air temperature
θ_1^{PV}, θ_2^{PV}, θ_2^{PV}	Parameters of PVUSA model
Θ^{PV}	Parameter vector of the PV model
$\mathcal{C}^{PV}$	Set of constraints of PV model
$*$ subscript	$* = i$ if present is referring to PV plant connected at bus i
Microgrid notation	
C_i^{CHP}	Cost of electricity production by the CHP system at bus i
C_i^B	Cost of heat production by the boiler at bus i
$J(k, \lambda)$	Objective function to be minimized over the interval $\mathcal{I}(k, \lambda + 1)$
P_i^{CHP}	Active power generated by the CHP system at bus i
Q_i^{CHP}	Reactive power generated by the CHP system at bus i
η_i^{CHP}	Electric efficiency of the CHP system at bus i
c_i^{CHP}	Operation cost of the CHP system at bus i per unit of electrical power generated in a time slot
p^g	Gas price
P_i^B	Heat power produced by the boiler at bus i
η_i^B	Efficiency of the boiler at bus i

Nomenclature

Name	Description
Microgrid notation	
P_i	Net active power injected at bus i
Q_i	Net reactive power injected at bus i
P_i^F	Active power demand of the i-th factory unit
Q_i^F	Reactive power demand of the i-th factory unit
P_i^G	Active power generation at bus i
P_i^D	Active power demand at bus i
G_{ij}	Real part of the electrical admittance between bus i and bus j
B_{ij}	Imaginary part of the electrical admittance between bus i and bus j
V_i	Voltage magnitude at bus i
θ_{ij}	Voltage phase difference between bus i and bus j
α_i^{CHP}	Waste heat factor of the CHP system at bus i
R	Thermal power required by the IMG
$\mathbf{\Pi}(k)$	Decision variable vector at time k
$\mathbf{\Pi}(k,\lambda)$	Decision variable vector sequence in $\mathcal{I}(k,\lambda+1)$
k_{max}^d	Maximum departure time for all the vehicles belonging to $\mathcal{H}_i(k) \cup \mathcal{H}_i(k,\lambda)$ for any i
Building basic notation	
m	Number of building zones
Z_i	$i-$th zone of the building
H_i	Heat exchanger device of zone i
HP_H, HP_C	Heat pump used for heating/cooling
HVAC model	
T^{SND}, T^{RET}	Fluid temperature at the inlet/outlet of heat exchangers
v_i	Heat exchanger actuation signal (commanded air flow) for H_i
$\mathbf{v}$	Vector of v_i, $i = 1,\ldots,m$
κ_i	Coefficient of heating performance of heat exchanger H_i
$\mathcal{C}_H^h$, $\mathcal{C}_C^h$	Set of constraints of HVAC model in heating/cooling mode

Nomenclature

Name	Description
Zone Thermal model	
h_i	Heat flow conveyed by H_i into zone Z_i
$\mathbf{h}$	Vector of h_i, $i = 1, \ldots, m$
T_i	Indoor temperature of zone Z_i
$\mathbf{T}$	Vector of T_i, $i = 1, \ldots, m$
$[\underline{T}_i, \overline{T}_i]$	Thermal comfort range for zone Z_i
$\underline{\mathbf{T}}$, $\overline{\mathbf{T}}$	Vector of $\underline{T}_i$ and $\overline{T}_i$, $i = 1, \ldots, m$
$\mathbf{e}$	Vector of measurements/predictions of exogenous inputs
$\mathbf{\Phi^T}$	Regression matrix of zone thermal model
$k_{\mathbf{T}}, k_{\mathbf{h}}, k_{\mathbf{e}}$	Model order of $\mathbf{T}$, $\mathbf{h}$ and $\mathbf{e}$ involved in $\mathbf{\Phi^T}$
$\Theta^{\mathbf{T}}$	Parameter matrix of zone thermal model
$\mathcal{C}^T$	Set of constraints of zone thermal model
$\mathcal{C}$	Set of comfort constraints
Heating mode operation	
$T_{in}^{HP_H}$, T^{HP_H}	Fluid temperature at HP_H inlet/outlet
$T_0^{HP_H}$	HP_H outlet temperature reference (HP_H command signal)
E^{HP_H}	HP_H electrical energy consumption in heating mode
T^{TES}	TES fluid temperature
α^{HP_H}	Coefficient of HP_H energy consumption
$\mathbf{\Phi}^{TES}$	Regression vector of the heating mode operation model
Θ^{TES}	Parameter vector of the heating mode operation model
$k_{TT},\ k_{TH},\ k_{T\mathbf{h}}$	Model order of T^{TES}, T^{HP_H} and $\mathbf{h}$ involved in $\mathbf{\Phi}^{TES}$
$\mathcal{C}_H$	Set of constraints of overall HVAC model in heating mode
Cooling mode operation	
$T_{in}^{HP_C}$, T^{HP_C}	Fluid temperature at HP_C inlet/outlet
$T_0^{HP_C}$	HP_C outlet temperature reference (HP_C command signal)
E^{HP_C}	HP_C electrical energy consumption in cooling mode
α^{HP_C}	Coefficient of HP_C energy consumption
$\mathbf{\Phi}^{C}$	Regression vector of the cooling mode operation model
Θ^{C}	Parameter vector of the cooling mode operation model
$k_{TC},\ k_{HC},\ k_{C\mathbf{h}}$	Model order of $T_{in}^{HP_C}$, T^{HP_C} and $\mathbf{h}$ involved in $\mathbf{\Phi}^{C}$
$\mathcal{C}_C$	Set of constraints of overall HVAC model in cooling mode

Nomenclature	
Name	**Description**
Energy consumption and DR model	
$E^G(k,\lambda)$	Total energy drawn from the grid within $\mathcal{I}(k,\lambda)$
$C(k,\lambda)$	Total cost of energy within $\mathcal{I}(k,\lambda)$
$\mathcal{R}_j$	$j-$th DR request
S_j	Total energy bound associated to $\mathcal{R}_j$
R_j	Monetary reward associated to $\mathcal{R}_j$
$\mathcal{F}$	DR program (a sequence of DR requests)
$\mathcal{F}(k,\lambda)$	Set of DR requests that occur within $\mathcal{I}(k,\lambda)$
$\mathcal{J}(k,\lambda)$	Set of indices j associated to $\mathcal{R}_j \in \mathcal{F}(k,\lambda)$
ζ_j	Binary variable associated to the fulfillment of $\mathcal{R}_j$
$C^{\mathcal{F}}(k,\lambda)$	Overall cost of operation under $\mathcal{F}$ within $\mathcal{I}(k,\lambda)$
M	Upper bound to the total building energy consumption per time step
$\mathcal{C}^{DR}(k,\lambda)$	Set of constraints of DR model within $\mathcal{I}(k,\lambda)$
Building optimization notation	
$\hat{\mathbf{e}}$	Forecasts/measurements of exogenous inputs
$\underline{\psi_i}$, $\overline{\psi_i}$	Slack variables
$\Psi(k,\lambda)$	Set including $\underline{\psi_i}$, $\overline{\psi_i}$ within $\mathcal{I}(k,\lambda)$
$\mathcal{C}_\Psi$	Relaxed comfort constraint set
$\Psi^{feas}(k,\lambda)$	Optimal value of $\Psi(k,\lambda)$ guaranteeing feasibility
Optimization problem (heating mode)	
$\mathbf{u}_*$	Vector grouping all command variables
$\mathbf{U}_*(k,\lambda)$	Vector grouping all $\mathbf{u}_*$ within $\mathcal{I}(k,\lambda)$
$\mathbf{T}_m$	Sensor measurement of $\mathbf{T}$
T_m^{TES}, E_m^{ESS}	Sensor measurement of T^{TES}
$T_m^{HP_*}$	Sensor measurement of T^{HP_*}
E_m^{ESS}	Sensor measurement of E^{ESS}
$T_{in,m}^{HP_C}$	Sensor measurement of $T_{in}^{HP_C}$
$\star$ subscript	$\star = H$ denotes heating mode; $\star = C$ denotes cooling mode
Test cases	
$\mathbf{G}'$	Vector of internal heat gains of the building zones
d	Noise signal affecting exogenous variables
a_2, a_1	Model coefficients of noise signal d
ε	Zero-mean Gaussian distributed random variable
T_{true}^A, $\widehat{T}^A$	Real/forecast outdoor temperature

Chapter 1

Introduction

The past decades have witnessed an increase of energy demand due to economic growth and technological development. However, traditional energy sources involve carbon-fossil fuels which are the primary causes of pollution and green house effect. Thus, worldwide countries are promoting incentive programs and research initiatives in order to reach a sustainable future [1]. In this setting, electric vehicles (EVs) and renewables represent one of the most trending solutions [2, 3]. Indeed, renewable generation provides electrical energy by exploiting natural phenomena such as sunlight or wind. Most popular applications are related to photovoltaic (PV) plants and wind turbines. On the other hand, EVs are reducing transportation emissions by employing high efficiency electrical engines and batteries. Battery recharge is commonly performed through public or home charging stations. In this context, the concept of microgrid plays a key role, since it represents the simplest aggregation level of different components and players of the grid for optimal management and control of the electricity system.

Conventionally, a microgrid is a group of interconnected loads and distributed energy resources that commonly cooperates with the local area electric power system. It can be perceived by the main grid as a single entity which reacts to specific control signals through a single connection point. However, a massive employment of renewable generation and EV charging stations raises additional challenges for the power system energy management. Because of their nature, both these technologies are an intrinsic source of uncertainty. In fact, renewables represent intermittent and uncontrollable energy resources where the actual production depends on meteorological conditions. Some of the main issues arising in this context relate to clean energy curtailment in periods of

system congestion and to difficult power balancing.
Concerning EVs, their energy demand dramatically changes during different periods of the day, due to traffic conditions and users preferences. If not prevented, the excess of EV demand could be the cause of several issues to the energy provider. Indeed, uncoordinated charging of EV batteries may lead to high power demand, causing voltage fluctuations and unstable grid operations. Modeling uncertainties related to this issues is essential to develop solutions that fully integrate these technologies into present power systems.

To overcome such issues, the development of optimization algorithms which explicitly take into account these uncertainties makes it possible to guarantee the correct quality of service on behalf of the energy provider. By a suitable modeling of the uncertain processes, it is possible to provide solutions where future loads and generation can be effectively forecasted and handled. Moreover, the definition of novel power system protocols may lead to additional benefits. In fact, several solutions to overcome the inflexibility of present end-user load patterns have been designed. Demand response (DR) is one of the most widespread paradigms introduced in the recent years [4]. Users that are participating in DR programs play an active role in the electricity system by adjusting their load patterns in response to the needs of the electricity provider. However, the participation to this programs does not take place on an individual basis, but rather through the aggregation of a community of individual customers. This community interacts with the electricity provider through an intermediary player, called aggregator, which has the objective of gathering the flexibility provided by each user. To achieve this task, the aggregator sends requests to its users asking for a change of their load patterns. If users comply with these requests, a monetary reward is granted. Typical participants in consumer communities are smart buildings, which involve a considerable fraction of the worldwide energy demand [5].

1.1 Thesis Contribution

In this thesis, some of the above mentioned problems have been investigated. The main issues addressed regard handling uncertainty affecting microgrids from the perspective of EV charging stations and buildings.

Concerning EVs, the main objectives are the formulation of optimization procedures in order to achieve proper and safe EV grid integration in the face of the numerous sources of uncertainty. The goal is to reduce peak power consumption, providing a competitive selling price and ensuring grid technical constraints. Actually, all the proposed procedures are suitable for any kind of statistical distribution describing the EV random processes.

Regarding smart buildings, the problem of optimal heating ventilation and air conditioning (HVAC) operation problem has been studied. Participation of the building into a DR program has been considered. A two-step receding horizon algorithm to handle the uncertainty affecting environmental variables and provide robust performance has been proposed.

In both addressed problems, considerable attention has been devoted to computational aspects of the proposed solutions. In fact, the obtained results show that the presented procedures feature feasible computational times for implementation in real-time applications.

1.2 Thesis Organization

The remainder of this thesis is organized as follows.

In Chapter 2, the problem of minimizing the daily peak power consumption of an EV charging station under vehicle uncertainty is analyzed. Uncertainties affecting EVs are related to arrival times, departure times and energy demanded. Three receding horizon algorithms to reduce the daily peak power are proposed. The differences between the algorithms reflect a different a-priori knowledge about the EV random processes and the flexibility on EV recharging.

In Chapter 3, the energy pricing problem of an EV parking lot under vehicle demand uncertainty is addressed. Here, the parking lot is supposed to be equipped with an electrical energy storage system (ESS) and a PV plant. The optimization procedure is formulated through a chance constrained program

where suitable relaxations are exploited to manage joint chance constraints.

In Chapter 4, optimal operation of an industrial microgrid (IMG) is considered. We suppose that the microgrid is equipped with combined heat and power (CHP) generation, EVs, renewables and ESS facilities. A chance constrained formulation to deal with uncertainty on EV arrivals is presented and a receding horizon algorithm is provided.

In Chapter 5, optimal HVAC operation of a smart building participating into a DR program is investigated. In this case, the uncertainty is related to environmental variables (i.e. ambient temperature, solar illuminance) and internal load forecasts. The HVAC optimization procedure is formulated as a two-step optimization problem. The first step is focused on providing a feasible HVAC operation, while the second one performs the optimization of the overall cost.

Chapter 6 describes extensive simulations performed to assess the performance and the computational feasibility of all the devised optimization procedures. In particular, for each of the presented problems, a specific simulation environment is developed and the related results are discussed.

Finally, in Chapter 7 conclusions about all investigated problems are drawn, outlining possible future research lines.

1.3 List of Publications

Most of the material of the thesis is based on published or submitted articles. EV energy management techniques are investigated in the following papers:

EV1 M. Casini, G. G. Zanvettor, M. Kovjanic, and A. Vicino, "Optimal energy management and control of an industrial microgrid with plug-in electric vehicles," *IEEE Access*, vol. 7, pp. 101 729–101 740, 2019.

EV2 M. Casini, A. Vicino, and G. G. Zanvettor, "A distributionally robust joint chance constraint approach to smart charging of plug-in electric vehicles," in *Proc. 58th IEEE Conf. on Decision and Control*, Nice, December 2019, pp. 4222–4227.

EV3 M. Casini, A. Vicino, and G. G. Zanvettor, "A receding horizon approach to peak power minimization for EV charging stations in the presence of uncertainty," *International Journal of Electrical Power & Energy Systems*, vol. 126, p. 106567, 2021.

EV4 M. Casini, A. Vicino, and G. G. Zanvettor, "A chance constraint approach to peak mitigation in electric vehicle charging stations," *Automatica (Accepted)*.

Building HVAC control and energy management under DR programs is addressed in the following articles:

B1 G. Bianchini, M. Casini, D. Pepe, A. Vicino, and G. G. Zanvettor, "Optimal demand-response operation of heating and energy storage in smart buildings," in *2017 AEIT International Annual Conference*, 2017, pp. 1–6.

B2 G. Bianchini, M. Casini, D. Pepe, A. Vicino, and G. G. Zanvettor, "An integrated MPC approach for demand-response heating and energy storage operation in smart buildings," in *2017 IEEE 56th Annual Conference on Decision and Control (CDC)*, 2017, pp. 3865–3870.

B3 G. Bianchini, M. Casini, D. Pepe, A. Vicino, and G. G. Zanvettor, "An integrated model predictive control approach for optimal HVAC and energy storage operation in large-scale buildings," *Applied Energy*, vol. 240, pp. 327–340, 2019.

Chapter 2

Peak Shaving Strategies for an EV Charging Station Under Vehicle Uncertainty

The increasing penetration of plug-in electric vehicles in recent years asks for specific solutions concerning the charging policies to be used in parking lots equipped with charging stations. In fact, simple policies based on uncoordinated vehicle charging usually lead to high peak power demand, which may cause high costs to the car park owner. In this chapter, the problem of minimizing the daily peak power of a charging station is addressed.

2.1 Introduction

The development of renewable generation technologies and electric vehicles (EVs) makes it possible to tackle several issues causing green house effect and pollution. On the energy production side, renewable generation has been adopted to produce green energy without impact on the environment. Concerning EVs, their utilization allows to move gas emissions outside living centers and to reduce the overall fossil fuel consumption by exploiting renewable sources [6, 7]. On the other hand, existing power systems might not be capable to manage the electricity demand needed for a high number of electric vehicles. In fact, safety and technical constraints may be violated in the presence of high penetration of EVs. Several studies available in the literature propose EV charging solutions to face different problems. In [8, 9], battery swap-

ping strategies have been developed to reduce the user waiting time, charging time and to maximize the station profit, while in [10], a centralized charging strategy based on battery swapping has been adopted to minimize the total charging cost, as well as to reduce power loss and voltage deviations in power networks. In [11], a study focused on the minimization of travel time and charging cost has been performed, whereas in [12], a price competition game aimed at maximizing charging station revenues has been developed. In [13], it has been shown that by exploiting smart metering tools and optimization techniques it is possible to handle a high penetration of EVs without changing the power system structure. Energy management of an industrial microgrid including the charging policy for EVs has been studied in [14], with the scope of minimizing the overall electricity bill and satisfying network stability constraints. To guarantee satisfactory EV charging service, sizing and siting of charging stations in the network have been investigated, see [15, 16, 17, 18]. In [19], vehicle arrivals are modeled through an ergodic Markov chain, and an algorithm to minimize the mean waiting time has been proposed, while in [20], a charging strategy to maximize the profit based on a distributionally robust joint chance constraint approach has been presented. Regarding location of charging stations for EVs, parking lots represent an opportunity which has been often exploited in several cities. To this purpose, a number of works are focused on the management of charging units located in parking lots, see e.g., [21, 22, 23, 24, 25].

Various charging strategies have been proposed to reduce the peak load consumption. A decentralized EV charging schedule aimed at filling the valleys in electric load profiles has been developed in [26], while in [27] a similar approach has been proposed taking into account future incoming vehicles, too. In [28], a coordinated strategy between renewables, EVs and electrical storage devices has been implemented to reduce domestic peak load, while in [29], the peak shaving problem has been addressed at network distribution level. The problem of reducing the peak load under demand response programs in a parking lot has been recently considered in [30].

A crucial aspect to consider when dealing with EVs is related to the uncertainty which inevitably affects their behavior, like the arrival time, the parking time and the demanded energy. If not properly handled, these uncertainties may generate drawbacks, degrading performance or causing problems to the grid. Different solutions have been devised to handle such issues. In [31], dynamic programming has been exploited to provide a real-time algorithm for

a cost saving/load flattening problem by clustering EVs on the basis of their departure time. A smart charging algorithm providing peak shaving is described in [32] for non-residential sites. Vehicle arrivals are uncertain, while times of departure are assumed to be known whenever a vehicle plugs-in. In a vehicle-to-grid framework, an event driven optimization has been proposed in [33], where rescheduling is performed when a new vehicle arrives or when an EV leaves the station before the declared time. In [34], a power schedule aimed at reducing the overall charging cost is considered. Incoming vehicles are supposed to be affected by uncertainty and the departure time is fixed when a vehicle arrives at the station. A similar setting is considered in [35], where vehicle arrivals are generated following a Poisson distribution. If the EV is not fully charged at departure, a monetary penalty is applied to the charging station. Photovoltaic generation in an EV charging station has been considered in [36]. Here, charging strategies based on Model Predictive Control have been devised to achieve peak reduction. In [37], peak reduction is achieved by two algorithms, based on interruption (on-off) and modulation strategies, respectively. In both cases, the energy to be charged and the departure time of vehicles are known once they reach the station. The above mentioned works require the knowledge of the departure time of plugged-in vehicles. Such information can be hard to be notified in several practical situations, like for instance, in charging stations located in commercial centers, where the parking time can be affected by several unpredictable events. To fill this gap, charging techniques which do not assume such information have been proposed.

Chapter Contribution and Organization

In this chapter, we consider a charging station equipped with a number of charging units for plug-in electric vehicles. The aim is to design a charging power schedule for each unit able to minimize the overall daily peak power while satisfying the customer requirements in terms of charged energy. Assuming that the energy price the car park owner (CPO) has to pay to the energy provider depends on the daily peak power, the minimization of such peak will lead to an increase of the CPO profit. Moreover, the station may participate in a demand response program [4], where a peak reduction is rewarded by a monetary remuneration. The arrival and departure times of EVs as well as the amount of energy to be charged are assumed to be uncertain. In the present setting, vehicle-to-grid power exchange is not considered.

The contribution of the chapter consists in the development of three novel algo-

rithms aimed at solving the above mentioned problem. Differently from other approaches available in the literature (like, e.g., [31, 32, 33, 34, 35, 36, 37]), the considered setting does not require the knowledge of the departure time of plugged-in vehicles. To deal with this setting, a suitable policy has been devised to assess the customer satisfaction, where a nominal charging power is guaranteed to the customer, which may decide to leave the station before the demanded energy is effectively charged. The proposed algorithms are formulated in a receding horizon framework. In particular, the first one refers to the case where the CPO has no prior knowledge about the uncertain variables affecting the system; the second one is suitable for the case when some information about them is available, e.g., in terms of probability distributions; the last one takes into account the possibility of leaving a fraction of the incoming users not satisfied, i.e. the energy charged is less than the one promised.

The chapter is structured as follows. In Section 2.2, a sketch of the considered problem is described, while in Section 2.3, a rigorous formulation is reported. The proposed charging algorithm assuming no information available on the uncertain variables is provided in Section 2.4. In Section 2.5, an improved version of the charging procedure is presented, assuming that some information on the uncertain variables are available. Finally, in Section 2.6 the optimization procedure based on a chance constrained program where a fraction of customers may be left not satisfied is provided.

2.2 Problem Description

In this chapter, we focus on a plug-in EV charging station, which can be supposed to belong to a parking lot.

We assume that the car park owner contracts with customers according to the following policy:

- The CPO promises a given nominal charging rate to customers.
- Once a vehicle arrives, the customer selects the desired amount of energy to be charged (DEC), or equivalently, the desired level of charge (LOC) at departure.
- Based on the promised charging rate, the charging unit estimates the time at which the request will be fulfilled (*fulfillment time*), and communicates it to the customer.

- When the customer leaves the parking lot, he/she will be marked as satisfied if the EV has been charged with an average charging power which is greater or equal to the promised one. Otherwise he/she will be not satisfied. For instance, if the customer leaves the parking lot at the fulfillment time (or later), he/she will be marked as satisfied if the vehicle has been charged with the DEC.

The charging profile promised by the CPO is depicted in Fig. 2.1. The slope of the quantized ramp represents the nominal charging power rate. The customer is marked as satisfied if the energy charged at departure lies in the satisfaction region (gray area in Fig. 2.1). In a realistic scenario, several uncertainties are

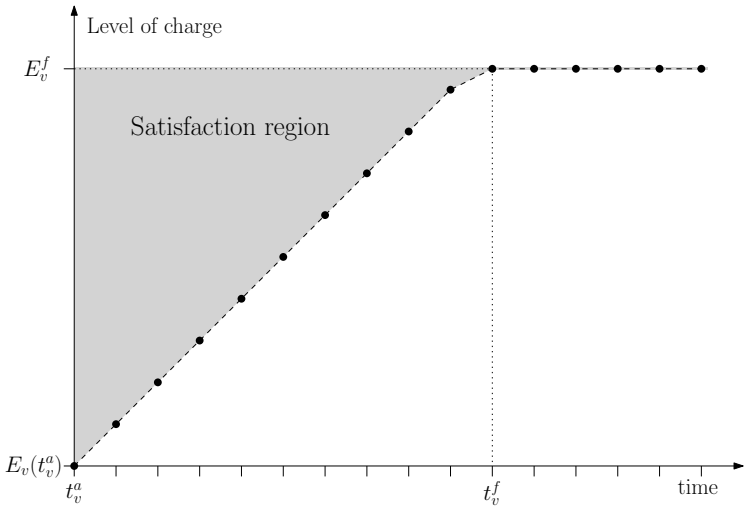

Figure 2.1: Customer satisfaction region for a generic vehicle v. $E_v^{EV}(t_v^a)$ denotes the LOC at arrival, t_v^a the arrival time, t_v^f the fulfillment time and E_v^f the desired LOC.

related to the incoming vehicles. To deal with such issues, in this chapter, three sources of uncertainty are considered for each vehicle: the arrival time, the parking time and the desired energy to be charged.

The aim of this chapter is to devise a charging policy for the station such to minimize the peak power on a daily basis while guaranteeing customer satisfaction. Reducing the peak power is convenient whenever the energy price the CPO has to pay to the energy provider is related to the daily peak power consumption. One more reason may concern the participation of the charging station in a demand response program, where a monetary reward is granted to the CPO in the face of a power reduction request [4]. To accomplish this goal, the problem is formulated in a receding horizon framework, where a suitable

optimization problem is solved in order to compute the charging power of all active units at each time step. Three different control algorithms are proposed depending on the prior knowledge the CPO has about the uncertain variables and on the flexibility on performing the EV recharge.

It is worthwhile to remark that the choice of a satisfaction region as in Fig. 2.1 allows to evaluate the customer satisfaction under uncertain departure time. In fact, differently from other works where a customer notifies its departure time when the vehicle arrives at the station, in this framework EVs leave the station at uncertain time. By assuring a minimum charging power, the CPO can modulate the actual charging power to reduce the daily peak, while guaranteeing customer satisfaction.

2.3 Problem Formulation

The problem is formulated in a discrete time setting, where Δ denotes the sampling time.

Let $v \in \mathbb{N}$ denote a vehicle involved in the charging process. For a given vehicle v, we denote by $t_v^a \in \mathbb{N}$ and $t_v^d \in \mathbb{N}$ the arrival and departure time steps, respectively. We denote by $E_v^{EV}(t)$ the energy charged till time t and by $P_v^{EV}(t)$ the mean charging power between the time step t and $t+1$.

Once a vehicle plugs-in to the charging unit, the customer declares a desired energy to be charged E_v^f. Assuming to charge the vehicle at a constant nominal power P_0^{EV}, and denoting by η_v^{EV} the charging efficiency, the number of time slots needed to fulfill the request is

$$\tau_v^f = \left\lceil \frac{E_v^f - E^{EV}(t_v^a)}{\Delta P_0^{EV} \eta_v^{EV}} \right\rceil . \tag{2.1}$$

Thus, the DEC will be reached at time

$$t_v^f = t_v^a + \tau_v^f . \tag{2.2}$$

Let us call t_v^f as the *fulfillment time* of vehicle v. Moreover, let t_v^d denote the departure time of vehicle v. Notice that in a realistic scenario t_v^d may be greater, less or equal than t_v^f.

The set of plugged-in vehicles in charge at the present time t is denoted by

$$\mathcal{V}(t) = \left\{ v \colon t_v^a \leq t < t_v^d \text{ and } E_v^{EV}(t) < E_v^f \right\} . \tag{2.3}$$

In this framework, we suppose that there is a sufficient number of charging units to ensure the connection of new arriving vehicles.

The dynamics of the charged energy of vehicle v can be expressed as

$$E_v^{EV}(t+1) = E_v^{EV}(t) + \Delta P_v^{EV}(t)\eta_v^{EV}. \tag{2.4}$$

It is assumed that the charging power is bounded, i.e.,

$$0 \leq P_v^{EV}(t) \leq \overline{P}^{EV} \ , \tag{2.5}$$

where $\overline{P}^{EV} > P_0^{EV}$ denotes the maximum power of the charging units.

According to (2.4), the customer satisfaction lower bound $r_v(t)$ can be expressed as follows (see Fig. 2.1)

$$r_v(t) = \min\left\{\Delta\, P_0^{EV}\, \eta_v^{EV}\, (t - t_v^a) + E_v(t_v^a),\ E_v^f\right\} \ . \tag{2.6}$$

Thus, the satisfaction region in Fig. 2.1 is defined by the constraint

$$r_v(t) \leq E_v^{EV}(t) \leq E_v^f. \tag{2.7}$$

It is worthwhile to remark that, for any possible departure time, customer satisfaction is guaranteed whenever (2.7) holds.

In the next sections, procedures aimed at minimizing the daily peak power consumed by the charging station are described. These procedures rely on different hypothesis on the information available to the CPO about the uncertain variables and on the possibility to leave a fraction of customers not satisfied.

2.4 EV Charging Policy without a-Priori Information

In this section, it is assumed that no information about vehicle arrival/departure time and DEC is available to the car park owner. The goal of the CPO is to minimize the daily electricity peak power while guaranteeing customer satisfaction.

Let us denote by $\widehat{\gamma}$ the peak power consumption occurred in the considered day till the present time t. At time t, we denote by $\widetilde{\gamma}$ the power needed to charge all the parked vehicles at the maximum rate without exceeding the DEC, i.e.,

$$\widetilde{\gamma} = \sum_{v \in \mathcal{V}(t)} \min \left\{ \overline{P}^{EV}, \frac{E_v^f - E_v^{EV}(t)}{\Delta \eta_v^{EV}} \right\} . \tag{2.8}$$

It is apparent that charging the vehicles with an overall power less than or equal to $\widehat{\gamma}$ does not increase the daily peak, i.e., $\widehat{\gamma}$ remains the same. So, a preliminary check can be done in order to evaluate if the power needed to charge all the parked vehicles at the maximum rate is less than or equal to $\widehat{\gamma}$, that is:

$$\widetilde{\gamma} \leq \widehat{\gamma} . \tag{2.9}$$

If (2.9) holds, then each vehicle is charged with power

$$P_v^{EV}(t) = \min \left\{ \overline{P}^{EV}, \frac{E_v^f - E_v^{EV}(t)}{\Delta \eta_v^{EV}} \right\} , \ \forall v \in \mathcal{V}(t) \tag{2.10}$$

without affecting $\widehat{\gamma}$. Notice that, as previously stated, $P_v^{EV}(t)$ represents the mean charging power from time t to $t+1$ for vehicle v.

If (2.9) does not hold, an optimization algorithm has to be devised in order to find a charging schedule aimed at minimizing the daily peak power. To accomplish this task, a receding horizon approach is adopted. Since we are interested in minimizing the daily peak power, we will consider an operation time horizon of one day.

In Algorithm 2.1, the pseudo-code of the proposed receding horizon optimization algorithm is reported. After the variable initialization at the beginning of the day, a loop is performed until the day is over. Each loop iteration corresponds to a time step. At a generic time step t, the set $\mathcal{V}(t)$ containing the indices of charging vehicles is obtained and the maximum overall power at time t is computed as in (2.8). If $\widetilde{\gamma} \leq \widehat{\gamma}$, the power schedule at time t is set

$\widehat{\gamma} = 0$;
$t = 0$;
while *day_not_over* **do**
  compute $\mathcal{V}(t)$;
  $\widetilde{\gamma} = \sum_{v \in \mathcal{V}(t)} \min \left\{ \overline{P}^{EV}, \frac{E_v^f - E_v^{EV}(t)}{\Delta \eta_v^{EV}} \right\}$;
  if $\widetilde{\gamma} \leq \widehat{\gamma}$ **then**
    $P_v^{EV*}(t) = \min \left\{ \overline{P}^{EV}, \frac{E_v^f - E_v^{EV}(t)}{\Delta \eta_v^{EV}} \right\}, \forall v \in V(t)$;
  else
    $[\mathbf{P}^{EV*}(t, \lambda(t)), \gamma_p^*] = charge\_no\_prior\_info(\mathcal{V}(t), \widehat{\gamma})$;
    $\widehat{\gamma} = \sum_{v \in \mathcal{V}(t)} P_v^{EV*}(t)$;
  end
  apply command $P_v^{EV*}(t)$, $\forall v \in \mathcal{V}(t)$;
  $t = t + 1$;
end

Algorithm 2.1: Receding horizon control algorithm.

according to (2.10), otherwise it is computed by the *charge_no_prior_info* routine. Such a function returns the solution of a suitable optimization problem (described below) in terms of charging power schedule ($P^{EV*}(t)$) for the next time slot; after that $\widehat{\gamma}$ is updated accordingly. Then, the computed charging power schedule is applied to vehicles and the loop iterates.

It is worthwhile to remark that the crucial step of Algorithm 2.1 resides in the optimization problem the function *charge_no_prior_info* has to solve at each time instant. The rest of this section is devoted to describe and comment such an optimization program, whose solution will define the charging power for all plugged-in vehicles at the present time t.

In view of the constraints introduced in Section 2.3 related to physical and customer satisfaction constraints, the following optimization problem is formulated.

Problem 2.1 (charge_no_prior_info)

$$
\begin{cases}
[\mathbf{P}^{EV*}(t,\lambda(t)),\gamma_p^*] = \arg \inf_{\mathbf{P}^{EV}(t,\lambda(t)),\gamma_p} \left(\gamma_p - \sum_{v\in V(t)} \alpha_v(t) P_v^{EV}(t) \right) & \text{(2.11a)} \\
\text{subject to:} & \\
0 \le P_v^{EV}(k) \le \overline{P}^{EV},\ \forall v \in \mathcal{V}(t),\ \forall k \in \mathcal{I}(t,\lambda(t)) & \text{(2.11b)} \\
E_v^{EV}(k+1) = E_v^{EV}(k) + \Delta P_v^{EV}(k)\eta_v^{EV},\ \forall v \in \mathcal{V}(t),\ \forall k \in \mathcal{I}(t,\lambda(t)) & \text{(2.11c)} \\
r_v(k) \le E_v^{EV}(k) \le E_v^f,\ \forall v \in \mathcal{V}(t),\ \forall k \in \mathcal{I}(t+1,\lambda(t)+1) & \text{(2.11d)} \\
\widehat{\gamma} \le \sum_{v\in\mathcal{V}(t)} P_v^{EV}(t) \le \gamma_p & \text{(2.11e)} \\
\sum_{v\in\mathcal{V}(t)} P_v^{EV}(t) \ge \sum_{v\in\mathcal{V}(t)} P_v^{EV}(k),\ \forall k \in \mathcal{I}(t,\lambda(t)) & \text{(2.11f)}
\end{cases}
$$

where $\mathbf{P}^{EV}(t,\lambda(t))$ is the matrix collecting all elements $P_v^{EV}(k)$ with $k \in \mathcal{I}(t,\lambda(t))$, and $\lambda(t)$ denotes the optimization time horizon defined as

$$\lambda(t) = \max\{t_v^f \colon v \in \mathcal{V}(t)\}\ , \tag{2.12}$$

while $\mathcal{I}(t,\lambda(t))$ refers to the time interval $[t, t+\lambda)$. Notice that, according to (2.2), all the vehicles belonging to $\mathcal{V}(t)$ will be fully charged or will have left the parking at time $\lambda(t)$.

The optimization variables in Problem 2.1 are the power schedule for all vehicles $P_v^{EV}(k),\ \forall v \in \mathcal{V}(t),\ \forall k \in \mathcal{I}(t,\lambda(t))$, and the predicted peak power γ_p, while the optimal variables of interest for Algorithm 2.1 are only the charging powers at the present time step t, i.e., $P_v^{EV}(t), v \in \mathcal{V}(t)$. Let us denote by the superscript * the optimal value of the optimization variables.

In Problem 2.1, we aim at minimizing the difference of two quantities: γ_p and $\sum_{v\in\mathcal{V}(t)} \alpha_v(t) P_v^{EV}(t)$. For the sake of simplicity, for the moment, let us neglect the latter one in (2.11a) and let us focus on the minimization of γ_p, i.e., the predicted peak power till the time horizon $\lambda(t)$. Constraints (2.11b) are related to the charging power bounds in (2.5), while (2.11c)-(2.11d) concern the dynamics of the charged energy and the customer satisfaction constraints as defined in (2.4) and (2.6), respectively. Constraint (2.11e) bounds the total power consumed at time t to belong to the interval $[\widehat{\gamma}, \gamma_p]$, while (2.11f) enforces the overall power consumed at time t to be greater or equal to the power absorbed at next time steps. So, constraints (2.11e)-(2.11f) impose that the maximum peak power until time $\lambda(t)$ be less than or equal to γ_p. Then, the optimal value of γ_p represents the minimum predicted peak power within the time horizon.

Remark 2.1 *Constraints* (2.11f) *may appear somehow obscure. Along with* (2.11e)*, these constraints impose that the optimal predicted peak* γ_p^* *be attained at the first time step* t*, that is,*

$$\sum_{v \in \mathcal{V}(t)} P_v^*(t) = \gamma_p^* \ . \tag{2.13}$$

Notice that, since $E_v^{EV}(k) \geq E_v^{EV}(t)$, $\forall k \in \mathcal{I}(t+1, \lambda(t))$*, according to* (2.8)*, the maximum charging power (of vehicles belonging to* $\mathcal{V}(t)$*) which can be consumed at time* t *is greater than or equal to those occurring at next time instants, i.e.,*

$$\begin{aligned} \widetilde{\gamma} &= \sum_{v \in \mathcal{V}(t)} \min \left\{ \overline{P}^{EV}, \frac{E_v^f - E_v^{EV}(t)}{\Delta \eta_v^{EV}} \right\} \\ &\geq \sum_{v \in \mathcal{V}(t)} \min \left\{ \overline{P}^{EV}, \frac{E_v^f - E_v^{EV}(k)}{\Delta \eta_v^{EV}} \right\}, \ \forall k \in \mathcal{I}(t+1, \lambda(t)). \end{aligned}$$

So, constraints (2.11f) *are surely feasible. Moreover, the introduction of* (2.11f) *does not change the optimal predicted peak* γ_p^**, but it forces such a peak to occur at the current time step* t*. In fact, assuming that* γ_p^* *be a reliable estimate of the future peak, it is convenient to force the present power consumption to equal this estimate.*

Remark 2.2 *Notice that Problem 2.1 is an LP problem, whose solution can be efficiently found through standard optimization solvers. Moreover, one may easily prove that such a problem is always feasible. In fact, by charging all the vehicles at the maximum power until the DEC is attained, one gets*

$$\sum_{v \in \mathcal{V}(t)} P_v^{EV}(t) = \widetilde{\gamma} \ .$$

Since Problem 2.1 is evaluated only if $\widetilde{\gamma} > \widehat{\gamma}$ *(due to line 6 in Algorithm 2.1), constraint* (2.11e) *is surely satisfied, as well as* (2.11b)-(2.11d)*. Finally, by Remark 2.1,* (2.11f) *holds, too.*

It is worthwhile to stress that since the problem is formulated in a receding horizon framework, only the charging powers related to the present time step will be actually applied. However, since the CPO has no information about the uncertainty affecting vehicles, each computation of Problem 2.1 involves only the vehicles which are plugged-in at time t.

In the above reasoning, we neglected the second part of the cost function, i.e.,

$$- \sum_{v \in \mathcal{V}(t)} \alpha_v(t) P_v^{EV}(t) \ . \tag{2.14}$$

In (2.14), $\alpha_v(t) > 0$ denote weights which satisfy $\sum_{v \in \mathcal{V}(t)} \alpha_v(t) = a$, for a fixed $a \ll 1$. In (2.13), it is stated that the optimal cost (neglecting (2.14) from (2.11a)) is

$$\gamma_p^* = \sum_{v \in \mathcal{V}(t)} P_v^*(t) \ .$$

So, it is straightforward to note that, since $a \ll 1$, the introduction of (2.14) in the cost function does not significantly change the optimal cost. However, it allows to allocate the optimal overall charging power at time t among vehicles on the basis of the weights $\alpha_v(t)$.

Such weights can be chosen in several ways. A heuristics which provides good results (see Section 6.1) is to assign greater charging power to vehicles which have longer fulfillment time. A possible way to do that is described below.

Let us define

$$\tilde{\alpha}_v(t) = t_v^f - t \quad , \quad v \in \mathcal{V}(t) \tag{2.15}$$

and let $\widetilde{\mathcal{A}}(t)$ be the vector collecting $\tilde{\alpha}_v(t)$. By the definition of $\mathcal{V}(t)$ in (2.3), one has $E_v^{EV}(t) < E_v^f$. Moreover, by (2.1)-(2.2) one gets $t < t_v^f$ and hence $\tilde{\alpha}_v(t) > 0$, for all $v \in \mathcal{V}(t)$. So, by defining the weighting vector $\mathcal{A}(t)$ as

$$\mathcal{A}(t) = a \frac{\widetilde{\mathcal{A}}(t)}{\|\widetilde{\mathcal{A}}(t)\|_1} \ , \tag{2.16}$$

it is easy to show that $\|\mathcal{A}(t)\|_1 = \sum_{v \in \mathcal{V}(t)} \alpha_v(t) = a$.

Thus, the amount of power given by γ_p^* will be split among vehicles to favor those with greater fulfillment time.

Let us call the procedure reported in Algorithm 2.1 as *receding horizon policy* (RHP). Moreover, let us denote by *nominal charging policy* (NCP) the uncoordinated charging schedule where each vehicle is charged with constant nominal power P_0^{EV} till departure or the DEC is attained.

In the following, we want to show that RHP always returns a peak power which is less or equal to that obtained by NCP. To this purpose, some notation needs be introduced. Let us call by $\widehat{\gamma}^r(t)$ and $\widehat{\gamma}^n(t)$ the peak power occurred up to time t by adopting the RHP and NCP strategy, respectively. Hereafter, we denote by the superscript r and n all the variables related to RHP and NCP, respectively. To simplify the exposure, let us define $\widehat{\mathcal{V}}(t) = \left\{v \colon t_v^a \leq t < t_v^d\right\}$. By (2.3), one has $\widehat{\mathcal{V}}(t) \supseteq \mathcal{V}(t)$ since $\widehat{\mathcal{V}}(t)$ contains also the vehicles which are

charged with the DEC but have not left the parking lot. Since the charging power is null for such vehicles, they do not contribute to the charging schedule.

The charging power applied by NCP at time step t is

$$P_v^{EV^n}(t) = \min\left\{P_0^{EV}, \frac{E_v^f - E_v^{EV^n}(t)}{\eta_v^{EV}\Delta}\right\} \ , \quad \forall v \in \widehat{\mathcal{V}}(t). \tag{2.17}$$

By definition, the peak power function up to time t satisfies

$$\widehat{\gamma}^n(t) = \max\left\{\widehat{\gamma}^n(t-1), \sum_{v\in\widehat{\mathcal{V}}(t)} P_v^{EV^n}(t)\right\}. \tag{2.18}$$

The fact that the peak power obtained by RHP cannot be greater than that of NCP is stated by the following theorem.

Theorem 2.1 *At a given time t, the following inequality holds*

$$\widehat{\gamma}^r(t) \leq \widehat{\gamma}^n(t) \quad , \quad \forall t \geq 0.$$

Proof: The theorem will be proven by induction.

At time $t = 0$, one has $\widehat{\gamma}^r(0) = \widehat{\gamma}^n(0) = 0$.

Let us suppose that at time $t-1$ it holds

$$\widehat{\gamma}^r(t-1) \leq \widehat{\gamma}^n(t-1). \tag{2.19}$$

We want to prove that $\widehat{\gamma}^r(t) \leq \widehat{\gamma}^n(t)$. If $\widetilde{\gamma} \leq \widehat{\gamma}^r(t-1)$, then by the condition in Line 6 of Algorithm 2.1, the peak power is not updated and so, by (2.19) and (2.18)

$$\widehat{\gamma}^r(t) = \widehat{\gamma}^r(t-1) \leq \widehat{\gamma}^n(t-1) \leq \widehat{\gamma}^n(t).$$

If $\widetilde{\gamma} > \widehat{\gamma}^r(t-1)$, the charging schedule provided by RHP is given by the solution of Problem 2.1, and according to Line 10 of Algorithm 2.1, it holds

$$\widehat{\gamma}^r(t) = \sum_{v\in\widehat{\mathcal{V}}(t)} P_v^{EV^r}(t) \ . \tag{2.20}$$

Let us define the charging command

$$\widehat{P}_v^{EV}(t) = \min\left\{P_0^{EV}, \frac{E_v^f - E_v^{EV^r}(t)}{\eta_v^{EV}\Delta}\right\} \ , \ \forall v \in \widehat{\mathcal{V}}(t). \tag{2.21}$$

Since RHP provides a charging schedule which guarantees the customer satisfaction, surely $E_v^{EV^r}(t) \geq E_v^n(t)$, and hence by comparing (2.17) and (2.21), one has

$$\widehat{P}_v^{EV}(t) \leq P_v^{EV^n}(t) \ , \ \forall v \in \widehat{\mathcal{V}}(t) \ . \tag{2.22}$$

We have to study two different cases.
First, let us consider the case $\sum_{v\in\widehat{\mathcal{V}}(t)} \widehat{P}_v^{EV}(t) < \widehat{\gamma}^r(t-1)$. Since $\widetilde{\gamma} > \widehat{\gamma}^r(t-1)$, then there surely exist $P_v^{EV^r}(t) \geq \widehat{P}_v^{EV}(t),\ v \in \widehat{\mathcal{V}}(t)$ such that

$$\sum_{v\in\widehat{\mathcal{V}}(t)} P_v^{EV^r}(t) = \widehat{\gamma}^r(t-1),$$

and hence

$$\widehat{\gamma}^r(t) = \widehat{\gamma}^r(t-1) \leq \widehat{\gamma}^n(t-1) \leq \widehat{\gamma}^n(t) \ .$$

It remains to study the case $\sum_{v\in\widehat{\mathcal{V}}(t)} \widehat{P}_v^{EV}(t) \geq \widehat{\gamma}^r(t-1)$. It is easy to note that $\widehat{P}_v^{EV}(t)$ satisfies constraints (2.11b)-(2.11e). Moreover, also constraints (2.11f) are satisfied. In fact, by choosing in (2.11f) the sequence $\widehat{P}_v^{EV}(k)$, $\forall k \in \mathcal{I}(t+1, \lambda(t))$ like in (2.21), one has $\widehat{P}_v^{EV}(t) \geq \widehat{P}_v^{EV}(k),\ \forall v \in \widehat{\mathcal{V}}(t),\ \forall k \in \mathcal{I}(t+1, \lambda(t))$. Hence, constraints (2.11f) are satisfied, and the charging sequence $\widehat{P}_v^{EV}(t)$ is a feasible solution of Problem 2.1, in the sense that it satisfies all its constraints.

Since the schedule $P_v^{EV^r}(t)$ is the optimal solution of Problem 2.1, one has $\sum_{v\in\widehat{\mathcal{V}}(t)} P_v^{EV^r}(t) \leq \sum_{v\in\widehat{\mathcal{V}}(t)} \widehat{P}_v^{EV}(t)$, and then, by (2.20), (2.22) and (2.18), it holds

$$\widehat{\gamma}^r(t) = \sum_{v\in\widehat{\mathcal{V}}(t)} P_v^{EV^r}(t) \leq \sum_{v\in\widehat{\mathcal{V}}(t)} \widehat{P}_v^{EV}(t) \leq \sum_{v\in\widehat{\mathcal{V}}(t)} P_v^{EV^n}(t) \leq \widehat{\gamma}^n(t).$$

□

This theorem states that, for any possible distribution involving the uncertain variables, the proposed algorithm outperforms the uncoordinated charging policy, that is RHP is able to reduce the daily peak power while guaranteeing customer satisfaction.

2.5 EV Charging Policy with a-Priori Information

In this section, it is assumed that the CPO has some knowledge about the uncertain variables involved in the charging process, i.e., the arrival and charging time of vehicles and the DEC. We suppose that the probability distributions (or an estimate of them) of the previously mentioned variables are available, obtained for instance by using historical data. Under such an assumption, the technique described in Section 2.4 can be refined, in order to obtain better performance, i.e., reduced daily peak power.

The main procedure is like to that reported in Algorithm 2.1, with the only difference that the function *charge_no_prior_info* used to solve Problem 2.1 in Line 9 is replaced by *charge_prior_info*, aimed at solving Problem 2.2.

Problem 2.2 (charge_prior_info)

$$
\begin{cases}
[\mathbf{P}^{EV*}(t,\lambda(t)),\gamma_p^*] = \arg \inf\limits_{\mathbf{P}^{EV}(t,\lambda(t)),\gamma_p} \left(\gamma_p - \sum\limits_{v\in V(t)} \alpha_v(t) P_v^{EV}(t) \right) & \text{(2.23a)} \\
\text{subject to:} & \\
0 \le P_v^{EV}(k) \le \overline{P}^{EV},\ \forall v \in \mathcal{V}(t),\ \forall k \in \mathcal{I}(t,\lambda(t)) & \text{(2.23b)} \\
E_v^{EV}(k+1) = E_v^{EV}(k) + \Delta P_v^{EV}(k)\eta_v^{EV},\ \forall v \in \mathcal{V}(t),\ \forall k \in \mathcal{I}(t,\lambda(t)) & \text{(2.23c)} \\
r_v(k) \le E_v^{EV}(k) \le E_v^f,\ \forall v \in \mathcal{V}(t),\ \forall k \in \mathcal{I}(t+1,\lambda(t)+1) & \text{(2.23d)} \\
\widehat{\gamma} \le \sum\limits_{v\in\mathcal{V}(t)} P_v^{EV}(t) \le \gamma_p & \text{(2.23e)} \\
\sum\limits_{v\in\mathcal{V}(t)} P_v^{EV}(t) \ge \sum\limits_{v\in\mathcal{V}(t)} P_v^{EV}(k),\ \forall k \in \mathcal{I}(t,\lambda(t)) & \text{(2.23f)} \\
\sum\limits_{v\in\mathcal{V}(t)} P_v^{EV}(k)\mathcal{P}\left(t_v^d > k | t_v^d > t\right) + P_a(k) \le \gamma_p,\ \forall k \in \mathcal{I}(t,\lambda(t)) & \text{(2.23g)}
\end{cases}
$$

where

$$
P_a(k) = N_m\, P_0^{EV}\ \min\left\{ k-t, \frac{E_m}{\Delta\eta_v^{EV} P_0^{EV}} \right\}\ , \tag{2.24}
$$

and N_m, E_m denote the average number of vehicles arriving at the station at each time step and the mean value of the charged energy, respectively.

Problem 2.2 differs from Problem 2.1 since constraints (2.23g) have been added in the former with the aim of obtaining a better estimate of the future peak power γ_p. Notation $\mathcal{P}\left(t_v^d > k | t_v^d > t\right)$ in (2.23g) denotes the probability that

the departure time of vehicle v be greater than k, conditioned to the fact that it is greater than t. The left hand side of (2.23g) can be decomposed in this way

$$\underbrace{\sum_{v\in\mathcal{V}(t)} P_v^{EV}(k)\mathcal{P}\left(t_v^d > k | t_v^d > t\right)}_{current\ vehicles} + \underbrace{P_a(k)}_{future\ vehicles}$$

where, at time k, the left part denotes the expected value of the overall power consumption given by the vehicles which are charging at time t, while $P_a(k)$ provides an estimate of the overall power consumption given by vehicles which will arrive at future time, assuming nominal charging power. In the expression of $P_a(k)$ in (2.24), it is assumed that each vehicle asks for an amount of energy to be charged equal to E_m. In (2.24), the expression $\frac{E_m}{\Delta\eta_v^{EV} P_0^{EV}}$ denotes the mean number of time slots needed to complete the charge. So, while plugged-in vehicles are considered individually in (2.23g), future EVs are managed in an aggregated way, by exploiting average values of uncertain variables.

The introduction of constraints (2.23g) in the optimization problem leads to a better estimate of the predicted peak power γ_p^*, improving the performance of the overall algorithm, as reported in Chapter 6.

2.6 EV Charging Policy with Chance Constrained Optimization

In this section, the optimization procedure may be further improved by assuming that a fraction of customer may be left not satisfied. Let ε be the maximum fraction of customers which may leave the parking not satisfied, i.e., such that (2.7) does not hold. Let us call this quantity as *dissatisfaction level*. For instance, a dissatisfaction level $\varepsilon = 0.05$ means that at most 5% of vehicles may leave the parking lot not satisfied. Since the departure time of vehicles is uncertain, a customer is not satisfied whenever

$$E_v^{EV}(t_v^d) < r_v(t_v^d)$$

that is, the charged energy at departure is less than promised. In other words, it occurs when the level of charge at departure lies outside the satisfaction region depicted in Fig. 2.1.

Then, a chance constrained program aimed to minimize the predicted peak with at least $1-\varepsilon$ customers satisfied is structured as follows

Problem 2.3 (charge_prior_info_chance_constraint)

$$
\begin{cases}
[\mathbf{P}^{EV*}(t,\lambda(t)),\gamma_p^*] = \arg \inf_{\mathbf{P}^{EV}(t,\lambda(t)),\gamma_p} \left(\gamma_p - \sum_{v\in\mathcal{V}(t)} \alpha_v(t) P_v^{EV}(t)\right) & \text{(2.25a)}\\
\text{subject to:} & \\
z_v(k) \in \mathcal{B},\ \forall v \in \mathcal{V}(t),\ \forall k \in \mathcal{I}(t+1,\lambda(t)+1) & \text{(2.25b)}\\
0 \le P_v^{EV}(k) \le \overline{P}^{EV},\ \forall v \in \mathcal{V}(t),\ \forall k \in \mathcal{I}(t,\lambda(t)) & \text{(2.25c)}\\
E_v^{EV}(k+1) = E_v^{EV}(k) + \Delta\eta_v^{EV} P_v^{EV}(k),\quad \forall v \in \mathcal{V}(t),\ \forall k \in \mathcal{I}(t,\lambda(t)) & \text{(2.25d)}\\
r_v(k) z_v(k) \le E_v^{EV}(k) \le E_v^f,\quad \forall v \in \mathcal{V}(t), \forall k \in \mathcal{I}(t+1,\lambda(t)+1) & \text{(2.25e)}\\
\widehat{\gamma} \le \sum_{v\in\mathcal{V}(t)} P_v^{EV}(t) \le \gamma_p & \text{(2.25f)}\\
\sum_{v\in\mathcal{V}(t)} P_v^{EV}(t) \ge \sum_{v\in\mathcal{V}(t)} P_v^{EV}(k),\ \forall k \in \mathcal{I}(t+1,\lambda(t)) & \text{(2.25g)}\\
\sum_{v\in\mathcal{V}(t)} P_v^{EV}(k)\mathcal{P}\left(t_v^d > k | t_v^d > t\right) + P_a(k) \le \gamma_p,\quad \forall k \in \mathcal{I}(t+1,\lambda(t)) & \text{(2.25h)}\\
\widehat{\varepsilon}_v + \sum_{\forall k\in\mathcal{I}(t+1,\lambda(t)+1)} (1 - z_v(k))\mathcal{P}(t_v^d = k) \le \varepsilon,\ \forall v \in \mathcal{V}(t). & \text{(2.25i)}
\end{cases}
$$

In Problem 2.3, the time horizon $\lambda(t)$ defined as

$$\lambda(t) = \max\{\overline{t}_v^d \colon v \in \mathcal{V}(t)\}, \tag{2.26}$$

has been modified to fit the chance constraint.

It is worthwhile to notice that Problem 2.3 is a mixed-integer linear programming (MILP) problem, where all the optimization variables are real with the exception of $z_v(k)$ which are binary variables. Although in the formulation reported in Problem 2.3 the number of binary variables may be large, from an implementation point of view it can be greatly reduced by considering the maximum time a vehicle can stay in charge. Such an aspect will be discussed in Section 6.1, where it will be shown the computation feasibility of the optimization program.

Problem 2.3 differs from Problem 2.2 by constraints (2.25b), (2.25e) and (2.25i). In (2.25b), the binary variables $z_v(k)$ are defined. Such variables are related to the fact that the satisfaction constraint involving the vehicle v at time k be surely satisfied (if $z_v(k) = 1$), or it could be violated (if $z_v(k) = 0$). Constraints (2.25e) are similar to (2.7); if $z_v(k) = 1$, it is imposed that the LOC at time k belongs to the satisfaction region (see Fig. 2.1), while if $z_v(k) = 0$, the left inequality is surely satisfied even if the LOC does not lie in the satisfaction

$\widehat{\gamma} = 0$;
$t = 0$;
while *day_not_over* **do**
  compute $\mathcal{V}(t)$;
  $\widetilde{\gamma} = \sum_{v \in \mathcal{V}(t)} \min \left\{ \overline{P}^{EV}, \frac{E_v^f - E_v^{EV}(t)}{\Delta \eta_v^{EV}} \right\}$;
  if $\widetilde{\gamma} \leq \widehat{\gamma}$ **then**
    $P_v^{EV*}(t) = \min \left\{ \overline{P}^{EV}, \frac{E_v^f - E_v^{EV}(t)}{\Delta \eta_v^{EV}} \right\}, \forall v \in V(t)$;
  else
    $[\mathbf{P}^{EV*}(t, \lambda(t)), \gamma_p^*] = charge\_prior\_info\_chance\_constraint(\mathcal{V}(t), \widehat{\gamma})$;
    $\widehat{\gamma} = \sum_{v \in \mathcal{V}(t)} P_v^{EV*}(t)$;
    foreach $v \in \mathcal{V}(t)$ **do**
      if $\left(E_v^{EV}(t) + \Delta \eta_v^{EV} P_v^{EV*}(t)\right) < r_v(t+1)$ **then**
        $\widehat{\varepsilon}_v = \widehat{\varepsilon}_v + \mathcal{P}(t_v^d = t+1 | t_v^d > t)$
      end
    end
  end
  apply command $P_v^{EV*}(t), \forall v \in \mathcal{V}(t)$;
  $t = t + 1$;
end

Algorithm 2.2: Chance constrained receding horizon control algorithm.

region. Finally, chance constraints (2.25i) allow a vehicle to leave the parking lot not satisfied with a probability no greater than ε. Specifically, $\widehat{\varepsilon}_v$ denotes the probability that the vehicle v had left the parking lot not satisfied at past time steps, while the second term represents the probability that the vehicle departs not satisfied at future times. The sum of these two terms is enforced to be no greater than ε, guaranteeing that the overall number of not satisfied vehicles do not exceed the prescribed threshold.

The chance constrained optimization procedure is reported in Algorithm 2.2. The main difference with respect to Algorithm 2.1 resides in the fact that, once the optimization step is performed, the chance constraint probabilities may need to be adjusted. Specifically, if the LOC of vehicle v at time $t+1$ is less than the corresponding customer satisfaction level, then $\widehat{\varepsilon}_v$ is increased by the probability that the considered vehicle will depart at time $t+1$.

Remark 2.3 *It is worthwhile to note that constraints* (2.23g), (2.25h) *and* (2.25i) *include some probability computations. Since the probability distribution of the parking time (or an estimate of it) is assumed to be known, when a vehicle arrives at the station also the distribution related to the departure time is known. So,* $\mathcal{P}(t_v^d = k)$ *is known for each* $v \in \mathcal{V}(t)$ *and the corresponding value can be substituted in* (2.25i). *Regarding constraints* (2.23g) *and* (2.25h), *the conditional probability* $\mathcal{P}\left(t_v^d > k | t_v^d > t\right)$ *has to be computed to solve Problem 2.2 and Problem 2.3. However, it can be easily evaluated by discarding from the unconditional probability mass function of the departure time, the mass accounting for vehicles such that* $t_v^d \leq t$, *and normalizing the obtained distribution. At this step, numerical values can be directly substituted in* (2.23g) *and* (2.25h). *Thus, Problem 2.2 and Problem 2.3 can be solved.*

Chapter 3

Energy Pricing of an EV Parking Lot Under Vehicle Demand Uncertainty

The increasing adoption of electric vehicles (EVs) and the related need for efficient battery charging leads to additional challenges to the power network and energy providers. One of the main issues regards the intrinsic uncertainty affecting the EV charging process, which calls for appropriate strategies to ensure reliable solutions. From parking lot perspective, the electric vehicle charging process should be managed in order to guarantee the recharge at competitive price. In this chapter, the problem of energy pricing under vehicle uncertainty is addressed.

3.1 Introduction

In Chapter 2, the general background about electric vehicle (EV) parking lots and charging stations has been covered. Thus, in this introduction we focus on describing the energy pricing problem of an EV parking lot. As already mentioned in the previous chapter, EVs represent a source of uncertainty to energy providers. In fact, their electricity demand depends on several factors such as user preferences and traffic conditions. In this context, electricity pricing of EV parking lot becomes a demanding task, particularly when the energy price must be chosen in a competitive environment. In the literature, several works about this problem have been proposed. In [38], a game theory

study is carried out in order to derive an optimal selling price for several charging stations. Considering power and transportation network frameworks, a pricing strategy to optimally manage a large number of EVs is developed in [39]. In [40], a two layer model is developed to generate electricity selling price under market price uncertainty, while in [41] an EV energy pricing procedure to lower the peak power absorption is proposed. To handle the uncertainty on EVs and renewables, an electricity pricing framework is developed in [42]. To provide a fair pricing scheme, the utility function of the users is considered in [43]. In [44], an EV pricing problem is addressed under renewable and load demand uncertainty. To provide a probabilistic guarantee for the EV charging profit, a chance constrained program under EV load uncertainty is formulated in [45].

Chapter Contribution and Organization

In this chapter, a parking lot equipped with a charging station, photovoltaic (PV) generation and electrical energy storage system (ESS) is considered. The main contribution of the chapter is twofold:

i) To design a procedure aimed at computing the daily selling price for charging EVs. In particular, such a price must be the lowest which ensures a given profit with a probabilistic guarantee. In the considered setting, the source of uncertainty is related to future incoming vehicles, specifically, to arrival time, departure time and daily number of incoming EVs. To handle such uncertainties, a chance constrained optimization problem aimed at finding the optimal selling price is designed, and a tractable formulation of such problem is provided.

ii) To provide a receding horizon control algorithm to operate the ESS during the day to achieve the expected profit of i). Contrary to the procedure designed in i), this algorithm takes advantage of the knowledge acquired in an online approach about the random process outcomes of arrived vehicles.

The major novelty of the contribution is to provide a robust selling price policy as the solution of an optimization problem where the uncertainty on the EVs is modeled through suitable probability distributions. The proposed approach allows one to deal with different setups and scenarios because no specific assumptions on probability distributions describing the EV uncertainties is made.

The chapter is organized as follows. In Section 3.2, problem variables, constraints and probability derivations are described. In Section 3.3, the optimiza-

tion problem aimed at finding the optimal daily selling price is analyzed and solved through a suitable algorithm. Section 3.4 is related to the formulation of a receding horizon procedure to operate the ESS during the day.

3.2 Problem Formulation

In this chapter, we focus on a charging station used to charge a large number of electric vehicles. Such charging station is assumed to be equipped with charging units, a PV plant and an electrical storage system. It is supposed that the number of charging units is enough to provide charging for all incoming vehicles. Moreover, it is assumed that the daily electricity cost profile and a forecast of the PV daily production are available in advance. In this setting, the charging station is not allowed to sell energy to the grid, i.e. no vehicle-to-grid energy flow is considered.

The problem is formulated in a discrete time setting, where the sampling time is denoted by Δ. The EV arrival and departure times, and the daily number of incoming vehicles are uncertain and their probability distributions, or estimates for them, are assumed to be available. Each plugged-in vehicle is charged at a constant power rate P_0^{EV} from the arrival time to its departure time. We assume that the reference day is divided into λ time slots where the initial time slot starts at $k = 0$, while the last one at $k = \lambda - 1$. Let t_v^a and t_v^d be the v-th vehicle arrival time and departure time, while t_v^c is the corresponding charging time, i.e. the number of time slots the vehicle remains in charge, hence $t_v^d = t_v^a + t_v^c$. The total number of incoming vehicles during each day is represented by the random variable N_V. Let us assume that the random variables related to arrival time and charging time of each vehicle are independent and identically distributed. Thus, the arrival time, departure time and charging time of a generic vehicle are denoted by t^a, t^d and t^c, respectively. Moreover, we assume that the supports of random variables t^c and N_V are bounded. We denote their minimum values by $\underline{t}^c$ and $\underline{N}_V$, and their maximum values by $\overline{t}^c$ and $\overline{N}_V$.

Let us define by $E_d^{EV}(k)$ the overall energy required to charge plugged in vehicles in the k-th time slot, i.e. between time k and $k+1$.

Concerning the ESS, we denote by $E^{ESS}(k)$ the stored energy at time k, and its charging/discharging power rates by $P^{ESS^+}(k)/P^{ESS^-}(k)$, respectively. We

use a simple dynamic model for the ESS

$$E^{ESS}(k+1) = E^{ESS}(k) + \eta^{ESS}\Delta P^{ESS^+}(k) - \frac{1}{\eta^{ESS}}\Delta P^{ESS^-}(k),$$

where η^{ESS} is the battery efficiency. Let E_0^{ESS} denote the energy stored at the initial time step of the day, i.e.

$$E^{ESS}(0) = E_0^{ESS}.$$

The ESS charging and discharging power rates are bounded by zero and a maximum rate $\overline{P}^{ESS}$, i.e.

$$0 \leq P^{ESS^+}(k) \leq \overline{P}^{ESS+}$$
$$0 \leq P^{ESS^-}(k) \leq \overline{P}^{ESS-},$$

while the energy level of the ESS is bounded by its capacity $\overline{E}^{ESS}$, i.e.

$$0 \leq E^{ESS}(k) \leq \overline{E}^{ESS}.$$

Let us define the net power exchanged by the battery as

$$P^{ESS}(k) = P^{ESS^+}(k) - P^{ESS^-}(k).$$

Notice that, in order to have a consistent ESS dynamics, $P^{ESS+}(k)$ and $P^{ESS-}(k)$ cannot be both nonzero. Thus, the following constraint needs to be enforced

$$P^{ESS+}(k)P^{ESS-}(k) = 0.$$

Let $P^{PV}(k)$ be the average power produced by the PV plant between time k and $k+1$ and let $\widehat{P}^{PV}(k)$ denote the power that is actually drawn from the PV plant in the same time interval. Hence $\widehat{E}^{PV}(k)$ is such that:

$$0 \leq \widehat{E}^{PV}(k) \leq E^{PV}(k).$$

Thus, the overall energy drawn from the grid $E^G(k)$ in time slot k is

$$E^G(k) = \max\Big\{\underbrace{E_d^{EV}(k) - \Delta\widehat{P}^{PV}(k) + \Delta P^{ESS}(k)}_{\widehat{E}^G(k)}, 0\Big\} = \max\Big\{\widehat{E}^G(k), 0\Big\}, \tag{3.1}$$

where the max function is needed since the parking lot is not allowed to sell energy to the grid.

Let us define the cost per time step $c(k)$ as

$$C^G(k) = E^G(k)p(k), \tag{3.2}$$

where $p(k)$ is the electricity price at time k.

The aim of this chapter is summarized in the following problem.

Problem 3.1 *For each day, compute the minimum electricity selling price s' such that the daily net profit is at least a fraction ρ of the daily cost, with probability at least $1-\varepsilon$.*

To fulfill Problem 3.1, the overall revenue must satisfy the following inequality with probability $1-\varepsilon$.

$$\sum_{k\in\mathcal{I}(0,\lambda)} E_d^{EV}(k)s' \geq (1+\rho)\sum_{k\in\mathcal{I}(0,\lambda)} C^G(k). \tag{3.3}$$

By defining $s = s'/(1+\rho)$, (3.3) is equivalent to

$$\sum_{k\in\mathcal{I}(0,\lambda)} E_d^{EV}(k)s \geq \sum_{k\in\mathcal{I}(0,\lambda)} c(k).$$

So, the goal is to find an *artificial* selling price s capable to cover the daily cost. Then, the *actual* selling price will be $s' = (1+\rho)s$. Hereafter, we will focus on the computation of s which, for the sake of simplicity, will be denoted as the *selling price*.

To compute the probability distribution of the daily net profit, we focus on finding the distribution of the energy drawn from the grid at each time step. Since the randomness is due to vehicle statistics, let us focus on random variables modeling the EV process.
Let us denote by $\mathcal{P}(e)$ the probability that a given event e occurs, by $\mathcal{P}(e,e')$ the joint probability that two events e and e' occur, and by $\mathcal{P}(e|e')$ the probability that an event e occurs conditioned to e'.

The probability that a generic vehicle is in charge at time k can be expressed as

$$\begin{aligned}\mathcal{P}\left(t^a \leq k,\ t^d > k\right) &= \sum_{\tau=\max\{k-\overline{t}^c+1,0\}}^{k} \mathcal{P}\left(t^d > k | t^a = \tau\right)\mathcal{P}\left(t^a = \tau\right) = \\ &= \sum_{\tau=\max\{k-\overline{t}^c+1,0\}}^{k} \mathcal{P}\left(t^c > k-\tau\right)\mathcal{P}\left(t^a = \tau\right),\end{aligned} \tag{3.4}$$

that is the convolution between the complement of the charging time cumulative distribution with the distribution of the arrival time. Notice that, the probability of having a vehicle in charge at time k follows a binomial distribution, so we can easily compute the probability that a given amount of vehicles be in charge at a given time step. In fact, let $\mathcal{H}(k)$ be the random variable

denoting the number of vehicles in charge at time k. Then, its probability distribution is derived as follows

$$\mathcal{P}\left(\mathcal{H}(k)=n\right)=\sum_{m=n}^{\overline{N}_V}\mathcal{P}\left(\mathcal{H}(k)=n|N_V=m\right)\mathcal{P}\left(N_V=m\right)=$$
$$=\sum_{m=n}^{\overline{N}_V}\binom{m}{n}\mathcal{P}\left(t^a\leq k,\ t^d>k\right)^n\left(1-\mathcal{P}\left(t^a\leq k,\ t^d>k\right)\right)^{m-n}\mathcal{P}\left(N_V=m\right). \tag{3.5}$$

The study of such probabilities is useful to derive the probability distribution of the energy needed by EVs at each time step. Indeed, the relation between $E_d^{EV}(k)$ and $\mathcal{H}(k)$ is expressed by the following equation

$$E_d^{EV}(k)=\mathcal{H}(k)\Delta P_0^{EV}.$$

Of course, the marginal cost distribution at each time step is immediately obtained from the marginal distribution of the EV energy. Unfortunately, computing the probability distribution of the EV daily cost starting from the marginal distributions of each time step is a hard task, since the energy required at different time slot are correlated. Indeed, it can be shown that it is a combinatorial problem which becomes intractable even for a small number of vehicles. To overcome such issue, the concept of *EV daily loss* is introduced. Let us define the EV daily loss as $\sum_{k\in\mathcal{I}(0,\lambda)}E_d^{EV}(k)(p(k)-s)$. Notice that, a negative loss means that the selling price s provides a profit. For a given selling price s, we are interested in computing the following probability

$$\mathcal{P}\left(\sum_{k\in\mathcal{I}(0,\lambda)}E_d^{EV}(k)(p(k)-s)=L^{EV}\right), \tag{3.6}$$

where L^{EV} denotes a realization of the EV daily loss.

Let us analyze the probability distribution of the daily loss for a single vehicle. For a fixed s, if vehicle v has been charged in the time interval $[k_1,k_2)$, then the corresponding loss is

$$c_v=\sum_{k=k_1}^{k_2-1}\Delta P_0^{EV}(p(k)-s).$$

Then, let us introduce the following set

$$\boldsymbol{\mathcal{C}}(h)=\left\{k_1\in[0,\lambda-1],k_2\in[0,\lambda-1]:\sum_{k=k_1}^{k_2-1}\Delta P_0^{EV}(p(k)-s)=h\right\}, \tag{3.7}$$

that defines all the possible time windows which can lead to a loss h. Therefore, the probability that the daily loss of a vehicle is h can be computed as

$$\mathcal{P}\left(c_v = h\right) = \sum_{(k_1,k_2)\in\mathcal{C}(h)} \mathcal{P}\left(t^a = k_1, t^d = k_2\right), \tag{3.8}$$

that is the probability that a loss h occurs is equal to the sum of the probabilities of every (k_1, k_2) leading to a loss h. Then, the probability of having a daily loss L^{EV} is

$$\begin{aligned}\mathcal{P}\left(\sum_{v=1}^{N_V} c_v = L^{EV}\right) &= \sum_{n=\underline{N}_V}^{\overline{N}_V} \mathcal{P}\left(\sum_{v=1}^{N_V} c_v = L^{EV} \middle| N_V = n\right) \mathcal{P}\left(N_V = n\right) \\ &= \sum_{n=\underline{N}_V}^{\overline{N}_V} \mathcal{P}\left(\sum_{v=1}^{n} c_v = L^{EV}\right) \mathcal{P}\left(N_V = n\right). \end{aligned} \tag{3.9}$$

Notice that, the single vehicle loss distributions are independent and identically distributed, since their relative arrival times and charging times are independent and identically distributed. So, the distribution of the sum of n losses is equivalent to the convolution of n single loss distributions. According to the previous reasoning, the following lemma is introduced.

Lemma 3.1 *The probability in* (3.6) *satisfies*

$$\mathcal{P}\left(\sum_{k\in\mathcal{I}(0,\lambda)} E_d^{EV}(k)(p(k)-s) = L^{EV}\right) = \mathcal{P}\left(\sum_{v=1}^{N_V} c_v = L^{EV}\right).$$

3.3 Selling Price Optimization

In this section, the chance constraint on the daily profit and the optimization problem to compute the optimal selling price are presented. The constraint on the selling price satisfying Problem 3.1 is

$$\mathcal{P}\left(\sum_{k\in\mathcal{I}(0,\lambda)} E_d^{EV}(k)s \geq \sum_{k\in\mathcal{I}(0,\lambda)} C^G(k)\right) \geq 1-\varepsilon$$

which by (3.2) is equivalent to

$$\mathcal{P}\left(\sum_{k\in\mathcal{I}(0,\lambda)} E_d^{EV}(k)s \geq \sum_{k\in\mathcal{I}(0,\lambda)} E^G(k)p(k)\right) \geq 1-\varepsilon.$$

To remove the max function in (3.1), the following chance constraint is introduced

$$\mathcal{P}\left(\begin{array}{l}\displaystyle\sum_{k\in\mathcal{I}(0,\lambda)} E_d^{EV}(k)s \geq \sum_{k\in\mathcal{I}(0,\lambda)} \max\left\{\widehat{E}^G(k),0\right\}p(k)\\ \widehat{E}^G(k)\geq 0,\ \forall k\in\mathcal{I}(0,\lambda)\end{array}\right)\geq 1-\varepsilon.$$

Notice that such constraint requires that two joint events occur. The first event concerns the selling price, which has to provide a desired amount of profit. The second one is aimed at ensuring a positive energy flow.

Let us define the vector $\mathbf{P}^{ESS}(k,\lambda)$ as

$$\mathbf{P}^{ESS}(k,\lambda)=\left[P^{ESS}(k),P^{ESS}(k+1),\ldots,P^{ESS}(\lambda-1)\right].$$

Therefore, the minimum selling price s will be the solution of the following optimization problem

Problem 3.2

$$\begin{cases}
\min\limits_{\mathbf{P}^{ESS}(0,\lambda),s} s & \text{(3.10a)}\\
\text{subject to:} & \text{(3.10b)}\\
\mathcal{P}\left(\begin{array}{l}\displaystyle\sum_{k\in\mathcal{I}(0,\lambda)} E_d^{EV}(k)s \geq \sum_{k\in\mathcal{I}(0,\lambda)} \max\left\{\widehat{E}^G(k),0\right\}p(k)\\ \widehat{E}^G(k)\geq 0,\ \forall k\in\mathcal{I}(0,\lambda)\end{array}\right)\geq 1-\varepsilon & \text{(3.10c)}\\
\widehat{E}^G(k)=E_d^{EV}(k)+\Delta P^{ESS}(k)-\Delta\widehat{P}^{PV}(k) \qquad \forall k\in\mathcal{I}(0,\lambda) & \text{(3.10d)}\\
0\leq\widehat{P}^{PV}(k)\leq P^{PV}(k) \qquad \forall k\in\mathcal{I}(0,\lambda) & \text{(3.10e)}\\
E^{ESS}(k+1)=E^{ESS}(k)+\eta^{ESS}\Delta P^{ESS^+}(k) - \frac{1}{\eta^{ESS}}\Delta P^{ESS^-}(k) \qquad \forall k\in\mathcal{I}(0,\lambda) & \text{(3.10f)}\\
0\leq E^{ESS}(k)\leq\overline{E}^{ESS} \qquad \forall k\in\mathcal{I}(0,\lambda+1) & \text{(3.10g)}\\
P^{ESS}(k)=P^{ESS^+}(k)-P^{ESS^-}(k) \qquad \forall k\in\mathcal{I}(0,\lambda). & \text{(3.10h)}\\
0\leq P^{ESS^+}(k)\leq\overline{P}^{ESS+} \qquad \forall k\in\mathcal{I}(0,\lambda) & \text{(3.10i)}\\
0\leq P^{ESS^-}(k)\leq\overline{P}^{ESS-} \qquad \forall k\in\mathcal{I}(0,\lambda) & \text{(3.10j)}\\
P^{ESS^+}(k)P^{ESS^-}(k)=0 \qquad \forall k\in\mathcal{I}(0,\lambda) & \text{(3.10k)}\\
E^{ESS}(0)=E_0^{ESS} & \text{(3.10l)}\\
s\geq 0. & \text{(3.10m)}
\end{cases}$$

Notice that the nonlinearity in constraint (3.10k) can be substituted by replacing (3.10i)-(3.10k) with the following constraints

$$0 \leq P^{ESS-}(k) \leq \overline{P}^{ESS+-}(1 - z^{ESS}(k)) \qquad \forall k \in \mathcal{I}(0,\lambda) \tag{3.11}$$

$$0 \leq P^{ESS+}(k) \leq \overline{P}^{ESS+} z^{ESS}(k) \qquad \forall k \in \mathcal{I}(0,\lambda) \tag{3.12}$$

$$z^{ESS}(k) \in \mathcal{B} \qquad \forall k \in \mathcal{I}(0,\lambda). \tag{3.13}$$

By using the conditional probability, chance constraint (3.10c) can be reformulated as

$$\mathcal{P}\left(\sum_{k\in\mathcal{I}(0,\lambda)} E_d^{EV}(k)s \geq \sum_{k\in\mathcal{I}(0,\lambda)} \widehat{E}^G(k)p(k)\Big|\widehat{E}^G(k) \geq 0,\ \forall k \in \mathcal{I}(0,\lambda)\right) \cdot \mathcal{P}\left(\widehat{E}^G(k) \geq 0,\ \forall k \in \mathcal{I}(0,\lambda)\right) \geq 1-\varepsilon.$$

By (3.10d), one has

$$\mathcal{P}\left(\sum_{k\in\mathcal{I}(0,\lambda)} E_d^{EV}(k)s \geq \sum_{k\in\mathcal{I}(0,\lambda)} \widehat{E}^G(k)p(k)\Big|\widehat{E}^G(k) \geq 0,\ \forall k \in \mathcal{I}(0,\lambda)\right) =$$

$$= \mathcal{P}\left(\sum_{k\in\mathcal{I}(0,\lambda)} E_d^{EV}(k)(p(k)-s) \leq \sum_{k\in\mathcal{I}(0,\lambda)} \left(\Delta\widehat{P}^{PV}(k) - \Delta P^{ESS}(k)\right)p(k)\right), \tag{3.14}$$

and

$$\mathcal{P}\left(\widehat{E}^G(k) \geq 0\ \forall k \in \mathcal{I}(0,\lambda)\right) = \mathcal{P}\left(E_d^{EV}(k) \geq \Delta\widehat{P}^{PV}(k) - \Delta P^{ESS}(k),\ \forall k \in \mathcal{I}(0,\lambda)\right).$$

Notice that, the probability in (3.14) can be easily computed if the power schedule of the battery, the energy produced by the PV, and the selling price are known.

Suppose that

$$\mathcal{P}\left(E_d^{EV}(k) \geq \Delta\widehat{P}^{PV}(k) - \Delta P^{ESS}(k),\ \forall k \in \mathcal{I}(0,\lambda)\right) \geq 1-\beta$$

where β is a risk level such that $\beta < \varepsilon$.

Then, chance constraint (3.10c) is satisfied if the following inequality holds

$$\mathcal{P}\left(\sum_{k\in\mathcal{I}(0,\lambda)} E_d^{EV}(k)(p(k)-s) \leq \sum_{k\in\mathcal{I}(0,\lambda)} \left(\Delta\widehat{P}^{PV}(k) - \Delta P^{ESS}(k)\right)p(k)\right) \geq \frac{1-\varepsilon}{1-\beta}.$$

Let us denote the quantity $\sum_{k\in\mathcal{I}(0,\lambda)}\left(\Delta\widehat{P}^{PV}(k)-\Delta P^{ESS}(k)\right)p(k)$ as *daily savings*. It is apparent that the larger the daily savings, the smaller the selling price s. So, for a fixed β, the following chance constrained program is introduced.

Problem 3.3

$$
\begin{cases}
r'_\beta = \max\limits_{\mathbf{P}^{ESS}(0,\lambda)} \sum\limits_{k\in\mathcal{I}(0,\lambda)}\left(\Delta\widehat{P}^{PV}(k)-\Delta P^{ESS}(k)\right)p(k) & \text{(3.15a)}\\
\text{subject to:} & \text{(3.15b)}\\
\mathcal{P}\left(E_d^{EV}(k)\geq \Delta\widehat{P}^{PV}(k)-\Delta P^{ESS}(k),\ \forall k\in\mathcal{I}(0,\lambda)\right)\geq 1-\beta & \text{(3.15c)}\\
0\leq \widehat{P}^{PV}(k)\leq P^{PV}(k) \qquad \forall k\in\mathcal{I}(0,\lambda) & \text{(3.15d)}\\
E^{ESS}(k+1)=E^{ESS}(k)+\eta^{ESS}\Delta P^{ESS^+}(k) - \frac{1}{\eta^{ESS}}\Delta P^{ESS^-}(k) \qquad \forall k\in\mathcal{I}(0,\lambda) & \text{(3.15e)}\\
0\leq E^{ESS}(k)\leq \overline{E}^{ESS} \qquad \forall k\in\mathcal{I}(0,\lambda+1) & \text{(3.15f)}\\
P^{ESS}(k)=P^{ESS^+}(k)-P^{ESS^-}(k) \qquad \forall k\in\mathcal{I}(0,\lambda) & \text{(3.15g)}\\
0\leq P^{ESS^+}(k)\leq \overline{P}^{ESS+}z^{ESS}(k) \qquad \forall k\in\mathcal{I}(0,\lambda) & \text{(3.15h)}\\
0\leq P^{ESS^-}(k)\leq \overline{P}^{ESS-}(1-z^{ESS}(k)) \qquad \forall k\in\mathcal{I}(0,\lambda) & \text{(3.15i)}\\
z^{ESS}(k)\in\mathcal{B} \qquad \forall k\in\mathcal{I}(0,\lambda) & \text{(3.15j)}\\
E^{ESS}(0)=E_0^{ESS}. & \text{(3.15k)}
\end{cases}
$$

Such optimization problem aims at finding the maximum daily savings r'_β guaranteeing constraint (3.15c), i.e. the probability that the energy flow is negative is less than β. Notice that equation (3.15c) is a joint chance constraint. In general, joint chance constrained optimization problems are notoriously difficult to solve. However, such constraint can be converted with its robust counterpart in order to derive a tractable formulation of this optimization problem [46]. Indeed, let us focus on the following optimization program

Problem 3.4

$$
\begin{cases}
r_\beta = \max\limits_{\mathbf{P}^{ESS}(0,\lambda)} \sum\limits_{k\in\mathcal{I}(0,\lambda)} \left(\Delta\widehat{P}^{PV}(k) - \Delta P^{ESS}(k)\right) p(k) & \text{(3.16a)}\\
\text{subject to:} & \text{(3.16b)}\\
\inf\limits_{\mathcal{P}\in\mathcal{D}} \mathcal{P}\left(E_d^{EV}(k) \geq \Delta\widehat{P}^{PV}(k) - \Delta P^{ESS}(k),\ \forall k \in \mathcal{I}(0,\lambda)\right) \geq 1-\beta & \text{(3.16c)}\\
0 \leq \widehat{P}^{PV}(k) \leq P^{PV}(k) \qquad \forall k \in \mathcal{I}(0,\lambda) & \text{(3.16d)}\\
E^{ESS}(k+1) = E^{ESS}(k) + \eta^{ESS}\Delta P^{ESS^+}(k) - \dfrac{1}{\eta^{ESS}}\Delta P^{ESS^-}(k) \qquad \forall k \in \mathcal{I}(0,\lambda) & \text{(3.16e)}\\
0 \leq E^{ESS}(k) \leq \overline{E}^{ESS} \qquad \forall k \in \mathcal{I}(0,\lambda+1) & \text{(3.16f)}\\
P^{ESS}(k) = P^{ESS^+}(k) - P^{ESS^-}(k) \qquad \forall k \in \mathcal{I}(0,\lambda) & \text{(3.16g)}\\
0 \leq P^{ESS^+}(k) \leq \overline{P}^{ESS+} z^{ESS}(k) \qquad \forall k \in \mathcal{I}(0,\lambda) & \text{(3.16h)}\\
0 \leq P^{ESS^-}(k) \leq \overline{P}^{ESS-}(1 - z^{ESS}(k)) \qquad \forall k \in \mathcal{I}(0,\lambda) & \text{(3.16i)}\\
z^{ESS}(k) \in \mathcal{B} \qquad \forall k \in \mathcal{I}(0,\lambda) & \text{(3.16j)}\\
E^{ESS}(0) = E_0^{ESS}, & \text{(3.16k)}
\end{cases}
$$

where constraint (3.15c) is converted to a distributionally joint chance constraint where the probability distribution $\mathcal{P}$ belongs to the ambiguity set $\mathcal{D}$. Such ambiguity set is defined as follows

$$
\mathcal{D} = \left\{\mathcal{P} : \mathcal{P} \in \mathcal{M}(\mathcal{P}_0, \ldots, \mathcal{P}_{\lambda-1}),\ E_d^{EV}(k) \sim \mathcal{P}_k\ \forall k \in \mathcal{I}(0,\lambda)\right\},
$$

where $\mathcal{P}_k$ denotes the probability distribution of $E_d^{EV}(k)$, and $\mathcal{M}(\mathcal{P}_0, \ldots, \mathcal{P}_{\lambda-1})$ denotes the set of all joint probability distributions whose marginals are $\mathcal{P}_k$. As described in [46] and since random variables $E_d^{EV}(k)$ are distributed along discrete distributions, Problem 3.4 is equivalent to the following mixed integer linear program (MILP).

Problem 3.5 (max_profit)

$$
\begin{cases}
r_\beta = \max\limits_{\mathbf{P}^{ESS}(0,\lambda)} \sum\limits_{k\in\mathcal{I}(0,\lambda)} \left(\Delta\widehat{P}^{PV}(k) - \Delta P^{ESS}(k)\right) p(k) & \text{(3.17a)}\\
\text{subject to:} & \text{(3.17b)}\\
\sum\limits_{n=0}^{\overline{N}_V} \left(\Delta P_0^{EV} n\right) z_n(k) \geq \Delta\widehat{P}^{PV}(k) - \Delta P^{ESS}(k) \qquad \forall k \in \mathcal{I}(0,\lambda) & \text{(3.17c)}\\
\sum\limits_{n=0}^{\overline{N}_V} \mathcal{P}_k\left(E_d^{EV}(k) \geq \Delta P_0^{EV} n\right) z_n(k) \geq 1-\beta_k \qquad \forall k \in \mathcal{I}(0,\lambda) & \text{(3.17d)}\\
0 \leq \widehat{P}^{PV}(k) \leq P^{PV}(k) \qquad \forall k \in \mathcal{I}(0,\lambda) & \text{(3.17e)}\\
E^{ESS}(k+1) = E^{ESS}(k) + \eta^{ESS}\Delta P^{ESS^+}(k) - \dfrac{1}{\eta^{ESS}}\Delta P^{ESS^-}(k) \qquad \forall k \in \mathcal{I}(0,\lambda) & \text{(3.17f)}\\
0 \leq E^{ESS}(k) \leq \overline{E}^{ESS} \qquad \forall k \in \mathcal{I}(0,\lambda+1) & \text{(3.17g)}\\
P^{ESS}(k) = P^{ESS^+}(k) - P^{ESS^-}(k) \qquad \forall k \in \mathcal{I}(0,\lambda) & \text{(3.17h)}\\
0 \leq P^{ESS^+}(k) \leq \overline{P}^{ESS+} z^{ESS}(k) \qquad \forall k \in \mathcal{I}(0,\lambda) & \text{(3.17i)}\\
0 \leq P^{ESS^-}(k) \leq \overline{P}^{ESS-}(1 - z^{ESS}(k)) \qquad \forall k \in \mathcal{I}(0,\lambda) & \text{(3.17j)}\\
z^{ESS}(k) \in \mathcal{B} \qquad \forall k \in \mathcal{I}(0,\lambda) & \text{(3.17k)}\\
E^{ESS}(0) = E_0^{ESS} & \text{(3.17l)}\\
\beta_k \geq 0 \qquad \forall k \in \mathcal{I}(0,\lambda) & \text{(3.17m)}\\
z_n(k) \in \mathcal{B} \qquad \forall k \in \mathcal{I}(0,\lambda),\ \forall n \in [0,\overline{N}_V] & \text{(3.17n)}\\
\sum\limits_{n=0}^{\overline{N}_V} z_n(k) = 1 \qquad \forall k \in \mathcal{I}(0,\lambda) & \text{(3.17o)}\\
\sum\limits_{k\in\mathcal{I}(0,\lambda)} \beta_k \leq \beta. & \text{(3.17p)}
\end{cases}
$$

In Problem 3.5, the original robust joint chance constraint (3.16c) has been approximated by using the Bonferroni inequality, where the optimizer is allowed to choose the best option for the Bonferroni weights β_k. Concerning the binary variables $z_n(k)$, they are used to satisfy each individual chance constraint (3.17d).

Remark 3.1 *Notice that, the number of binary variables $z_n(k)$ in Problem 3.5 may be large, since it equals $\lambda(\overline{N}_V + 1)$. Thus, the computational burden of Problem 3.5 might be intractable, in general. However, constraint (3.17o) enforces that only one binary variable can be equal to 1 at each time step, letting the problem structure suitable to be efficiently managed by standard solvers.*

Data: ε, $p(k)$, E_0^{ESS}, ρ, distributions on t_a, t_c, N_V, and step size γ
$s^* = \max_{k\in\mathcal{I}(0,\lambda)} p(k)$;
$\beta^* = 0$;
for $\beta = 0$ **to** $(\varepsilon - \gamma)$ **by** γ **do**
  $r_\beta = max\_savings(\beta)$;
  $s_\beta = min\_selling\_price(\beta, r_\beta)$;
  if $s_\beta < s^*$ **then**
    $s^* = s_\beta$;
    $\beta^* = \beta$;
  end
end
return s^*, β^*;

Algorithm 3.1: Main procedure to solve Problem 3.1.

In Problem 3.5, the maximum daily savings r_β for a fixed β is computed. Then, the corresponding minimum selling price s_β can be obtained by solving the following optimization problem.

Problem 3.6 (min_selling_price)

$$\begin{cases} s_\beta = \min \ s & \text{(3.18a)} \\ \quad \text{subject to:} & \text{(3.18b)} \\ \quad \mathcal{P}\left(\sum_{k\in\mathcal{I}(0,\lambda)} E_d^{EV}(k)(p(k) - s) \le r_\beta \right) \ge \dfrac{1-\varepsilon}{1-\beta} & \text{(3.18c)} \\ \quad s \ge 0. & \text{(3.18d)} \end{cases}$$

3.3.1 Optimal selling price algorithm

To compute the optimal selling price satisfying Problem 3.1, the procedure reported in Algorithm 3.1 has been devised.

First, initialization of some variables are performed. In particular, the candidate optimal selling price s^* is set to the maximum of the grid electricity price, while the candidate optimal value of β is set to 0. Since $0 \le \beta < \varepsilon$, a grid search in β with step γ from 0 to $\varepsilon - \gamma$ is performed. For any value of β, the subroutine *max_savings* provides the solution of Problem 3.5 returning the related daily savings r_β, while *min_selling_price* returns s_β, i.e. the solution of

Data: β, r_β, ε, $p(k)$, distributions on t_a, t_c, N_V and tolerance γ_ε

$s_{bot} = 0$; $s_{top} = \max_{k\in\mathcal{I}(0,\lambda)} p(k)$; $\varepsilon_{sat} = \frac{1-\varepsilon}{1-\beta}$;

$\varepsilon_{bot} = \mathcal{P}\left(\sum_{k\in\mathcal{I}(0,\lambda)} E_d^{EV}(k)(p(k) - s_{bot}) \leq r_\beta\right)$;

$\varepsilon_{top} = \mathcal{P}\left(\sum_{k\in\mathcal{I}(0,\lambda)} E_d^{EV}(k)(p(k) - s_{top}) \leq r_\beta\right)$;

while $\frac{\varepsilon_{top}-\varepsilon_{sat}}{\varepsilon_{sat}} > \gamma_\varepsilon$ **do**

  $s_{mid} = \frac{s_{top}+s_{bot}}{2}$;

  $\varepsilon_{mid} = \mathcal{P}\left(\sum_{k\in\mathcal{I}(0,\lambda)} E_d^{EV}(k)(p(k) - s_{mid}) \leq r_\beta\right)$;

  if $\varepsilon_{mid} \geq \varepsilon_{sat}$ **then**

    $\varepsilon_{top} = \varepsilon_{mid}$;

    $s_{top} = s_{mid}$;

  else

    $\varepsilon_{bot} = \varepsilon_{mid}$;

    $s_{bot} = s_{mid}$;

  end

end

return s_{top};

Algorithm 3.2: Bisection procedure to solve Problem 3.6 for given β and r_β.

Problem 3.6. If the current selling price is less than the current optimal value, s^* and β^* are updated accordingly. Finally, the optimal values are returned.

Since Problem 3.5 is a MILP, it can be easily implemented in the *max_savings* subroutine. Instead, the solution of Problem 3.6 requires an ad-hoc procedure. Notice that, Problem 3.6 involves an individual chance constraint where the only decision variable is related to the selling price s. Moreover, the probability on the left hand side of constraint (3.18c) is monotonically non-decreasing with respect to s, and so a bisection procedure on s can be designed, see Algorithm 3.2. The lowest value of the selling price has been set to $s_{bot} = 0$, while the highest one coincides with the maximum of the electricity price over the day, i.e. $s_{top} = \max_{k\in\mathcal{I}(0,\lambda)} p(k)$, which guarantees a non-negative profit. The computation of ε_{top}, ε_{bot}, and ε_{mid} is performed by exploiting (3.7)-(3.8)-(3.9). The algorithm stops when the relative difference between the maximum and the minimum probability level in (3.18c) is less than a given tolerance γ_ε. Thanks to the bisection formulation, computation of *min_selling_price* is efficiently performed.

3.4 Optimal ESS operation

The above mentioned method is used to compute the optimal selling price at the beginning of the day. However, during the day, the energy schedule of the ESS may be adapted to further improve the daily profit, taking into account the actual realizations of the stochastic processes modeling the EVs. In fact, at each time step, it is reasonable to assume the knowledge of the energy to be charged in each connected vehicle and their departure times, as well as the number of EVs arrived till the present time. To this purpose, a receding horizon procedure to online operate the ESS can be designed, following a similar reasoning to that described in Section 3.3.

Let us denote the present time step by t, and let $\mathcal{H}(t,k)$ be the number of connected vehicles which will be still in charge at time $k > t$, i.e.

$$\mathcal{H}(t,k) = |\left\{v : t_v^a \leq t, t_v^d > k\right\}|.$$

where $|\cdot|$ denotes the cardinality operator of a set. Notice that, at time t, $\mathcal{H}(t,k)$ is known for any $k > t$.

Let $N_V(0,t)$ be the random variable associated to the number of incoming vehicles during the interval $\mathcal{I}(0,t+1)$, and let us denote by n_a the actual number of vehicles arrived till the present time step, i.e. in the interval $\mathcal{I}(0,t+1)$. So, the distribution of the daily incoming vehicles can be refined by exploiting the knowledge of the already arrived vehicles n_a,

$$\mathcal{P}\left(N_V = n | N_V(0,t) = n_a\right) = \frac{\mathcal{P}\left(N_V(0,t) = n_a | N_V = n\right)\mathcal{P}\left(N_V = n\right)}{\mathcal{P}\left(N_V(0,t) = n_a\right)}, \quad (3.19)$$

where

$$\mathcal{P}\left(N_V(0,t) = n_a\right) = \sum_{m=n_a}^{\overline{N}_V} \mathcal{P}\left(N_V(0,t) = n_a | N_V = m\right)\mathcal{P}\left(N_V = m\right),$$

and

$$\mathcal{P}\left(N_V(0,t) = n_a | N_V = m\right) = \binom{m}{n_a}\mathcal{P}\left(0 \leq t_a \leq t\right)^{n_a}\left(1 - \mathcal{P}\left(0 \leq t_a \leq t\right)\right)^{m-n_a}.$$

For a given $k > t$, the arrival time distribution can be updated as

$$\mathcal{P}\left(t^a = k | t^a > t\right) = \frac{\mathcal{P}\left(t^a > t | t^a = k\right)\mathcal{P}\left(t^a = k\right)}{\mathcal{P}\left(t^a > t\right)} = \frac{\mathcal{P}\left(t^a = k\right)}{\mathcal{P}\left(t^a > t\right)}. \quad (3.20)$$

Let us denote by $\widetilde{\mathcal{H}}(k)$ the random variable describing the number of vehicles in charge at time $k > t$, ignoring the EVs which are in charge at time t. In

Data: ε, $p(k)$, E_0^{ESS}, and distributions on t_a, t_c, N_V
Set $\beta = \beta^*$ as returned in Algorithm 3.1;
Set $t = 0$ and $E_0^{ESS}(0) = E_0^{ESS}$;
while $t < \lambda - 1$ **do**
  $n_a = |\{v : t_v^a \leq t\}|$;
  $H(t,k) = |\{v : t_v^a \leq t, t_v^d \geq k\}|\ ,\ \forall k > t$;
  compute $P(N_V = n | N_V(0,t) = n_a),\ \forall n \in [n_a, \overline{N}_v]$ as in (3.19);
  compute $P(t_a = k | t_a > t),\ \forall k \in \mathcal{I}(t+1, \lambda - t - 1)$ as in (3.20);
  compute distributions of $\widetilde{\mathcal{H}}(k),\ \forall k \in \mathcal{I}(t+1, \lambda - t - 1)$;
  solve Problem 3.5 by using the updated constraints (3.21)-(3.22), and get $P^{ESS}(t)$;
  $E_0^{ESS}(t+1) = E_0^{ESS}(t) + \eta \Delta P^{ESS^*+}(t) - \frac{1}{\eta} \Delta P^{ESS^*-}(t)$;
  $t = t + 1$;
end

Algorithm 3.3: Receding horizon algorithm.

other words, $\widetilde{\mathcal{H}}(k)$ coincides with $\mathcal{H}(k)$ if one assumes empty parking lots and initial time step equal to t. Then, the probability distribution of $\widetilde{\mathcal{H}}(k)$ can be computed similarly as that of $\mathcal{H}(k)$ in (3.5), by using the updated distributions of the total number of incoming vehicles and the EV arrival times, i.e. (3.19) and (3.20), respectively.

To exploit the same reasoning described in Section 3.3, the receding horizon procedure is based on the solution of Problem 3.5, where the optimization is performed in $\mathcal{I}(t, \lambda - t)$, and constraints (3.17c)-(3.17d) are adjusted as follows

$$\sum_{n=0}^{\overline{N}_V} \left(\Delta P_0^{EV} n\right) z_n(k) \geq \Delta \widehat{P}^{PV}(k) - \Delta P^{ESS}(k) - \mathcal{H}(t,k) \Delta P_0^{EV} \quad \forall k \in \mathcal{I}(t, \lambda - t) \tag{3.21}$$

$$\sum_{n=0}^{\overline{N}_V} \mathcal{P}_k \left(\widetilde{E}_d^{EV}(k) \geq \Delta P_0^{EV} n\right) z_n(k) \geq 1 - \beta_k \qquad \forall k \in \mathcal{I}(t, \lambda - t) \tag{3.22}$$

where

$$\widetilde{E}_d^{EV}(k) = \Delta P_0^{EV} \widetilde{\mathcal{H}}(k).$$

A sketch of the receding horizon procedure to online operate the ESS is reported in Algorithm 3.3.

Chapter 4

Robust Energy Management of an IMG Under EV Arrival Uncertainty

An industrial microgrid (IMG) consists in a microgrid involving manufacturer plants which are usually equipped with distributed generation facilities, industrial electric vehicles, energy storage systems, etc. In this chapter, the problem of IMG efficient operation in presence of electric vehicle uncertainty is addressed. To this purpose, schedule of the different device operations of IMGs has to be optimally computed, minimizing the operation cost while guaranteeing electrical network stability and production constraints.

4.1 Introduction

Due to the technological development of low carbon technologies such as renewable generation sources, local energy storage systems and electric vehicles, several issues came up to properly integrate these new features into existing power systems. In fact, the intermittent nature of the energy from renewables may affect negatively network stability and grid power quality. To this end, attention of the scientific community has focused on local communities, and in particular on microgrids [47, 48, 49]. In [50], a novel model of microgrid in the presence of renewables and electric vehicles has been presented, whereas in [51], a coordinated electric vehicle charging algorithm has been proposed to guarantee the power quality of the system. In this framework, secure grid

operation under huge penetration of plug-in electric vehicles (EVs) has been addressed [52, 53]. In [54] a smart charging control to minimize the operation cost under different user preferences is reported, while an optimal storage sizing procedure to minimize the microgrid planning cost has been presented in [55].

Besides residential microgrids, recent years have witnessed a growing interest towards industrial microgrids (IMGs), i.e., microgrids involving manufacturing plants. In addition to the above mentioned features, this kind of microgrids has to take into account production loads, industrial electric vehicles, and possibly spatially distributed combined heat and electrical power generation sources [56]. In [57], an optimal microgrid planning for an industrial site in the presence of distributed generation (DG) plants has been proposed, while in [58] a multi-objective optimization of an industrial microgrid considering demand response, maximization of the total revenue, and total emission reduction, has been developed.

To guarantee robust operation of microgrids, uncertainties affecting various components and processes of the considered systems should be handled, as well. These uncertainties may affect directly the system behavior leading to possible violations of both technological and security constraints. In fact, since these constraints often depend on uncertain variables, a suitable modeling paradigm is needed to formulate them in probabilistic terms. A rigorous way to model this uncertainty is to make use of chance constraints [59, 60], which generally lead to complex formulations difficult to handle. In order to overcome this issue, several approximation techniques have been proposed, e.g., scenario-based [61] or distributionally chance constraint approaches [62]. For instance, a scenario-based approach has been introduced in [13] to guarantee network performance against uncertainties of power loads and electric vehicles arrivals, and in [63] to tackle uncertainty on renewable generation in an EV parking lot.

In this chapter, we consider an industrial microgrid involving a manufacturing plant composed of several spatially distributed buildings, hereafter referred to as *factory units* (FUs), connected to different buses. Such FUs perform different tasks of the production plan and some of them are assumed to be equipped with DG systems. In particular, PV systems coupled with electrical energy storage systems are considered. Further, we assume that FUs are provided with combined heat and power (CHP) systems able to produce electrical and heat power to be exchanged inside the IMG. In addition to CHP systems, heat

power can also be generated through boilers. A fleet of plug-in electric vehicles is assumed to be assigned to each FU. Such vehicles can be of different types, ranging from picker to lift trucks, from bucket to delivery trucks [56]. The arrival (charging) time of each EV is assumed to be uncertain, while the departure (plug-out) time is considered to be known in advance, since it is assumed to be scheduled in the FU production plan. In this setting, vehicle-to-grid power exchange will not be allowed. A sketch of the considered IMG is reported in Fig. 4.1.

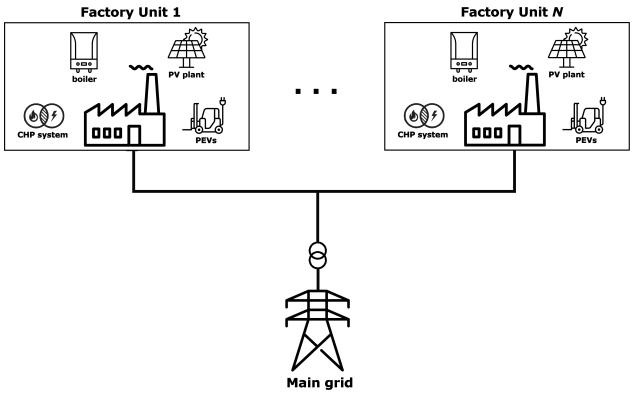

Figure 4.1: Sketch of an industrial microgrid.

Chapter Contribution and Organization

The aim of the chapter is to derive an optimal management and control policy for the IMG in order to minimize the energy bill, while satisfying electrical network stability constraints, heat and power exchange among FUs, and guaranteeing a suitable charge level to EVs. Electricity and gas prices change over time and they are assumed to be known in advance. The optimization problem is formulated in a receding horizon framework [64, 65], where at each time step a sequence of dynamic optimal power flow (DOPF) instances [66, 67] is solved. To tackle the uncertainty associated to each EV, a chance constraint approach [59] is adopted. Due to power flow equations and chance constraints, the obtained optimization problem is nonconvex. Relaxations based on [68] and [62] make it possible to reformulate the nonconvex constraints as a set of linear matrix inequalities for power flow and chance constraints, respectively.

The novel contribution of this chapter with respect to the existing literature can be summarized as follows:
i) the uncertainty related to EVs is managed through a chance constraint approach. This solution allows one to consider also vehicles which are not in charge in the optimization problem;

ii) nonconvex constraints arisen by using chance constraints are relaxed by means of worst-case Conditional Value at Risk (CVaR) constraints [62], allowing for computationally feasible solution of the optimization problem.

The chapter is organized as follows. In Section 4.2, the problem of optimal control of an IMG is formulated and all the relevant variables and constraint on such IMG are presented. While in Section 4.3, the uncertainty concerning electric vehicles has been modelled and the receding horizon approach is presented.

4.2 Formulation of the Optimal Control of an IMG

In this chapter, a discrete-time approach with sampling time Δ is considered. Let x be a generic variable, the notation $x(k)$ stands for the average value of x from time step k to $k+1$. Let the set of buses involved in the IMG be denoted by $\mathcal{N} = \{1, \ldots, N\}$, where N is the number of buses. By x_i we mean a generic variable x related to bus i.

The aim of this chapter is to minimize the overall cost of an IMG while respecting the physical and security constraints imposed by its components, i.e., power lines, DG facilities, ESSs, EVs, etc. Moreover, operation constraints related to heat requirements and EV charging set-points have to be respected, as well.

4.2.1 Objective Function

Let t denote the present time step and let λ be the horizon length. The objective function to be minimized is defined as the sum of all the costs of the IMG over the time interval $\mathcal{I}(t, \lambda + 1) = [t,\, t + \lambda + 1)$. Electrical power can be generated by PV and CHP systems or it can be drawn from the main grid. Heat may be produced by boilers and CHP systems. Thus, for all the factory units, the cost of using CHP systems (C_i^{CHP}) and boilers (C_i^B) has to be taken into account in the objective function, as well as the cost of the electricity drawn from the main grid (C^G). Thus, the objective function to be

minimized is:

$$J(t,\lambda) = \sum_{i=1}^{N} \sum_{k=t}^{t+\lambda} C_i^{CHP}(k) + \sum_{i=1}^{N} \sum_{k=t}^{t+\lambda} C_i^{B}(k) + \sum_{t=k}^{t+\lambda} C^{G}(k) \ . \tag{4.1}$$

Let P_i^{CHP} be the electrical power produced by the i-th CHP system, and let η_i^{CHP} and p^g be the CHP efficiency and the gas price, respectively. Denoting by c_i^{CHP} the operation cost of the i-th CHP system per unit of electrical power generated in a time slot, the CHP cost can be expressed as:

$$C_i^{CHP}(k) = \frac{P_i^{CHP}(k)\Delta}{\eta_i^{CHP}} p^g(k) + P_i^{CHP}(k)\, c_i^{CHP} \ .$$

Let P_i^B be the heat power generated by the i-th boiler, then the corresponding cost is:

$$C_i^{B}(k) = \frac{P_i^{B}(k)\Delta}{\eta_i^{B}} p^g(k) \ ,$$

where η_i^B denotes the boiler efficiency.

Let us denote the net active and reactive power at bus i by P_i and Q_i, respectively. By convention, the slack bus is indexed by 1, so the net active and reactive powers drawn from the main grid correspond to P_1 and Q_1, respectively. Let $p(k)$ be the electricity price at time k, the overall electricity cost from the main grid can be written as:

$$C^G(k) = P_1(k)\Delta\, p(k) \ .$$

It is worthwhile to remark that $P_1(k)$ is the difference between the overall electric power needed by the IMG (for factory operation, power losses, EV and ESS charging), and the electric power generated by CHP and PV systems.

In this chapter, to avoid arbitrage on electricity price, it is assumed that the IMG cannot inject electric power into the main grid, i.e., $P_1(k) \geq 0$ for all k.

4.2.2 Physical and Security Constraints

In this subsection, the physical and security constraints needed to ensure safe operation and physical stability of the IMG are defined.

First, the power balance equations are recalled. Let P_i^F be the active power demand of the factory unit connected to bus i and let the charge/discharge power of the i-th ESS be denoted by P_i^{ESS+} and P_i^{ESS-}, respectively. For a

generic EV v connected to bus i, $P_{i,v}^{EV}(k)$ represents the charge power at time k. Let $\widehat{P}_i^{PV}(k)$ be the actual power drawn from PV plant connected at bus i at time k. Denoting by P_i^G and P_i^D the total generated and demanded active power at bus i, one has:

$$P_i^G(k) = P_i^{CHP}(k) + \widehat{P}_i^{PV}(k) + P_i^{ESS-}(k) \ ,$$

$$P_i^D(k) = P_i^F(k) + P_i^{ESS+}(k) + \sum_{v=1}^{N_{V_i}} P_{i,v}^{EV}(k) \ ,$$

where N_{V_i} is the maximum number of vehicles related to bus i.

The net active and reactive power at bus i can be written as [69, 66, 67]:

$$P_i(k) = V_i(k) \sum_{j=1}^{N} V_j(k) \big(G_{ij} \cos\theta_{ij}(k) - B_{ij} \sin\theta_{ij}(k) \big) \ ,$$

$$Q_i(k) = V_i(k) \sum_{j=1}^{N} V_j(k) \big(G_{ij} \sin\theta_{ij}(k) - B_{ij} \cos\theta_{ij}(k) \big) \ ,$$

where G_{ij} and B_{ij} are the real and imaginary part of the electrical admittance between bus i and j, V_i is the voltage magnitude at bus i, and θ_{ij} is the voltage phase angle difference between buses i and j. Thus, the active power balance equality constraint at bus i is:

$$P_i(k) - P_i^G(k) + P_i^D(k) = 0 \ .$$

The reactive powers of the PV systems and EVs are neglected since these small generators are typically connected to the network through high quality grid-tie converters that feature a fixed power factor close to 1 [70]. The reactive power demand consists of the reactive power of the different FU loads. Denoting by Q_i^{CHP} and Q_i^F the reactive powers exchanged by the CHP system and the FU connected to bus i, the reactive power balance equation is:

$$Q_i(k) - Q_i^{CHP}(k) + Q_i^F(k) = 0 \ .$$

Let us now introduce the inequality constraints concerning network security, CHP and boiler systems, PV systems and EVs. The network security constraints enforce limits on voltages at the different buses and capacities of the lines, the latter depending on physical properties of the lines [70]. No voltage limits are set on the slack bus since it is considered a fixed-voltage bus. As previously stated, we assume that the slack bus is labeled with $i = 1$. Let us

denote by $S_{ij}(k)$ the power flowing from bus i to bus j in the k-th time slot. Network security constraints can be written as:

$$\underline{V}_i \leq V_i(k) \leq \overline{V}_i \ , \qquad \forall i \in \mathcal{N} \ ,$$

and

$$|S_{ij}(k)| \leq \overline{S}_{ij} \ , \qquad i \neq j \ ,$$

while the slack bus constraints are:

$$0 \leq P_1(k) \leq \overline{P}_1 \ ,$$
$$\underline{Q}_1 \leq Q_1(k) \leq \overline{Q}_1 \ ,$$

where $\overline{P}_1$, $\underline{Q}_1$ and $\overline{Q}_1$ are given bounds.

Constraints on active and reactive power generation by the i-th CHP system are expressed as:

$$\underline{P}_i^{CHP} \leq P_i^{CHP}(k) \leq \overline{P}_i^{CHP} \ ,$$
$$\underline{Q}_i^{CHP} \leq Q_i^{CHP}(k) \leq \overline{Q}_i^{CHP} \ ,$$

while the heat power produced by a generic boiler i is constrained as:

$$0 \leq P_i^B(k) \leq \overline{P}_i^B \ .$$

Let E_i^{ESS} be the energy stored in the ESS connected to bus i, and let η_i^{ESS} be the corresponding efficiency. The constraints involving the ESS enforce limits on the charge/discharge power, the storage capacity and the energy balance. Thus:

$$0 \leq P_i^{ESS+}(k) \leq \overline{P}_i^{ESS+} \ ,$$
$$0 \leq P_i^{ESS-}(k) \leq \overline{P}_i^{ESS-} \ ,$$
$$\underline{E}_i^{ESS} \leq E_i^{ESS}(k) \leq \overline{E}_i^{ESS} \ ,$$
$$E_i^{ESS}(k) = E_i^{ESS}(k-1) + \eta_i^{ESS} P_i^{ESS+}(k-1)\Delta - \frac{1}{\eta_i^{ESS}} P_i^{ESS-}(k-1)\Delta.$$

Regarding EVs, let us consider the generic vehicle v connected to bus i and denote by $E_{i,v}^{EV}$ the energy stored in its battery and by $\eta_{i,v}^{EV}$ the corresponding charging efficiency. The electrical vehicle charging process is represented by the following constraints:

$$E_{i,v}^{EV}(k) = E_{i,v}^{EV}(k-1) + \eta_{i,v}^{EV} P_{i,v}^{EV}(k-1)\Delta \ , \tag{4.2}$$

$$0 \leq P_{i,v}^{EV}(k) \leq \overline{P}_{i,v}^{EV} \ , \tag{4.3}$$

$$E_{i,v}^{EV}(k) \leq \overline{E}_{i,v}^{EV} \ . \tag{4.4}$$

Lastly, the power drawn from the PV plant at bus i is constrained as follows

$$0 \leq \widehat{P}_i^{PV}(k) \leq P_i^{PV}(k),$$

where $P_i^{PV}(k)$ is the maximum PV power produced at bus i.

4.2.3 Operational Constraints

Let $t_{i,v}^a$ and $t_{i,v}^d$ denote the time a generic EV v connected to bus i starts and stops the charging process, respectively. We assume that the departure time $t_{i,v}^d$ is known, being it related to the factory production schedule, while the arrival time $t_{i,v}^a$ is uncertain. We also assume that the battery capacity at plug-in time is known. To assure that a vehicle is fully charged at the time it is plugged-out, the following constraint is introduced. It enforces the stored energy at departure time to be equal to the maximum battery capacity:

$$E_{i,v}^{EV}(t_{i,v}^d) = \overline{E}_{i,v}^{EV} \ . \tag{4.5}$$

In the considered setting, we assume that factory units can exchange heat among themselves, and that their CHP systems and boilers cooperate to satisfy the overall heat requirement. Denoting by α_i^{CHP} the waste factor that describes how much useful heat power is generated per electric power produced by the i-th CHP system, the constraint on the overall heat demand R of the IMG can be expressed as:

$$\sum_{i=1}^{N} \left(\alpha_i^{CHP} P_i^{CHP}(k) + P_i^B(k)\right) \geq R(k) \ .$$

4.3 Optimal Control Implementation

In this section, a receding horizon algorithm ensuring optimal operation of the IMG is derived. To this purpose, the objective function (4.1) has to be minimized in order to compute the optimal control sequence.

Let t denote the current time step. The arrival time of a vehicle is supposed to be uncertain, and therefore the constraint representing its charging process is meaningful only when that EV is plugged into the network. For this reason, let us define $\mathcal{V}_i(t) = \left\{v : \ t_{i,v}^a \leq t \leq t_{i,v}^d\right\}$ as the set of indices identifying vehicles

plugged into the i-th bus at time t. Since the cardinality of this set varies over time, the optimization procedure needs to be adapted at each time step. Therefore, an adaptive optimization problem need be formulated at each time step in order to find the best solution for the IMG operation.

Notice that $\mathcal{V}_i(t)$ takes into account only the vehicles charging at time t, but it provides no information about the incoming ones. Ignoring such an aspect may lead to situations in which network safety constraints may be violated, e.g., due to voltage drops and/or power overloads caused by arrivals of vehicles in future steps. Thus, in order to prevent these events, a chance constrained approach is adopted to handle uncertainty affecting EVs arrival times.

4.3.1 Uncertainty Modeling

The real arrival time of the v-th vehicle at bus i, $t^a_{i,v}$, is supposed to be a random variable with a bounded closed support $[\underline{t}^a_{i,v}, \overline{t}^a_{i,v}]$, and let us assume that the corresponding discrete distribution function is known. To take into account the incoming vehicles, let us define the index set $\mathcal{V}_i(t,\lambda) = \left\{v : t < \underline{t}^a_{i,v} < t+\lambda\right\}$ which contains the indices of the vehicles whose minimum arrival time falls into the prediction horizon. Notice that, by construction, sets $\mathcal{V}_i(t)$ and $\mathcal{V}_i(t,\lambda)$ are disjoint, i.e., $\mathcal{V}_i(t) \cap \mathcal{V}_i(t,\lambda) = \emptyset$, for all i and t.

Being the arrival time $t^a_{i,v}$ a random variable, also the evolution of the vehicle state of charge $E^{EV}_{i,v}$ becomes a random variable itself. So, to manage the charging process involving incoming vehicles, constraint (4.5) is replaced by the following chance constraint:

$$\mathcal{P}\left(E^{EV}_{i,v}(t^d_{i,v}) \geq \overline{E}^{EV}_{i,v}\right) \geq 1-\epsilon \ , \qquad v \in \mathcal{V}_i(t,\lambda) \ , \tag{4.6}$$

where $0 < \epsilon < 1$ denotes a given failure tolerance level.

In order to model the uncertainty on the state of charge, let us define the binary random vector $\Gamma_{i,v}$ as

$$\Gamma_{i,v} = \left[\gamma_{i,v}(\underline{t}^a_{i,v}), \ldots, \ \gamma_{i,v}(\overline{t}^a_{i,v})\right]'$$

where,

$$\gamma_{i,v}(k) = \begin{cases} 1 & \text{if} \quad k \geq t^a_{i,v} \\ 0 & \text{otherwise} \end{cases} \ , \ k = \underline{t}^a_{i,v}, \ldots, \overline{t}^a_{i,v}$$

describes if a vehicle is in charge at time k.

Combining (4.6) with $\Gamma_{i,v}$, the chance constraint can be rearranged as

$$\mathcal{P}\left(\eta_{i,v}^{EV}\Delta\Big(\sum_{k=\underline{t}_{i,v}^{a}}^{\overline{t}_{i,v}^{a}}P_{i,v}^{EV}(k)\gamma_{i,v}(k)+\sum_{k=\overline{t}_{i,v}^{a}+1}^{t_{i,v}^{d}-1}P_{i,v}^{EV}(k)\Big)\geq\overline{E}_{i,v}^{EV}-E_{i,v}^{EV}(t_{i,v}^{a})\right)\geq 1-\epsilon\ .$$

By using (4.2), the second sum can be rewritten as

$$\mathcal{P}\left(\eta_{i,v}^{EV}\Delta\sum_{k=\underline{t}_{i,v}^{a}}^{\overline{t}_{i,v}^{a}}P_{i,v}^{EV}(k)\gamma_{i,v}(k)+E_{i,v}^{EV}(t_{i,v}^{d})-E_{i,v}^{EV}(\overline{t}_{i,v}^{a}+1)\geq\overline{E}_{i,v}^{EV}-E_{i,v}^{EV}(t_{i,v}^{a})\right)\geq 1-\epsilon\ ,$$

and finally

$$\mathcal{P}\left(\eta_{i,v}^{EV}\Delta\left(\pi_{i,v}^{t_a}\right)'\Gamma_{i,v}+\mathcal{E}_{i,v}^{EV}\geq 0\right)\geq 1-\epsilon, \tag{4.7}$$

where,

$$\pi_{i,v}^{k^a}=\left[P_{i,v}^{EV}(\underline{t}_{i,v}^{a}),\ldots,\ P_{i,v}^{EV}(\overline{t}_{i,v}^{a})\right]',$$

and

$$\mathcal{E}_{i,v}^{EV}=E_{i,v}^{EV}(t_{i,v}^{d})-E_{i,v}^{EV}(\overline{t}_{i,v}^{a}+1)-\overline{E}_{i,v}^{EV}+E_{i,v}^{EV}(t_{i,v}^{a}).$$

Notice that, if the vehicle arrival time interval overlaps the current time, the arrival distribution $\Gamma_{i,v}$ can be replaced by the corresponding conditional distribution.

4.3.2 Optimization Problem Formulation

Let us define the command row vector $\mathbf{\Pi}(t)$ as

$$\begin{aligned}\mathbf{\Pi}(t)=\Big[&P_{1,1}^{EV}(t),...,P_{1,N_{V_1}}^{EV}(t),...,P_{N,1}^{EV}(t),...,P_{N,N_{V_N}}^{EV}(t),\\&P_1^{ESS+}(t),...,P_N^{ESS+}(t),P_1^{ESS-}(t),...,P_N^{ESS-}(t),\\&P_1^{CHP}(t),...,P_N^{CHP}(t),\ Q_1^{CHP}(t),...,Q_N^{CHP}(t),\\&P_1^{B}(t),...,P_N^{B}(t)\Big]\ .\end{aligned}$$

Furthermore, let us introduce the vector $\mathbf{\Pi}(t,\lambda)$ in order to collect the control sequence over the time interval $\mathcal{I}(t,\lambda+1)$:

$$\mathbf{\Pi}(t,\lambda)=\left[\mathbf{\Pi}(t),\ldots,\ \mathbf{\Pi}(t+\lambda)\right].$$

The DOPF problem can be formulated as reported in Problem 4.1.

Problem 4.1 (Dynamic Optimal Power Flow Problem)

$$\boldsymbol{\Pi}^*(t,\lambda) = \underset{\boldsymbol{\Pi}(t,\lambda)}{\operatorname{argmin}} \quad J(t,\lambda)$$

subject to:

$$\left.\begin{aligned}
&P_i(k) = P_i^{CHP}(k) + \widehat{P}_i^{PV}(k) + P_i^{ESS-}(k) \\
&\qquad - \quad P_i^{F}(k) - P_i^{ESS}(k) - \sum_{v\in\mathcal{V}_i(k)\cup\mathcal{V}_i(k,\lambda)} P_{i,v}^{EV}(k) \\
&Q_i(k) = Q_i^{CHP}(k) - Q_i^{F}(k) \\
&|S_{ij}(k)| \le \overline{S}_{ij} \ , \quad j \neq i \\
&\underline{P}_i^{CHP} \le P_i^{CHP}(k) \le \overline{P}_i^{CHP} \\
&\underline{Q}_i^{CHP} \le Q_i^{CHP}(k) \le \overline{Q}_i^{CHP} \\
&0 \le P_i^{B}(k) \le \overline{P}_i^{B} \\
&0 \le P_i^{ESS+}(k) \le \overline{P}_i^{ESS+} \\
&0 \le P_i^{ESS-}(k) \le \overline{P}_i^{ESS-} \\
&\underline{E}_i^{ESS} \le E_i^{ESS}(k) \le \overline{E}_i^{ESS} \\
&0 \le \widehat{P}_i^{PV}(k) \le P_i^{PV}(k)
\end{aligned}\right\} \begin{array}{l}\forall k \in \mathcal{I}(t,\lambda+1), \\ \forall i \in \mathcal{N}\end{array}$$

$$\left.\begin{aligned}
&0 \le P_1(k) \le \overline{P}_1 \\
&\underline{Q}_1 \le Q_1(k) \le \overline{Q}_1 \\
&R(k) \le \sum_{i=1}^{N} \left(\alpha_i^{CHP} P_i^{CHP}(k) + P_i^{B}(k)\right)
\end{aligned}\right\} \forall k \in \mathcal{I}(t,\lambda+1)$$

$$\left.\begin{aligned}
&\underline{V}_i \le V_i(k) \le \overline{V}_i
\end{aligned}\right\} \begin{array}{l}\forall k \in \mathcal{I}(t,\lambda+1), \\ \forall i \in \mathcal{N}\end{array}$$

$$\left.\begin{aligned}
&E_i^{ESS}(k) = E_i^{ESS}(k-1) + \eta_i^{ESS} P_i^{ESS+}(k-1)\Delta \\
&\qquad - \quad \frac{1}{\eta_i^{ESS}} P_i^{ESS-}(k-1)\Delta
\end{aligned}\right\} \begin{array}{l}\forall k \in \mathcal{I}(t+1,\lambda+1), \\ \forall i \in \mathcal{N}\end{array}$$

$$\left.\begin{aligned}
&E_{i,v}^{EV}(k) = E_{i,v}^{EV}(k-1) + \eta_{i,v}^{EV} P_{i,v}^{EV}(k-1)\Delta \\
&0 \le P_{i,v}^{EV}(k) \le \overline{P}_{i,v}^{EV} \\
&E_{v}^{EV}(k) \le \overline{E}_{k}^{EV}
\end{aligned}\right\} \begin{array}{l}\forall k \in \mathcal{I}\left(t_{i,v}^{a}+1, t_{i,v}^{d}+1\right) \\ \forall i \in \mathcal{N}, \\ \forall v \in \mathcal{V}_i(k)\cup\mathcal{V}_i(k,\lambda)\end{array}$$

$$\left.\begin{aligned}
&\mathcal{P}\left(\eta_{i,v}^{EV}\Delta\left(\pi_{i,v}^{y_a}\right)'\Gamma_{i,v} + \mathcal{E}_{i,v}^{EV} \ge 0\right) \ge 1-\epsilon
\end{aligned}\right\} \begin{array}{l}\forall i \in \mathcal{N}, \\ \forall v \in \mathcal{V}_i(k,\lambda)\end{array}$$

$$\left.\begin{aligned}
&E_{i,v}^{EV}(t_{i,v}^{d}) = \overline{E}_{i,v}^{EV}
\end{aligned}\right\} \begin{array}{l}\forall i \in \mathcal{N}, \\ \forall v \in \mathcal{V}_i(k) \ .\end{array}$$

Notice that, since $\mathcal{V}_i(k) \cap \mathcal{V}_i(k,\lambda) = \emptyset$, $\forall i, \forall k$, the last two constraints of Problem 4.1 are mutually exclusive in the adaptive optimization procedure.

It is worthwhile to remark that this optimization problem is nonconvex. In fact, it involves power flow equations, which describe a highly nonlinear system, and chance constraints in which the feasible set is typically nonconvex.

From the optimal power flow perspective, the nonconvexity can be handled by using its dual formulation and by relaxing a rank constraint to obtain a convex problem. It has been proven that for radial networks like those considered in this chapter, such a relaxation is exact, see [68] for details.

Regarding chance constrained optimization, in the next subsection a method to approximate such constraints is adopted.

4.3.3 Chance Constraint Approximation

In the literature, there exist mainly two approaches to approximate chance constraints. The first one regards scenario based methods, where a number of realizations of the random process is collected in order to approximate the original chance constraints [61, 71]. The drawback of this approach is that the number of samples needed increases considerably as the failure tolerance level decreases, leading to computationally demanding problems when satisfaction probability approaches 1. This feature may be dramatically amplified by the increasing number and dimension of the random vectors necessary to model uncertainty. In the considered setting, the number of EVs employed into the IMG, and then the number of random vectors, amounts to tens or even hundreds, leading to computationally unfeasible problems.

The second approximation family involves robust optimization methods, where chance constraints are relaxed by exploiting stochastic properties of the uncertain variables involved. Hereafter, we refer to the technique proposed in [62], where the first and second order moments of the considered random variable are used to obtain a convex problem reformulation involving linear matrix inequalities. Then, such a problem can be efficiently solved by using standard optimization tools (e.g., [72, 73, 74]).

Thus, let us now focus on the random variable $\mathbf{\Gamma}_{i,v}$, whose expected value is given by

$$\mathbb{E}[\mathbf{\Gamma}_{i,v}] = \boldsymbol{\mu}_{i,v} = \left[\mu_{i,v}(\underline{t}^a_{i,v}), \ldots, \ \mu_{i,v}(\overline{t}^a_{i,v})\right]',$$

where

$$\mu_{i,v}(k) = \mathbb{E}[\gamma_{i,v}(k)] = P(\gamma_{i,v}(k) = 1) = P(t^a_{i,v} \leq k) \ .$$

Let $\mathbf{\Sigma}_{i,v}$ denote the covariance matrix of $\mathbf{\Gamma}_{i,v}$, one has:

$$\mathbf{\Sigma}_{i,v} = \begin{bmatrix} \sigma_{i,v}(\underline{t}^a_{i,v}, \underline{t}^a_{i,v}) & \ldots & \sigma_{i,v}(\underline{t}^a_{i,v}, \overline{t}^a_{i,v}) \\ \vdots & \ddots & \vdots \\ \sigma_{i,v}(\overline{t}^a_{i,v}, \underline{t}^a_{i,v}) & \ldots & \sigma_{i,v}(\overline{t}^a_{i,v}, \overline{t}^a_{i,v}) \end{bmatrix} ,$$

where

$$\sigma_{i,v}(p,q) = \begin{cases} \mu_{i,v}(p)(1-\mu_{i,v}(q)) & \text{if } p \leq q \\ \mu_{i,v}(q)(1-\mu_{i,v}(p)) & \text{if } p > q. \end{cases}$$

The first and second order moments of $\Gamma_{i,v}$ can be combined as follows:

$$\boldsymbol{\Omega}_{i,v} = \begin{bmatrix} \boldsymbol{\Sigma}_{i,v} + \boldsymbol{\mu}_{i,v}\boldsymbol{\mu}'_{i,v} & \boldsymbol{\mu}_{i,v} \\ \boldsymbol{\mu}'_{i,v} & 1 \end{bmatrix}.$$

Let us refer to a generic vehicle v connected to bus i. In the following, for ease of notation, subscripts i and v are omitted. According to [62], chance constraint (4.7) can be approximated through CVaR and then replaced with the following set of convex constraints:

$$\begin{cases} \exists \chi \in \mathbb{R},\ \mathbf{M} \in \mathbb{S}^{(\overline{t}^a - \underline{t}^a + 2)}, \\ \exists \boldsymbol{\nu} \in \mathbb{R}^{(\overline{t}^a - \underline{t}^a + 1)},\ \boldsymbol{\omega} \in \mathbb{R}^{(\overline{t}^a - \underline{t}^a + 1)}, \\ \boldsymbol{\nu} \geq 0, \\ \boldsymbol{\omega} \geq 0, \\ \chi + \frac{1}{\epsilon} Tr(\mathbf{M}\boldsymbol{\Omega}) \leq 0, \\ \mathbf{M} + \sum_{j=1}^{(\overline{t}^a - \underline{t}^a + 1)} \mathbf{W}_j \nu_j \succeq 0, \\ \mathbf{M} + \sum_{j=1}^{(\overline{t}^a - \underline{t}^a + 1)} \mathbf{W}_j \omega_j - \begin{bmatrix} 0 & -\frac{1}{2}\eta^{EV}\Delta\boldsymbol{\pi}^{t^a} \\ -\frac{1}{2}\eta^{EV}\Delta\left(\boldsymbol{\pi}^{t^a}\right)' & -\mathcal{E}^{EV} - \chi \end{bmatrix} \succeq 0\ , \end{cases} \tag{4.9}$$

where $Tr(\cdot)$ is the trace operator and W_j are symmetric matrices of dimension $\overline{t}^a - \underline{t}^a + 1$. Such matrices are used to approximate the support Ξ of $\boldsymbol{\Gamma}$ as:

$$\Xi \subseteq \left\{ \boldsymbol{\Gamma} \in \mathbb{R}^{(\overline{t}^a - \underline{t}^a + 1)} :\ [\boldsymbol{\Gamma}',\ 1] W_j [\boldsymbol{\Gamma}',\ 1]' \leq 0,\ j = 1, \ldots, \overline{t}^a - \underline{t}^a + 1 \right\},$$

where $\mathbf{W}_j$ are such that each entry of $\boldsymbol{\Gamma}$ must lie between 0 and 1.

4.3.4 Receding Horizon Implementation

Notice that optimization Problem 4.1 does not take into account vehicles whose departure time falls outside the prediction horizon. To overcome this issue, a dynamic adaptation of the prediction horizon λ is proposed as follows:

1. Let the nominal prediction horizon λ be given.

2. At time t, let us check for each bus i if there is any EV with index v such that $v \in \mathcal{V}_i(t) \cup \mathcal{V}_i(t, \lambda)$:

   (a) if there is not any EV belonging to $\mathcal{V}_i(t) \cup \mathcal{V}_i(t, \lambda)$, then the prediction horizon remains unchanged;

   (b) if there are some vehicles belonging to $\mathcal{V}_i(t) \cup \mathcal{V}_i(t, \lambda)$, the corresponding departure times $t^d_{i,v}$ have to be considered. Let us call t^d_{max} the maximum departure time for all the vehicles belonging to $\mathcal{V}_i(t) \cup \mathcal{V}_i(t, \lambda)$. The prediction horizon has to be updated with the maximum value between t^d_{max} and λ.

The overall receding horizon algorithm is reported in Algorithm 4.1.

```
Let λ_0 be the nominal prediction horizon;
Set t = 0;
Set λ = λ_0;
for i = 1 to N do
    for v ∈ V_i(t) do
        Update the horizon as λ = max{λ, t^d_{i,v}};
        Add constraints (4.2)-(4.3)-(4.4)-(4.5) for vehicle v;
    end
    for v ∈ V_i(t, λ) do
        Update the horizon as λ = max{λ, t^d_{i,v}};
        Add constraints (4.2)-(4.3)-(4.4)-(4.9) for vehicle v;
    end
end
Solve Problem 4.1 to obtain Π*(t, λ);
Apply command Π*(t);
t = t + 1;
Repeat from step 3
```

Algorithm 4.1: Receding Horizon procedure

Chapter 5

Smart Buildings Energy Management Under Environmental Uncertainty and DR

This chapter deals with the problem of cost-optimal operation of smart buildings that integrate a centralized HVAC system, photovoltaic generation and both thermal and electrical storage devices. Building participation in a Demand-Response program is also considered.

5.1 Introduction

It is well-known that buildings represent one of the major electricity consumers worldwide. About a half of the total energy consumption is devoted to heating, ventilation and air conditioning (HVAC). While HVAC devices in older buildings are operated through simple rules, newer buildings exploit the opportunities offered by information and communication technologies to efficiently operate such appliances [75]. An efficient control of most of the building devices yields to a global reduction of energy consumption, with a consequent reduction of emissions and energy bills [76].

Although a large part of the currently deployed building management systems are rule-based, Model Predictive Control (MPC) is gaining a lot of importance, owing to its flexibility and its ability to take a number of different requirements

and constraints into account [77]. Indeed, to optimize the building operation cost, several applications of MPC can be found in the literature, where both linear [78] and non-linear [79] dynamics are considered. In [80], an MPC-based enthalpy control algorithm has been derived. Other works deal with uncertainty in models and/or exogenous variables by using stochastic MPC approaches. Specifically, in [81, 82] a tractable reformulation using chance constraints has been devised, while a scenario-based approach has been exploited in [83].

In order to reduce the computational complexity which often affects MPC implementations, in [84] a machine learning approach based on multivariate regression and dimensionality reduction algorithms has been proposed, and a case study involving a 6-zone building has been carried out. In [85], a cooperative Fuzzy MPC has been implemented on a real building composed of five zones.

Due to the relevance of buildings as players in smart grids, an important aspect recently considered in the building management literature is participation in Demand-Response (DR) programs, which enables end-users to become active players in the electricity system [86, 87, 88]. DR is usually managed by an intermediary player (known as the aggregator [89]) whose role is to gather flexibility from its affiliated consumers, in order to build services to be sold either to the grid operator or on the wholesale market. In response to the aggregator's requests, which become known in advance, consumers may choose to adjust their consumption patterns in order to comply and receive a monetary reward [90, 91, 92]. Reduction of energy cost in presence of DR has been studied in [93] via an agent-based modeling approach.

Considering the growing importance of distributed generation and the relevant share of energy consumption by buildings, energy storage systems are expected to become increasingly used. Such systems are employed to achieve high levels of self-sufficiency, as well as system resiliency [94, 95]. Furthermore, optimal sizing and efficient management of electrical storage in smart buildings, mainly in the presence of photovoltaic (PV) generation [96] and plug-in electric vehicles [97], is a widely investigated topic. In view of the participation of a building in DR programs, the presence of energy storage facilities contributes to achieve a high level of consumption flexibility.

Chapter Contribution and Organization

The aim of this chapter is to propose a novel MPC-based control strategy

aimed at the minimization of the electricity bill in a large-scale building. The building is assumed to be equipped with a central HVAC system powered by heat pumps (HPs), a PV plant, thermal (TES) and electrical (ESS) storage devices, and to participate in a DR program. In the proposed approach, heat pumps, heater actuators, storage devices, and PV generation facilities are managed in an optimal fashion by a centralized control unit. The employed DR paradigm consists of price-volume signals sent by an aggregator, which specify a monetary reward granted to the building operator upon the fulfillment of energy consumption constraints within a given time period [98, 99].

The control law for the different actuating devices of the overall HVAC system is computed through a receding horizon algorithm involving a two-step optimization strategy. Several constraints are taken into account, namely thermal comfort, DR programs, operating limits of heat exchangers, PV power availability, storage capacity and maximum charging/discharging rates. Meteorological variables, building occupancy, light and internal appliance loads are considered as exogenous disturbances where their measured/predicted values are assumed to be available.

The main contributions of the chapter in the above context are as follows.

- Since the computational complexity of the control algorithm is a crucial aspect when dealing with large-scale buildings, a framework is adopted in which heat flows in the different building zones are regulated by controlling the air mass flow through each fan coil. This choice, along with approximate linear modeling of the building zones, allows for formulating the optimal control problem at each step as a Linear Program (LP). Hence, the involved computational burden scales nicely with the problem dimension and the solver provides a fast solution even for a large number of optimization variables and constraints [100]. Actually, the presence of DR programs calls for the introduction of binary decision variables, changing the nature of the problem from LP to Mixed Integer Linear Program (MILP). Nevertheless, the number of such variables amounts at most to few units, i.e., the number of time intervals that contain a DR request falling inside the optimization horizon and, more importantly, it is independent of the building size (i.e., the number of zones). As a result, the computational burden of the overall optimization algorithm is affordable even for large-scale instances, making the proposed approach suitable for real-world applications with hundreds of zones.

- As it is well-known in the literature, multiple sources of uncertainty come into the picture when dealing with building heating/cooling control, such as modeling inaccuracies, disturbances, weather forecasting errors and possibly undersized HVAC system. For this reason, when implementing a constrained MPC strategy, the presence of such uncertainties often causes infeasibility of the optimization problem. A standard way to deal with this issue is to replace hard bounds with soft bounds on the constraints and introduce penalties in the cost function accounting for constraint violations. Unfortunately, the choice of appropriate weights for the different penalty terms becomes a formidable task, especially in view of the high number of variables/constraints involved and the hard-to-predict "size" of constraint violations. To overcome these issues, in this chapter a different approach based on a two-step optimization strategy is proposed. At each time step, first an ancillary LP is solved in order to reset the comfort constraints, by minimizing the l_1 norm of the bound violations. Then, the feasible overall optimization problem is solved using the modified constraints. A further advantage of this approach is that it allows for quick recovery from realistic situations in which the original comfort constraints cannot be satisfied.

To validate the proposed control algorithm, numerical simulations have been performed on EnergyPlus [101], an industry-standard realistic building model simulator. In particular, performance analysis in the presence of uncertain forecasts of exogenous variables has been carried out.

The chapter is organized as follows: in Section 5.2, an overview of the proposed control architecture is presented while in Section 5.3, the relevant models are introduced. In Section 5.4, the control problem is formulated, its solution derived and implementation issues discussed.

5.2 System Architecture Overview

This chapter focuses on a building composed of several zones and equipped with a central HVAC system. Heating and cooling power is provided by electrical heat pumps. The heating pump HP_H is assumed to be connected to a thermal storage device (TES), while the cooling pump HP_C is not. Although thermal storage is quite common for both heating and cooling use, it is here employed in the first case only, with the aim of illustrating the performance

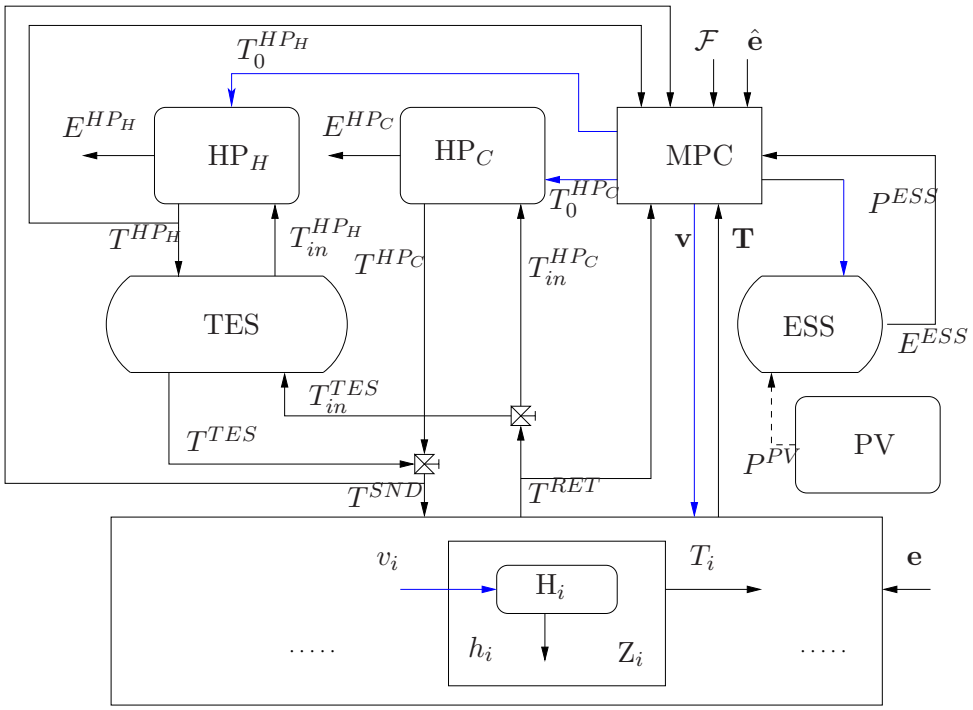

Figure 5.1: Overall HVAC and energy storage system architecture. Blue lines denote control signals.

of the proposed control strategy both in the presence and in the absence of a storage device. Heat exchange at zone level is provided by fan coil units, one for each zone, exchanging heat with the TES at constant water throughput. Heat flow regulation is achieved by controlling the air mass flow through each fan coil. It is also assumed that each zone is equipped with a temperature sensor. The building also features short-term energy storage system (ESS) facilities (e.g., via a rechargeable battery system) and PV generation. Participation of the building in a Demand-Response (DR) program is also assumed. Regulation of the HPs, TES, fan coil air flow, ESS and PV is implemented via a digital centralized control unit that operates in discrete time with sampling period Δ.

5.3 System Modeling

A block diagram of the overall control system is depicted in Figure 5.1 along with the relevant signals. The modeling of each component is detailed in the following subsections.

5.3.1 Zone Thermal Model

The m building zones are denoted by $\mathrm{Z}_1, \ldots, \mathrm{Z}_m$, and the respective heat exchanger devices by $\mathrm{H}_1, \ldots, \mathrm{H}_m$. All zones are equipped with temperature sensors, and the air flow of the heat exchangers can be independently regulated by the control unit. The control action must ensure that each room temperature satisfies a time-varying comfort constraint.
Let us define the following variables:

- $h_i(k) \in \mathbb{R}$: heat flow conveyed by H_i at time k into room Z_i,
- $\mathbf{h}(k) = [h_1(k) \ldots h_m(k)]' \in \mathbb{R}^m$,
- $T_i(k)$: indoor temperature of zone Z_i at time k,
- $\mathbf{T}(k) = [T_1(k) \ldots T_m(k)]' \in \mathbb{R}^m$,
- $[\underline{T}_i(k), \overline{T}_i(k)]$: thermal comfort range for Z_i at time k,
- $\underline{\mathbf{T}}(k) = [\underline{T}_1(k) \ldots \underline{T}_m(k)]' \in \mathbb{R}^m$, $\overline{\mathbf{T}}(k) = [\overline{T}_1(k) \ldots \overline{T}_m(k)]' \in \mathbb{R}^m$,

The dynamics of the indoor temperatures $\mathbf{T}(k)$ depend on the heat flows $\mathbf{h}(k)$ and on exogenous variables like outdoor temperature, solar radiation, appliances, lighting, occupancy, etc. For the sake of simplicity, available measurements/forecasts of some/all of such variables are collected in a vector $\mathbf{e}(k)$. Assuming linear time-invariant dynamics, the zone temperature vector evolution can be modeled in regressive form as:

$$\mathbf{T}(k+1) = \Theta^{\mathbf{T}} \ \mathbf{\Phi}^{\mathbf{T}}(k), \tag{5.1}$$

where the regression matrix $\mathbf{\Phi}(k)$ is given by

$$\begin{aligned} \mathbf{\Phi}^{\mathbf{T}}(k) = [\mathbf{T}'(k) \ \ldots \ \mathbf{T}'(k - k_{\mathbf{T}}) \\ \mathbf{h}'(k) \ \ldots \ \mathbf{h}'(k - k_{\mathbf{h}}) \\ \mathbf{e}'(k) \ \ldots \ \mathbf{e}'(k - k_{\mathbf{e}})]', \end{aligned} \tag{5.2}$$

being $k_{\mathbf{T}}, k_{\mathbf{h}}, k_{\mathbf{e}}$ suitable nonnegative integers that define the model order. The matrix $\Theta^{\mathbf{T}}$ collects the model parameters.

According to the above, thermal comfort achievement at time k is expressed by the element-wise constraint

$$\underline{\mathbf{T}}(k) \leq \mathbf{T}(k) \leq \overline{\mathbf{T}}(k). \tag{5.3}$$

It is appropriate to group constraint sets (5.1),(5.2),(5.3) as follows:

$$\mathcal{C}^T(k) = \{(5.1),(5.2)\}, \quad \mathcal{C}(k) = \{(5.3)\}.$$

5.3.2 HVAC System Model

The HVAC system operates at constant water flow rate. With reference to Figure 5.1, let us define the following quantities:

- $T^{SND}(k) \in \mathbb{R}$: fluid temperature at the inlet of heat exchangers,
- $T^{RET}(k) \in \mathbb{R}$: temperature of return fluid,
- $v_i(k) \in \mathbb{R}$: heat exchanger actuation signal, i.e., commanded air flow at time k for H_i,
- $\mathbf{v}(k) = [v_1(k) \dots v_m(k)]' \in \mathbb{R}^m$,
- $\overline{v}_i$: maximum air flow rate allowed for H_i, i.e.,

$$0 \leq v_i(k) \leq \overline{v}_i. \tag{5.4}$$

For each zone Z_i, the heat flow rate $h_i(k)$ can be expressed as

$$h_i(k) = \kappa_i \left(T^{SND}(k) - T_i(k)\right) v_i(k), \tag{5.5}$$

where κ_i is a coefficient of heating performance pertaining to heat exchanger H_i. Note that, in view of (5.5), enforcing limitation (5.4) for all zones yields the linear constraint sets

$$\mathcal{C}_H^h(k) = \{0 \leq h_i(k) \leq \kappa_i \left(T^{SND}(k) - T_i(k)\right) \overline{v}_i, \quad i = 1, \dots, m\} \tag{5.6}$$

and

$$\mathcal{C}_C^h(k) = \{0 \geq h_i(k) \geq \kappa_i \left(T^{SND}(k) - T_i(k)\right) \overline{v}_i, \quad i = 1, \dots, m\} \tag{5.7}$$

when the heat exchanger operates in heating and cooling mode, respectively.

Heating Mode Operation with Thermal Storage

The dynamics of the HVAC system in heating mode is now described. As pointed out in Section 5.2, the heat pump HP_H is coupled to a thermal energy storage (TES). Define:

- $T_{in}^{HP_H}(k) \in \mathbb{R}$: thermal fluid temperature at HP inlet,
- $T^{HP_H}(k) \in \mathbb{R}$: thermal fluid temperature at HP outlet,
- $T_0^{HP_H}(k) \in \mathbb{R}$: HP outlet temperature reference, i.e., HP command signal,
- $E^{HP_H}(k) \in \mathbb{R}$: HP electrical energy consumption within the $k-$th time step,
- $T^{TES}(k) \in \mathbb{R}$: TES fluid temperature.

The inlet temperature of each heat exchanger H_i is assumed to be uniform and equal to the TES outlet temperature, i.e.,

$$T^{SND}(k) = T^{TES}(k).$$

Under the realistic assumption that the time constants of the HP thermal fluid dynamics in response to a change in the reference $T_0^{HP}(k)$ are much smaller than the control sampling period Δ, the HP outlet fluid temperature can be expressed by

$$T^{HP_H}(k+1) = T_0^{HP_H}(k), \tag{5.8}$$

so that the HP can be modeled as a unit time step delay system.
A further reasonable assumption is that the heat exchange at TES level is efficient enough such that

$$T_{in}^{HP_H}(k) = T^{TES}(k). \tag{5.9}$$

It is worth noting that the above assumptions are indeed satisfied by the real-world devices emulated by EnergyPlus [101], the widely used realistic building simulation software used here for experimental validation.
The HP has to be switched on when the reference temperature is greater than the fluid temperature at the HP inlet, i.e., as long as

$$T_0^{HP_H}(k) > T_{in}^{HP_H}(k) = T^{TES}(k),$$

which leads to an electrical energy consumption

$$E^{HP_H}(k) = \alpha^{HP_H}\left(T_0^{HP_H}(k) - T^{TES}(k)\right), \tag{5.10}$$

where α^{HP_H} represents a device specification. Otherwise, the HP is switched off and $E^{HP_H}(k) = 0$. Therefore, the condition

$$T_0^{HP_H}(k) \geq T^{TES}(k) \tag{5.11}$$

can be assumed without loss of generality.
Concerning the TES dynamics, it is worth observing that $T^{TES}(k)$ depends on $T^{HP_H}(k)$ and on the return water temperature $T^{RET}(k) = T_{in}^{TES}$, which in turn dynamically depends on $T^{SND}(k) = T^{TES}(k)$ and on the total heat exchange at the heater level, i.e., $h(k) = h_1(k) + \cdots + h_m(k)$. Therefore, the TES temperature dynamics can be modeled in regressive form as

$$T^{TES}(k+1) = \Theta^{TES}\mathbf{\Phi}^{TES}(k), \tag{5.12}$$

where the regression vector $\mathbf{\Phi}^{TES}(k)$ is given by

$$\begin{aligned}\mathbf{\Phi}^{TES}(k) = [&T^{TES}(k) \ \ldots \ T^{TES}(k-k_{TT}) \\ &T^{HP_H}(k) \ \ldots \ T^{HP_H}(k-k_{TH}) \\ &\mathbf{h}'(k) \ \ldots \ \mathbf{h}'(k-k_{T\mathbf{h}})]',\end{aligned} \tag{5.13}$$

being Θ^{TES} the (row) parameter vector and k_{TT}, k_{TH}, $k_{T\mathbf{h}}$ suitable model orders.

Given the models introduced above, and observing that the thermal energy stored in the TES is proportional to $T^{TES}(k)$, it is worth remarking that full control of individual zone temperatures and thermal energy storage can be achieved by manipulating the control variables $T_0^{HP_H}(k)$ and $\mathbf{v}(k)$.

Cooling Mode Operation

In order to derive a model of HVAC system in cooling mode, let us define the following:

- $T_{in}^{HP_C}(k) \in \mathbb{R}$: thermal fluid temperature at the inlet of the cooling heat pump,
- $T^{HP_C}(k) \in \mathbb{R}$: thermal fluid temperature at HP outlet,
- $T_0^{HP_C}(k) \in \mathbb{R}$: HP outlet temperature reference, i.e., HP command signal,

- $E^{HP_C}(k) \in \mathbb{R}$: HP electrical energy consumption within the $k-$th time step,

Similarly to the heating mode, the cooling HP dynamics can be modeled as:

$$T^{HP_C}(k+1) = T_0^{HP_C}(k). \tag{5.14}$$

As long as $T_0^{HP_C}(k) \leq T_{in}^{HP_C}$, the HP is switched on and the corresponding electrical energy consumption is given by

$$E^{HP_C}(k) = \alpha^{HP_C}\left(T_{in}^{HP_C}(k) - T_0^{HP_C}(k)\right), \tag{5.15}$$

where α^{HP_C} pertains to the given device. Otherwise, it is switched off and $E^{HP_C}(k) = 0$. Therefore, it can be assumed that

$$T_0^{HP_C}(k) \leq T_{in}^{HP_C}(k). \tag{5.16}$$

In this mode, it holds that $T^{SND}(k) = T^{HP_C}(k)$ and $T^{RET}(k) = T_{in}^{HP_C}(k)$. The latter quantity dynamically depends on $T^{SND}(k)$ and on the total zone heat flow $h(k) = h_1(k) + \cdots + h_m(k)$. Therefore, the following regressive model can be used for $T_{in}^{HP_C}(k)$:

$$T_{in}^{HP_C}(k+1) = \Theta^C \mathbf{\Phi}^C(k), \tag{5.17}$$

where the regression vector $\mathbf{\Phi}^C(k)$ is given by

$$\begin{aligned}\mathbf{\Phi}^C(k) = [&T_{in}^{HP_C}(k) \ \ldots \ T_{in}^{HP_C}(k-k_{TC}) \\ &T^{HP_C}(k) \ \ldots \ T^{HP_C}(k-k_{HC}) \\ &\mathbf{h}'(k) \ \ldots \ \mathbf{h}'(k-k_{C\mathbf{h}})]'\end{aligned} \tag{5.18}$$

where Θ^C is the (row) parameter vector and $k_{TC},\ k_{HC},\ k_{C\mathbf{h}}$ define the model orders.

The constraint sets pertaining to the HVAC system operating in heating and cooling mode, respectively, can be grouped as follows:

$$\begin{aligned}\mathcal{C}_H(k) &= \{(5.8),(5.10),(5.11),(5.12),(5.13)\}, \\ \mathcal{C}_C(k) &= \{(5.14),(5.15),(5.16),(5.17),(5.18)\}.\end{aligned}$$

5.3.3 Electrical Storage Model

The characterization of the storage system based on rechargeable batteries used in this chapter is as follows (see, e.g., [102, 70]). Let $E^{ESS}(k)$ represent

the state of charge at time k. Denote as $P^{ESS+}(k) \geq 0$ and $P^{ESS-}(k) \geq 0$ the battery charge and discharge signals, i.e., the amount of power fed to and drawn from the battery in the $k-$th time interval, respectively. It holds that

$$E^{ESS}(k+1) = E^{ESS}(k) + \eta^{ESS}\Delta P^{ESS+}(k) - \frac{1}{\eta^{ESS}}\Delta P^{ESS-}(k), \tag{5.19}$$

where $0 < \eta^{ESS} < 1$ is the battery efficiency. Furthermore, the average battery power exchange in the same interval reads

$$P^{ESS}(k) = P^{ESS+}(k) - P^{ESS-}(k). \tag{5.20}$$

The following additional constraints

$$0 \leq P^{ESS+}(k) \leq \overline{P}^{ESS+}, \tag{5.21}$$

$$0 \leq P^{ESS-}(k) \leq \overline{P}^{ESS-}, \tag{5.22}$$

$$0 \leq E^{ESS}(k) \leq \overline{E}^{ESS}, \tag{5.23}$$

where $\overline{P}^{ESS+}$, $\overline{P}^{ESS-}$ and $\overline{E}^{ESS}$ depend on the storage size and technology, and represent the maximum charge/discharge rate and capacity, respectively. The constraint sets pertaining to ESS can be grouped as:

$$\mathcal{C}^{ESS}(k) = \{(5.19),(5.20),(5.21),(5.22),(5.23)\}.$$

In order for the model to be consistent, $P^{ESS+}(k)$ and $P^{ESS-}(k)$ cannot both be nonzero. This can be guaranteed by introducing the nonlinear constraint $P^{ESS+}(k)P^{ESS-}(k) = 0$, $\forall k$. See Remark 5.2 in Section 5.4 on how the introduction of this constraint can be circumvented.

5.3.4 PV Generation Model

In this chapter, the well-known PVUSA model of a PV plant [103] is exploited. In this model, the average power produced by the plant in the $k-$th time interval is expressed as a function of irradiance and environmental temperature as follows:

$$P^{PV}(k) = \theta_1^{PV} I(k) + \theta_2^{PV} I^2(k) + \theta_3^{PV} I(k) T^A(k), \tag{5.24}$$

where $I(k)$ is the global solar irradiance and $T^A(k)$ is the outside air temperature. Despite its simplicity, this model is very accurate when its parameters are fit to measured data and several efficient methods for their estimation under various conditions have been proposed (see [104],[105],[106] and references

therein). Without loss of generality, it can be assumed that $I(k)$,$I^2(k)$, and $I(k)T_a(k)$ are part of the exogenous variable vector $\mathbf{e}(k)$. Therefore, (5.24) can be written in the form

$$P^{PV}(k) = \Theta^{PV}\mathbf{e}(k) \tag{5.25}$$

which represents a static linear-in-the-parameters model.

Denoting with $\widehat{P}^{PV}(k)$ the average power actually drawn from the PV plant in the $k-$th interval, the following constraint must hold:

$$0 \leq \widehat{P}^{PV}(k) \leq P^{PV}(k). \tag{5.26}$$

The latter two equations are grouped in the constraint set

$$\mathcal{C}^{PV}(k) = \{(5.25),(5.26)\}.$$

5.3.5 Energy Consumption and Demand-Response Model

Let $E^G(k)$ represent the amount of energy drawn from the grid by the building in the $k-$th time interval. According to the model introduced above, the electrical energy balance equation reads:

$$E^G(k) = E^{HP}(k) + \Delta P^{ESS}(k) - \Delta\widehat{P}^{PV}(k), \tag{5.27}$$

with $E^G(k) \geq 0$, since the possibility of injecting excess energy into the grid is not currently considered.

Let $p(k)$ represent the unit energy price or a forecast thereof, and consider a generic time horizon $\mathcal{I}(t,\lambda)$. The total energy drawn from the grid within $\mathcal{I}(t,\lambda)$ is given by

$$E^G(t,\lambda) = \sum_{k=t}^{t+\lambda-1} E^G(k), \tag{5.28}$$

and the total expected cost of energy in the same interval is equal to

$$C(t,\lambda) = \sum_{k=t}^{t+\lambda-1} p(k)E^G(k). \tag{5.29}$$

A Demand-Response model based on price-volume signals is considered in this chapter. Such a model was introduced in [99] and is recalled next. A DR program is modeled as a sequence of DR requests $\mathcal{R}_j$, each carrying a time

horizon $\mathcal{I}(h_j, q_j)$, a total energy bound S_j, and a monetary reward R_j. A request $\mathcal{R}_j$ is satisfied if the total building consumption within $\mathcal{I}(h_j, q_j)$, i.e., $E^G(h_j, q_j)$, is less or equal to the threshold S_j. In this case, a monetary reward R_j is granted.

Definition 5.1 *A DR program $\mathcal{F}$ is a sequence of DR requests $\mathcal{R}_j$, $j = 1, 2, \ldots$, where $\mathcal{R}_j$ is the set*

$$\mathcal{R}_j = \{\mathcal{I}(h_j, q_j), S_j, R_j\}, \tag{5.30}$$

being $\mathcal{I}(h_j, q_j) \subseteq \mathcal{K}$ and $\mathcal{I}(h_{j_1}, q_{j_1}) \cap \mathcal{I}(h_{j_2}, q_{j_2}) = \emptyset,\ \forall j_1 \neq j_2$.

The request $\mathcal{R}_j$ is satisfied if and only if

$$E^G(h_j, q_j) \leq S_j. \tag{5.31}$$

For any given time horizon $\mathcal{I}(t, \lambda)$, let

$$\mathcal{F}(t, \lambda) = \{\mathcal{R}_j : \mathcal{I}(h_j, q_j) \subseteq \mathcal{I}(t, \lambda)\}, \tag{5.32}$$

be the set of DR requests that occur within the time horizon. Moreover, define $\mathcal{J}(t, \lambda)$ as the set of indices identifying such DR requests, i.e.,

$$\mathcal{J}(t, \lambda) = \{j : \mathcal{R}_j \in \mathcal{F}(t, \lambda)\}. \tag{5.33}$$

To each request $\mathcal{R}_j$, let us associate a binary variable $\zeta_j \in \mathcal{B}$ defined as

$$\zeta_j = \begin{cases} 1 & \text{if } \mathcal{R}_j \text{ is satisfied} \\ 0 & \text{otherwise.} \end{cases} \tag{5.34}$$

The overall expected cost of operation of the building HVAC system within the time horizon $\mathcal{I}(t, \lambda)$ under the DR program $\mathcal{F}$, is therefore given by

$$C^{\mathcal{F}}(t, \lambda) = C(t, \lambda) - \sum_{j \in \mathcal{J}(t,\lambda)} \zeta_j R_j, \tag{5.35}$$

i.e., the expected cost of energy minus the total reward for the satisfied DR requests. Let M be an a-priori known upper bound to the total building energy consumption per time step. Then, the set of constraints

$$\mathcal{C}^{DR}(t, \lambda) = \left\{E^G(h_j, q_j) \leq \zeta_j S_j + (1 - \zeta_j) M q_j, \quad j \in \mathcal{J}(t, \lambda), \quad \zeta_j \in \mathcal{B}\right\} \tag{5.36}$$

drives each variable ζ_j to 1 if the respective DR request can be fulfilled, and to 0 otherwise.

The reader is referred to [99] for further details on this model and its MPC implementation.

5.4 Optimal HVAC and Storage Operation Problem

The goal of this section is to devise an optimal schedule for the operation of the overall system (HVAC, PV, thermal and electrical storage) in order to minimize the building electricity bill under a DR program $\mathcal{F}$, while preserving comfort constraints. On a given interval $\mathcal{I}(t,\lambda)$, such a problem amounts to the optimal manipulation of the control variables $\mathbf{v}(k)$, $T_0^{HP_H}(k)$ $[T_0^{HP_C}(k)]$, $P^{ESS}(k)$ for $k \in \mathcal{I}(t,\lambda)$ in order to minimize $C^{\mathcal{F}}(t,\lambda)$. To this purpose, it should be observed that the model is not linear in the above variables due to (5.5). Nevertheless, the model becomes linear if $\mathbf{h}(k)$ instead of $\mathbf{v}(k)$ are considered as decision variables. Once the optimal values $h_i^*(k)$ of $h_i(k)$ are available for zone Z_i, the corresponding optimal heat exchanger actuation is given by

$$v_i^*(k) = \frac{h_i^*(k)}{\kappa_i \left(T^{SND}(k) - T_i(k)\right)}. \tag{5.37}$$

In the formulation of the optimization problem, suitable forecasts or sensor measurements $\hat{\mathbf{e}}(k)$ of the exogenous variables are assumed to be available. Therefore, in the sequel, $\mathbf{e}(k) = \hat{\mathbf{e}}(k)$.

5.4.1 Heating Mode Operation with Thermal Storage

In order to formulate the optimal operation problem in heating mode over a time interval $\mathcal{I}(t,\lambda)$, the set of command variables $\mathbf{U}_H(t,\lambda)$, where

$$\mathbf{u}_H(k) = [\mathbf{h}'(k),\ T_0^{HP_H}(k),\ P^{ESS}(k)]',$$

is considered. Moreover, sensor measurements $\mathbf{T}_m(k)$, $T_m^{TES}(k)$, $T_m^{HP_H}(k)$, $E_m^{ESS}(k)$ of $\mathbf{T}(k)$, $T^{TES}(k)$, $T^{HP_H}(k)$, $E^{ESS}(k)$, respectively, are assumed to be available. Hence, the problem of minimizing the total energy cost $C^{\mathcal{F}}(t,\lambda)$ over the time interval $\mathcal{I}(t,\lambda)$ can be cast as a mixed-integer linear program (MILP) as follows.

Problem 5.1 *Optimal combined heating/storage control under DR program* $\mathcal{F}$.

$$\begin{aligned}
&\mathbf{U}_H^{opt}(t,\lambda) = \arg \min_{\substack{\mathbf{U}_H(t,\lambda) \\ \zeta_j : j \in \mathcal{J}(t,\lambda)}} C^{\mathcal{F}}(t,\lambda) \\
&\text{subject to} \\
&\mathcal{C}^T(k), \mathcal{C}(k), \mathcal{C}_H^h(k), \mathcal{C}_H(k), \mathcal{C}^{ESS}(k), \mathcal{C}^{PV}(k) \quad \forall k \in \mathcal{I}(t,\lambda) \\
&\mathcal{C}^{DR}(t,\lambda)
\end{aligned} \tag{5.38}$$

5.4.2 Cooling Mode Operation

In cooling mode, the set of control variables amounts to $\mathbf{U}_C(t,\lambda)$, where

$$\mathbf{u}_C(k) = [\mathbf{h}'(k),\ T_0^{HP_C}(k),\ P^{ESS}(k)]'.$$

Sensor measurements $\mathbf{T}_m(k)$, $T_{in,m}^{HP_C}(k)$, $T_m^{HP_C}(k)$, $E_m^{ESS}(k)$ of $\mathbf{T}(k)$, $T_{in}^{HP_C}(k)$, $T^{HP_C}(k)$, $E^{ESS}(k)$, respectively, are considered. The problem of minimizing the total energy cost over $\mathcal{I}(t,\lambda)$ has the following formulation.

Problem 5.2 *Optimal combined cooling/storage control under DR program* $\mathcal{F}$.

$$\begin{aligned}
&\mathbf{U}_C^{opt}(t,\lambda) = \arg \min_{\substack{\mathbf{U}_C(t,\lambda) \\ \zeta_j : j \in \mathcal{J}(t,\lambda)}} C^{\mathcal{F}}(t,\lambda) \\
&\text{subject to} \\
&\mathcal{C}^T(k), \mathcal{C}(k), \mathcal{C}_C^h(k), \mathcal{C}_C(k), \mathcal{C}^{ESS}(k), \mathcal{C}^{PV}(k) \quad \forall k \in \mathcal{I}(t,\lambda) \\
&\mathcal{C}^{DR}(t,\lambda)
\end{aligned} \tag{5.39}$$

5.4.3 Managing Constraint Violations and Uncertainty

The feasibility of the optimization problems introduced in the previous subsections cannot be guaranteed in general due to a number of circumstances that may occur in real use cases. Among such factors are the presence of uncertainties in the building component models, errors in sensor measurements or exogenous variable forecasts $\hat{\mathbf{e}}(k)$, inappropriate sizing or faults of the HVAC system, etc. Hence, a certain degree of constraint violation must always be accepted. In order to mitigate this issue, a common approach in MPC is to resort to soft constraints, that is, removing the relevant hard constraints and replace them with penalization terms in the objective function. However, in

complex scenarios such as the one dealt with in this chapter, designing suitable constraint penalization coefficients to be used in the cost function can be a very difficult task, and the optimal solution of the relaxed problem may turn out to be very sensitive to such design. To overcome this issue, a two-step procedure is adopted in this chapter, which is based on the observation that the constraints that may actually incur violations are the comfort constraints $\mathcal{C}(\cdot)$. In the first step, such constraints are relaxed by introducing a set of slack variables, and a modified version of Problem 5.1 or 5.2 is solved, in which the objective to be minimized is the $1-$norm of all constraint violations over $\mathcal{I}(t,\lambda)$. In the second step, Problem 5.1 or 5.2 is solved replacing the original comfort constraints with the optimal relaxed bounds computed in the first step. Note that this substitution always ensures feasibility of the latter problems.

In order to illustrate the procedure, the following set of positive slack variables pertaining to each time interval $\mathcal{I}(t,\lambda)$ is introduced:

$$\Psi(t,\lambda)=\left\{(\underline{\psi}_i(k),\overline{\psi}_i(k)),\ \underline{\psi}_i(k)\geq 0,\ \overline{\psi}_i(k)\geq 0,\ i=1,\dots,m,\ k\in\mathcal{I}(t,\lambda)\right\},$$

along with the relaxed constraint set

$$\mathcal{C}_\Psi(k)=\left\{\underline{T}_i(k)-\underline{\psi}_i(k)\leq T_i(k)\leq \overline{T}_i(k)+\overline{\psi}_i(k)\ \ \forall i=1,\dots,m\right\}.$$

Then, the following linear program, which is a modified version of Problems 5.1 and 5.2, is considered:

Problem 5.3

$$\Psi^{feas}(t,\lambda)=\arg\min_{\Psi(t,\lambda),\mathbf{U}_\star(t,\lambda)}\ \sum_{k\in\mathcal{I}(t,\lambda),\ i=1,\dots,m}\overline{\psi}_i(k)+\underline{\psi}_i(k) \tag{5.40}$$

subject to

$$\mathcal{C}^T(k),\mathcal{C}_\Psi(k),\mathcal{C}^h_\star(k),\mathcal{C}_\star(k)\quad\forall k\in\mathcal{I}(t,\lambda)$$

where $\star=H$ for heating mode (Problem 5.1) and $\star=C$ for cooling mode (Problem 5.2). All other constraints (battery, DR, etc.) do not influence feasibility and can be omitted. Notice that the optimum of Problem 5.3 represents the minimum 1-norm of the constraint violations that must be accepted.

5.4.4 MPC Algorithm

The proposed control procedure is implemented in a receding horizion fashion as the two-step optimization strategy in Algorithm 5.1.

1 $t = 0$;

2 Acquire sensor measurements $\mathbf{T}_m(t)$, $T_m^{TES}(t)$, $T_m^{HP_H}(t)$ $[T_{in,m}^{HP_C}(t)$, $T_m^{HP_C}(t)]$, $E_m^{ESS}(t)$ and exogenous variable forecasts $\hat{\mathbf{e}}(k)$, $k \in \mathcal{I}(t,\lambda)$;

3 Solve Problem 5.3 for

$$\Psi^{feas}(t,\lambda) = \left\{ (\underline{\psi_i}^{feas}(k), \overline{\psi_i}^{feas}(k)),\ i = 1,\dots,m,\ k \in \mathcal{I}(t,\lambda) \right\};$$

4 Define the constraint set

$$\mathcal{C}_\Psi^{feas}(k) = \left\{ \underline{T}_i(k) - \underline{\psi_i}^{feas}(k) \le T_i(k) \le \overline{T}_i(k) + \overline{\psi_i}^{feas}(k) \ \ \forall i = 1,\dots,m \right\};$$

5 Solve Problem 5.1 [Problem 5.2] for $\mathbf{U}_\star^{opt}(t,\lambda)$ setting

$$\mathcal{C}(k) = \mathcal{C}_\Psi^{feas}(k);$$

6 Actuate $\mathbf{u}_\star^{opt}(t)$;

7 $t = t + 1$ and repeat from 2;

Algorithm 5.1: MPC controller implementation

Remark 5.1 *At each step t, the proposed procedure consists of the solution of an LP (Problem 3) and of a MILP (Problem 1 or 2) involving a number of binary variables equal to the number of DR requests falling inside the prediction horizon $\mathcal{I}(t,\lambda)$. In realistic scenarios, the number of integer variables in the MILP is at most a few units [89] . The number of continuous variables as well as of constraints in all optimization problems scales in a linear fashion with the number of building zones. This makes the proposed procedure readily applicable to real-world scenarios involving large-scale buildings consisting of hundreds of zones, as demonstrated by the simulation experiments reported in Section 6.4.*

Remark 5.2 *The formulation of the optimization problems involved in Algorithm 5.1 does not take into account the constraint that the electrical storage cannot charge and discharge simultaneously, i.e., that $P^{ESS+}(k)$ and $P^{ESS-}(k)$ cannot be both nonzero. However, unless $E^{ESS}(k+1) = 0$ or $E^{ESS}(k+1) = \overline{E}^{ESS}$, such condition is always met because the battery efficiency satisfies $\eta^{ESS} < 1$. On the contrary, when the battery state of charge hits one of the bounds, $P^{ESS}(k)$ can be set such that $E^{ESS}(k+1) = 0$ or $E^{ESS}(k+1) = \overline{E}^{ESS}$ according to (5.19),(5.20).*

Chapter 6

Numerical Simulations

In this chapter, numerical simulations and discussions for all the strategies are presented. In Section 6.1, simulation results and discussion about algorithms aimed at minimizing the daily peak power consumption are presented. In Section 6.2, results concerning the pricing strategy are discussed, while in Section 6.3, numerical results referring the procedure focused on the robust operation of an industrial microgrid are provided. Finally, in Section 6.4, numerical simulations about the techniques for HVAC energy management of a smart building are presented.

6.1 EV Peak Power Minimization

To assess the performance of algorithms described in Chapter 2, numerical simulations and comparisons have been performed.

6.1.1 Simulation Setup

A parking lot equipped with charging units is considered. The simulated scenario covers 100 days with a sampling time $\Delta = 10$ minutes. EV arrivals have been modeled through an exponential distribution with rate of 5 vehicles per hour, while the desired energy to be charged has been taken from a uniform distribution in the interval [10, 50] kWh. The parking time has been chosen according to a triangular distribution with support $[t_v^f - 12, t_v^f + 12]$ with mean value t_v^f. We suppose that the parking lot is open to arrivals from 6:00 till 24:00, while departure may occur at any time. The nominal power P_0^{EV} has been set to 11 kW, while the maximum power $\overline{P}^{EV}$ is 22 kW. Charg-

ing efficiencies have been set to 0.9 for all the vehicles, while the optimization weights $\alpha_v(t)$ are chosen according to (2.15)-(2.16).

The number of plugged-in vehicles changes during a day. For instance, the evolution of plugged-in vehicles in the 48-th day of simulation is depicted in Fig. 6.1. One may notice that vehicles starts to arrive in the parking lot from 6:00, while after 24:00 no more vehicle arrives and the number of charging EVs quickly decreases.

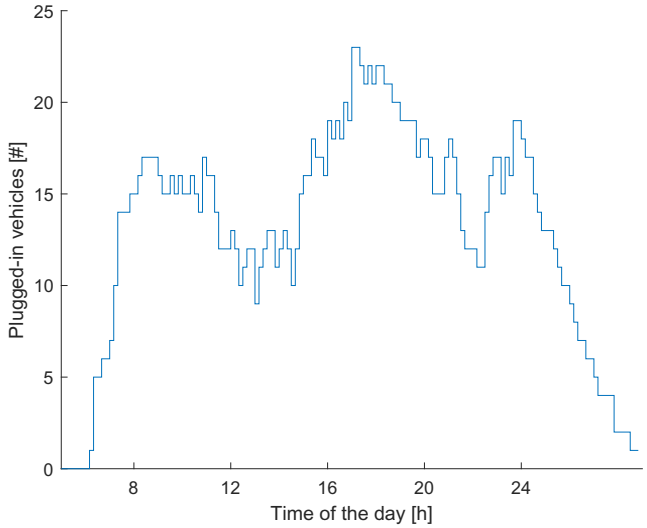

Figure 6.1: Number of plugged-in vehicles during the 48-th day of simulation.

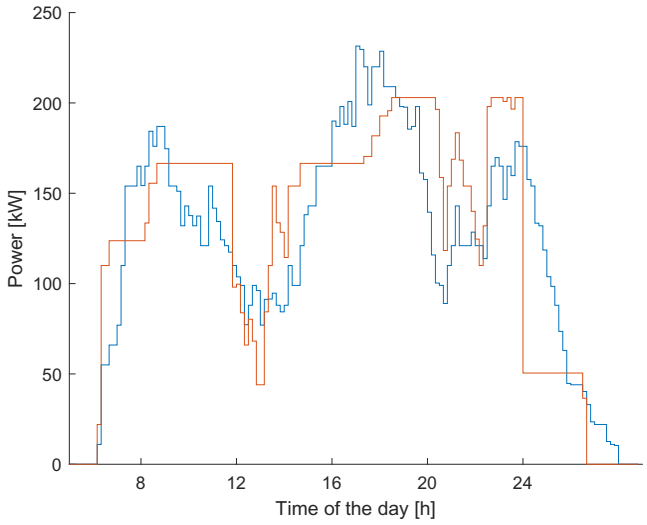

Figure 6.2: Power consumption of NCP (blue) and RHP (red) in simulation day 48.

Let us recall the acronyms RHP and NCP which are related to the receding horizon strategy with no a-priori information and the nominal charging policy,

respectively. Moreover, let us call the procedure described in Section 2.5 as *receding horizon policy-prior* (RHPP), the procedure presented in Section 2.6 as *receding horizon with chance constraint* (RHCC), and let the *ideal charging policy* (ICP) be the procedure aimed at minimizing the daily peak power assuming all the future realizations of the uncertain variables are available. It is clear that this charging strategy is unrealistic, since it relies on future outcomes of stochastic variables. However, ICP will be useful for assessing algorithm performance since it provides a lower bound for the daily peak power.

6.1.2 Simulation Results

To evaluate the effectiveness of RHP, the power schedules of NCP and RHP for the simulation day 48 are depicted in Fig. 6.2. As it can be observed, RHP tries to coordinate the vehicle charging to maintain the power consumption equal to the current peak power $\widehat{\gamma}$. In Fig. 6.2, this corresponds to the intervals where a flat behavior occurs. According to the condition in Line 6 of Algorithm 2.1, power values below $\widehat{\gamma}$ are related to situations in which all the vehicles are charging at the maximum power rate. In the considered day, RHP is able to lower the NCP peak by 32.6 kW, corresponding to a relative peak power reduction of about 12%.

In Fig. 6.3, daily peak powers of NCP and RHP are depicted. As stated in Theorem 2.1, RHP cannot perform worse than NCP. Indeed, the daily peak differences between the proposed procedure and NCP are represented by the blue bars above the red ones. The peak power reduction provided by RHP w.r.t. NCP in the simulated 100 days amounts to 24.1 kW, on average.

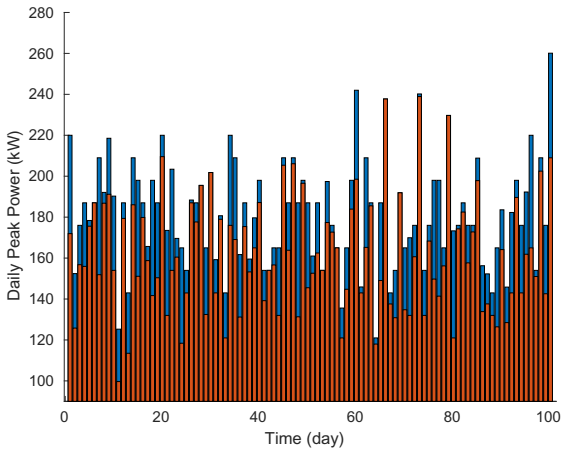

Figure 6.3: Daily peak power of NCP (blue) and RHP (red).

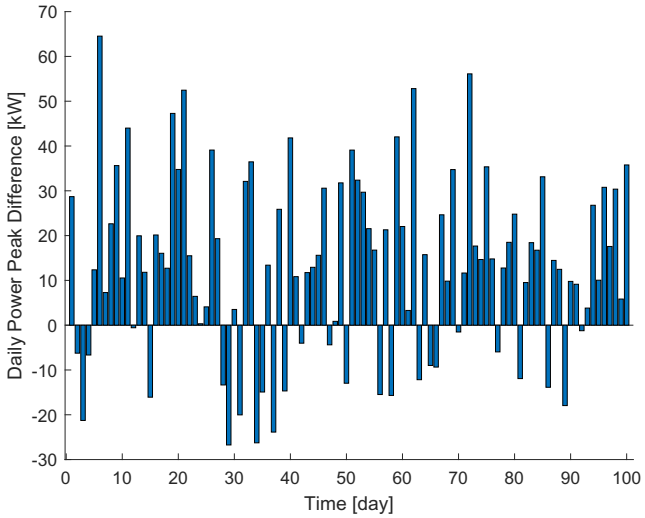

Figure 6.4: Daily peak power difference between RHP and RHPP.

Focusing on RHPP, its performance has been compared with that of RHP. In particular, daily peak power differences between the two procedures are reported in Fig. 6.4. It can be noticed that RHPP performs better than RHP in most of the days. In fact, the peak power obtained by RHPP is on average 13.2 kW lower than of RHP (37.4 kW lower than NCP).

The effectiveness of the RHPP can be noticed also comparing it with ICP. In Fig. 6.5, daily peaks of NCP, RHPP and ICP are reported. For ease of reading, the peaks provided by ICP are sorted in ascending order, and those obtained by NCP and RHPP are reported accordingly. It can be noticed that RHPP performs well also when compared with the best admissible solution. Indeed, knowledge of reliable statistical information about arrivals, charging time and DEC, makes RHPP capable to provide peak powers close to the those given by the benchmark charging policy. However, it is worthwhile to remind that the ICP provides a lower bound on the peak power and it is not feasible from a practical viewpoint since it depends on the knowledge of actual realizations of stochastic variables.

To evaluate the improvement given by the introduction of the weights (2.14) in the cost function, we will refer to the RHPP procedure. Specifically, in Fig. 6.6, daily peak power differences between RHPP without weights and RHPP with weights chosen as in (2.15)-(2.16) is depicted. As it can be noticed, the use of weights leads to a reduction of the daily peak power, which, in the considered simulation, amounts to 5.2 kW, on average.

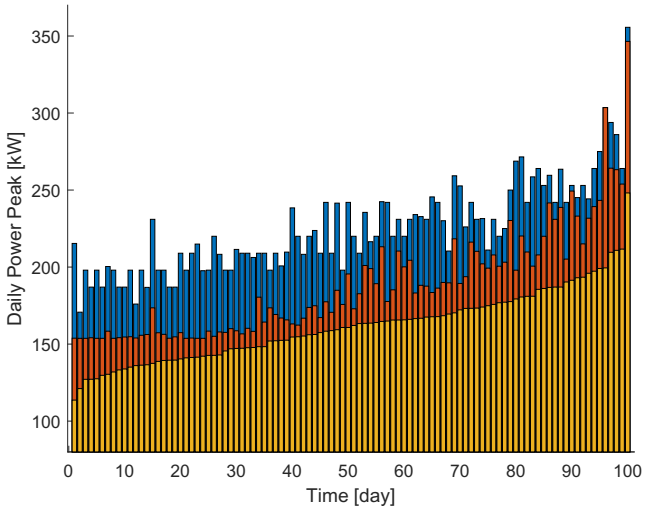

Figure 6.5: Daily peak power of NCP (blue), RHPP (red) and ICP (yellow), sorted in ascending order of ICP.

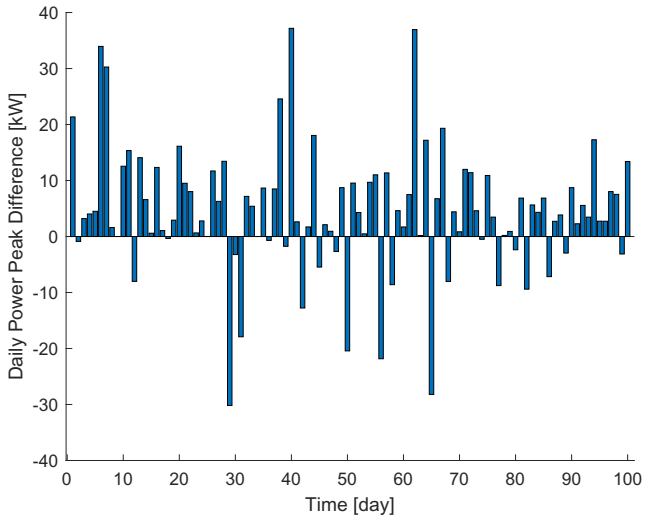

Figure 6.6: Daily peak power difference between RHPP without weights and RHPP with weights.

	$\varepsilon = 1\%$	$\varepsilon = 5\%$	$\varepsilon = 10\%$
Unsatisfied customers [%]	0.20	0.21	0.06
Peak reduction w.r.t. NCP [%]	18.57	18.80	18.82
Peak reduction w.r.t. RHPP [%]	4.29	3.68	4.85

Table 6.1: CSS-ε performance for different values of ε

To assess RHCC performance, several simulations by changing the tolerance level ε have been carried out and results are summarized in Table 6.1. It can be noticed that, RHCC strategy performs better with respect to both NPC and RHPP.

In Fig. 6.7, the RHCC policy with $\varepsilon = 10\%$ has been compared with the RHPP strategy. On average, the RHCC strategy provides a lower daily peak. In this case, the peak reduction is on average 4.8 kW with respect to RHPP (42.2 kW less than NCP).

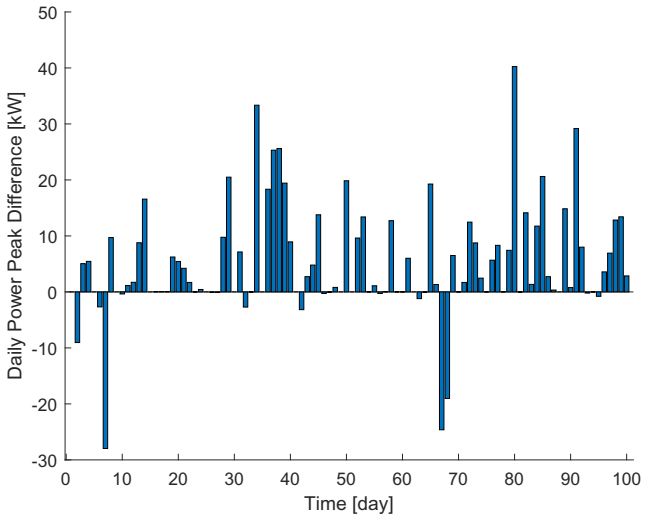

Figure 6.7: Daily peak power difference between RHCC with $\varepsilon = 10\%$ and RHPP.

In Fig. 6.8, the charging schedule of one single vehicle is depicted. One may observe that the algorithm, during the first charging period, lets the vehicle LOC to be outside the satisfaction region due to and high power demand. However, in the last time steps it recognizes that the vehicle departure is more probable and then it brings the level of charge to the satisfaction region. Another noticeable aspect is the number of violations obtained during simulations. Indeed, the fraction of customer left not satisfied is much below the chosen value of ε.

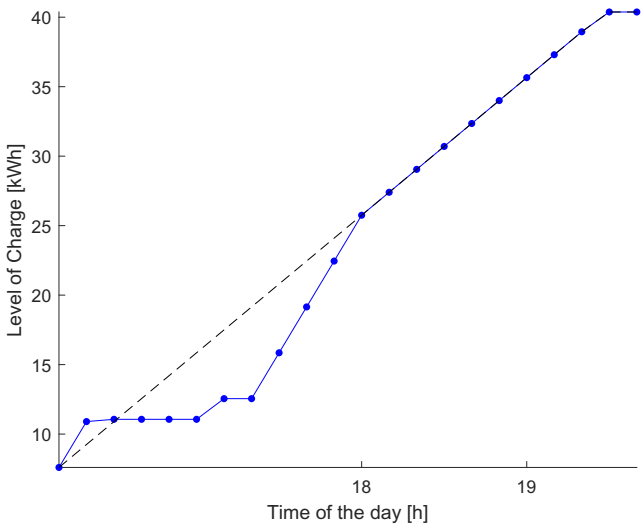

Figure 6.8: Vehicle LOC dynamics by using RHCC with $\varepsilon = 10\%$ during the 48-th day.

Computational time and scalability issues

To validate the computational feasibility of the proposed algorithms, several simulations with different EV arrival rates have been performed. Since the time needed to perform a single iteration differs significantly whether condition in Line 6 of Algorithm 2.1 holds or not, we only considered the worst case setting when $\widetilde{\gamma} > \widehat{\gamma}$. In fact, in this case, the computation of the solution of a linear program or a MILP is required. In Fig. 6.9, the mean time of each

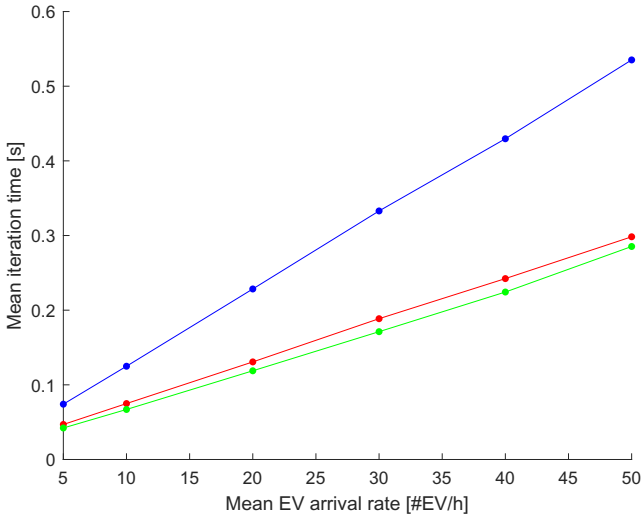

Figure 6.9: Mean computation time for an optimization loop using RHP (green), RHPP (red) and RHCC (blue) with $\varepsilon = 10\%$.

iteration is depicted for different EV arrival rates. It can be observed that

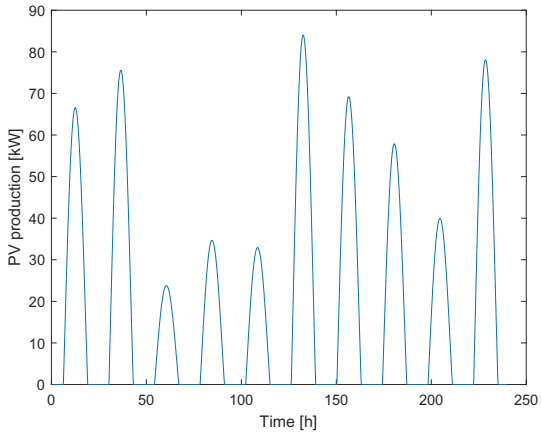

Figure 6.10: Photovoltaic production in 10 simulated days.

the computational burden scales almost linearly with the EV penetration. It is worthwhile to note that even for an arrival rate of 50 vehicles per hour all algorithms require computation times much lower than the sampling time (10 minutes), which shows their actual potential for real applications. Simulations have been performed using Matlab, the Yalmip toolbox [107] and the CPLEX solver [108], on an Intel Core i7-9700 CPU @3.00 GHz, 16 GB RAM.

6.2 Energy Pricing Optimization

6.2.1 Simulation Setup

In order to validate the proposed procedure, numerical simulations have been performed. It is assumed that the charging station is located in a commercial center and it supplies energy from $4:00$ till $24:00$. The sampling time is set to 10 minutes, i.e. $\Delta = 1/6$ hours, while the nominal charging power for electric vehicles is 22 kW. The ESS capacity is 1000 kWh, while its maximum charging and discharging power rates are 500 kW, with an efficiency $\eta = 0.9$. Concerning the PV plant, its peak power is assumed equal to 90 kW. To perform simulations, for each day the PV production has been scaled by a uniform distribution in the interval $[0.2, 1]$ (see Fig. 6.10). Fig. 6.11 reports the EV arrival time distribution, while the probability distribution of the charging time is shown in Fig. 6.12. By computing the convolution in (3.4), it is possible to obtain the probabilities that a generic vehicle is in charge at a fixed time, see Fig. 6.13.

The number of daily incoming vehicles has been modeled by a symmetric

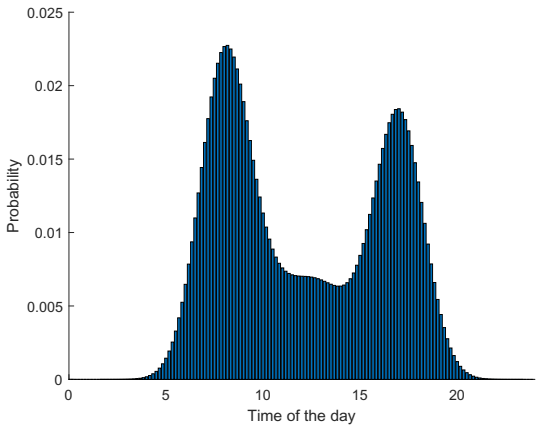

Figure 6.11: Arrival time distribution of incoming EVs.

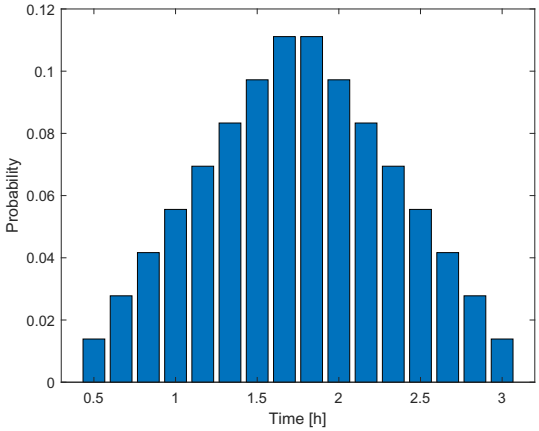

Figure 6.12: EV charging time distribution.

triangular distribution with $\underline{N}_V = 100$ and $\overline{N}_V = 200$, as shown in Fig. 6.14. Concerning the daily profit, the fraction ρ has been set to 0.2, corresponding to an earnings/cost ratio of 1.2, while the probability level ε is 10%. The electricity price has been taken from the Italian electricity market [109].

6.2.2 Simulation Results

The considered setup has been simulated for 300 days. In Fig. 6.15, the relation between β and the selling price for a generic day is depicted. In this case, the best selling price is obtained when β is around 3.4%. To validate the satisfaction of constraint (3.10c), the computed selling price and the battery schedule obtained by using Algorithm 3.1 have been considered. In this simulation, the number of days where such constraint is not satisfied amounts to 14, corresponding to 4.67%.

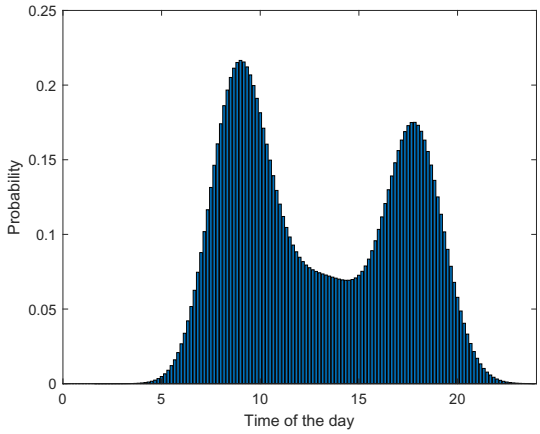

Figure 6.13: Probability to have a generic vehicle in charge at a fixed time.

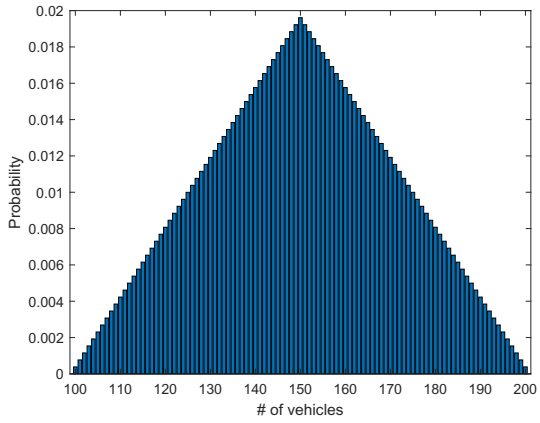

Figure 6.14: Probability distribution on the number of daily vehicles.

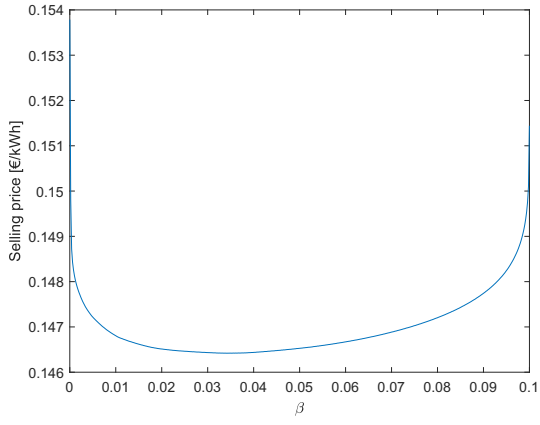

Figure 6.15: Values of the selling price with respect to β (day 93).

About the selling price, on average it lies between the mean and the maximum value of the daily electricity price, as shown in the box plots of Fig. 6.16. In Fig. 6.17, the daily electricity price and daily selling price for day 93 are

reported.

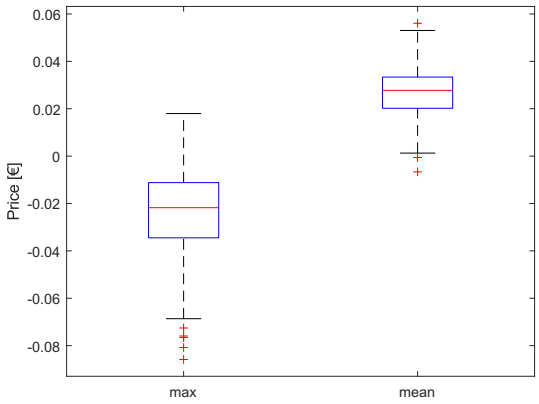

Figure 6.16: Left: Boxplot of the difference between the selling price and the maximum of the energy price. Right: Boxplot of the difference between the selling price and the mean of the energy price.

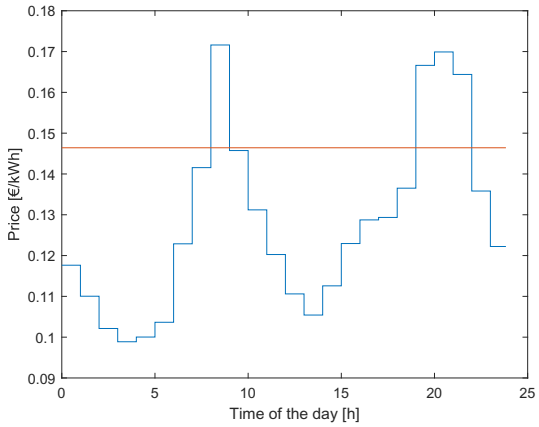

Figure 6.17: Daily electricity price (blue) and daily optimal selling price (red).

To assess the performance of the receding horizon battery schedule, a comparison with respect to the one computed at the beginning of the day has been carried out. Fig. 6.18 shows profiles of both the ESS energy schedules in day 93. Notice that, during the first time period, both solutions almost coincide because no vehicles have arrived yet. However, when vehicles start arriving to the parking lot, the two profiles separate. During this day, the receding horizon strategy provides an earnings/cost ratio of 1.24, while that related to the battery schedule computed at the beginning of the day is 1.21. As expected, in general, the receding horizon strategy outperforms the energy schedule computed at the beginning of the day, see Fig. 6.19. Moreover, the number of days when constraint (3.10c) is violated has been reduced to 4.

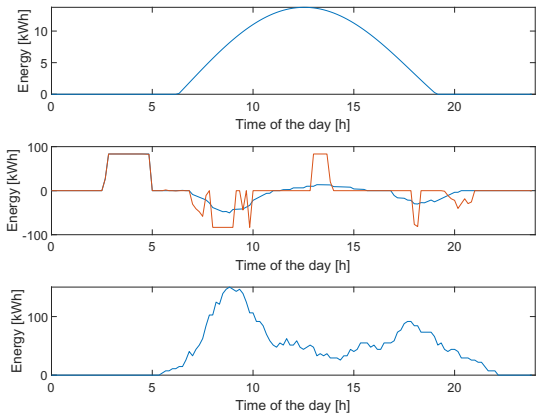

Figure 6.18: Energy schedule in day 93. Top: PV production. Middle: ESS energy schedule at the beginning of the day (blue) and receding horizon ESS energy schedule (red). Bottom: Energy needed by the EVs.

6.2.3 Discussion

In the following, analysis and discussion about the presented results are reported. First, it is worthwhile to note that the proposed technique exploits the EV distributions without requiring limiting assumptions on them. This means that the approach allows one to deal with different daily scenarios, possibly accounting for weekdays, holidays, strikes, etc.

By looking at Fig. 6.20 (right), one may notice that the selling price computed by Algorithm 3.1 at the beginning of a day leads to an earnings/cost ratio greater than the required threshold, in general. This result fully agrees with the requirements. In fact, the small number of days falling below the threshold are less than the prescribed 10%-limit, but at the same time, it is greater than zero, showing a low degree of conservativeness.

Once the selling price has been fixed, the proposed receding horizon algorithm can be used to operate the ESS during the day. Such procedure takes advantage of the knowledge of the random processes outcomes related to EVs, which are clearly missing at the beginning of the day when Algorithm 3.1 is run. So, it is expected that the daily profit obtained by the receding horizon procedure outperforms that given by operating the ESS with the commands provided at the beginning of the day. Such expectation has been confirmed by numerical simulations as reported in Fig. 6.19, where the difference between the daily earnings/cost ratio provided by the two procedures is shown. Besides, the receding horizon algorithm shows better performance in terms of violations of constraint (3.10c).

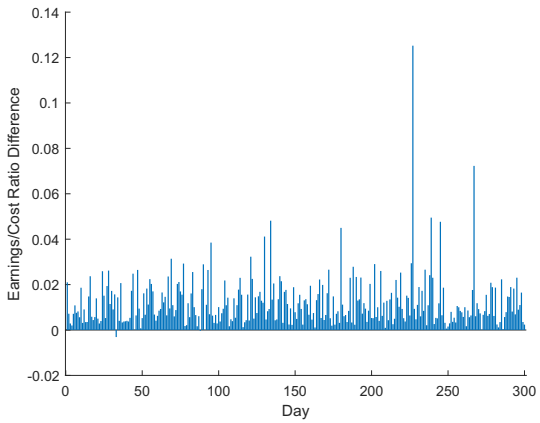

Figure 6.19: Difference between the earnings/cost ratio obtained by the receding horizon procedure and that computed by Algorithm 3.1 at the beginning of the day.

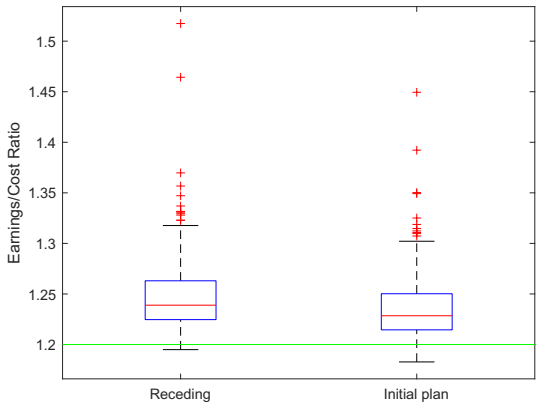

Figure 6.20: Boxplot of the earnings/cost ratio for the receding horizon ESS schedule (left) and the policy computed at the beginning of the day (right). The green line denotes the required threshold.

Regarding the computation of the best value of β, notice that in order to obtain the best selling price, its optimal value changes day by day on the basis of the expected PV production and of the electricity price profile. Moreover, as shown in Fig. 6.15, the flat behavior of the selling price around the optimal value β^*, allows one to perform the grid search in Algorithm 3.1 with fairly few iterations.

Concerning computational aspects, Algorithm 3.2 needs about 20 iterations to return the optimal value of Problem 3.6, with a tolerance $\gamma_\varepsilon = 10^{-6}$, while the loop in Algorithm 3.1 has been run over 100 equally spaced values between 0 and ε, i.e. with a resolution of 10^{-3}. As previously stated, such a resolution is

	$\mathbf{FU}_1$	$\mathbf{FU}_2$	$\mathbf{FU}_3$	$\mathbf{FU}_4$	$\mathbf{FU}_5$	$\mathbf{FU}_6$	$\mathbf{FU}_7$
CHP system	X	X	X	X	X	X	X
Boiler	X	X	X	X		X	
PV plant	X	X					

Table 6.2: Distributed generation facilities assigned to each factory unit.

enough to obtain a value of s_β very close to the optimal one, see Fig. 6.15. In the considered setup, Algorithm 3.1 takes on average 3.5 minutes to compute the optimal selling price, while the receding horizon strategy performs one iteration step in 0.18 seconds. Simulations have been run in MATLAB, the optimization problems have been formulated using YALMIP [107] and solved by CPLEX [108] on an Intel(R) Core(TM) i7-7700 CPU @3.60 GHz with 32 GB of RAM. Thanks to the low computational burden, both algorithms can be effectively used in practical applications even with a larger number of incoming vehicles.

6.3 Industrial Microgrid Management

In this section, an IMG is simulated in order to test the effectiveness and the computational feasibility of the proposed approach presented in Chapter 4.

6.3.1 Simulation Setup

Simulations have been performed over three days with a sampling time $\Delta = 1$ hour, a standard prediction horizon $\lambda_0 = 4$ hours and a chance constraint failure tolerance level $\epsilon = 0.1$.

An IMG composed of 10 buses and 7 FUs is considered, see Fig. 6.21. Factory units are referred to as FU_1 , . . . , FU_7 and they may be equipped with CHP systems, boilers, PV plants and EVs. DG facilities installed in each FU are summarized in Table 6.2.

Technical data regarding DG systems and EVs are taken from [56]. Data of CHP systems, that is, maximum and minimum active power generation, electric efficiency, waste heat factor and operational cost are reported in Table 6.3, while technical data regarding boilers are given in Table 6.4.

Each PV plant is assumed to be coupled with an ESS able to store the power in excess into batteries. Technical specifications about storage systems are

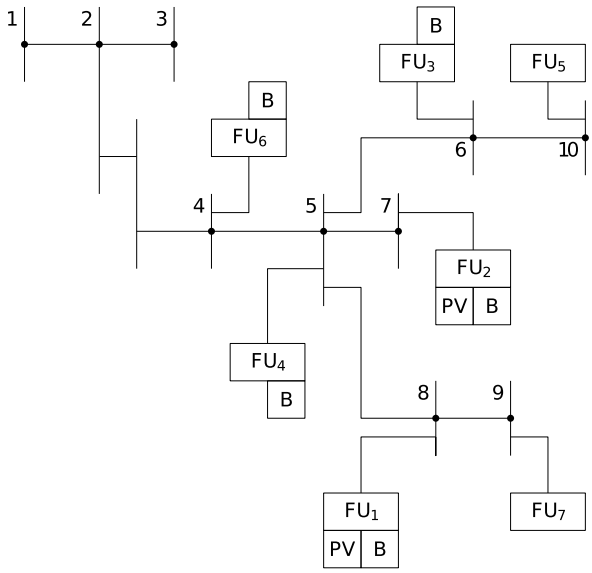

Figure 6.21: Structure of the considered 10-bus industrial microgrid. "B" denotes boilers while "PV" photovoltaic plants.

	$\mathbf{FU}_1$	$\mathbf{FU}_2$	$\mathbf{FU}_3$	$\mathbf{FU}_4$	$\mathbf{FU}_5$	$\mathbf{FU}_6$	$\mathbf{FU}_7$
$\underline{P}^{CHP}[kW]$	150	90	9	9	3	3	3
$\overline{P}^{CHP}[kW]$	1500	900	90	90	30	30	30
η^{CHP}	0.27	0.34	0.31	0.31	0.30	0.30	0.26
α^{CHP}	1.84	1.20	1.85	1.85	2.05	2.05	1.71
$c^{CHP}[\frac{€}{kW}]$	0.006	0.009	0.013	0.013	0.018	0.018	0.015

Table 6.3: CHP systems technical data.

reported in Table 6.5.

Forecasts of factory load patterns, PV generation and heat requirements are assumed to be known enough time in advance. The overall factory electrical load and heat requirement are depicted in Fig. 6.22, whereas the overall PV generation is reported in Fig. 6.23. The IMG is supposed to be equipped with three types of EVs (light service vehicles, heavy service vehicles and large industrial vehicles) each one divided in two subclasses. Technical data on EV charging systems are reported in Table 6.6, while in Table 6.7, the number of vehicles assigned to each FU is reported.

Daily arrival and departure schedules of EVs are reported in Table 6.8. The actual arrival times of vehicles are taken from a symmetric triangular distri-

	$\mathbf{FU}_1$	$\mathbf{FU}_2$	$\mathbf{FU}_3$	$\mathbf{FU}_4$	$\mathbf{FU}_6$
$\overline{P}^B\ [kW]$	800	400	80	80	80
η^B	0.8	0.85	0.85	0.85	0.83

Table 6.4: Boilers technical data.

	$\mathbf{FU}_1$	$\mathbf{FU}_2$
$\underline{E}^{ESS}\ [kWh]$	0	0
$\overline{E}^{ESS}\ [kWh]$	1000	250
$\overline{P}^{ESS+}\ [kW]$	350	100
$\overline{P}^{ESS-}\ [kW]$	350	100
$\underline{\eta}^{ESS}$	0.92	0.9

Table 6.5: ESS technical data.

Vehicle Type	η^{EV}	$\overline{E}^{EV}$	$\overline{P}^{EV}$
Light Service 1	0.88	16	23
Light Service 2	0.88	24	4
Heavy Service 1	0.9	170	24
Heavy Service 2	0.92	85	14
Large Industrial 1	0.95	100	100
Large Industrial 2	0.95	200	200

Table 6.6: EVs technical data.

	$\mathbf{FU}_1$	$\mathbf{FU}_2$	$\mathbf{FU}_3$	$\mathbf{FU}_4$	$\mathbf{FU}_5$	$\mathbf{FU}_6$	$\mathbf{FU}_7$
Light Service 1	5	4	3	3	3	3	3
Light Service 2	10	4	4	4	4	4	4
Heavy Service 1	5	1	0	0	0	0	0
Heavy Service 2	8	4	0	0	0	0	0
Large Industrial 1	5	3	3	0	0	0	0
Large Industrial 2	5	2	0	0	0	0	0

Table 6.7: Number of vehicles for each FU.

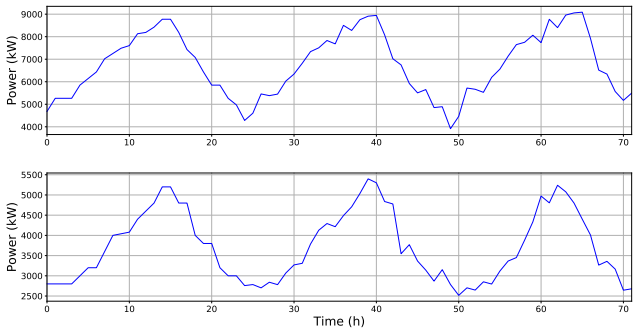

Figure 6.22: Top: overall FU electrical load. Bottom: overall heat requirement.

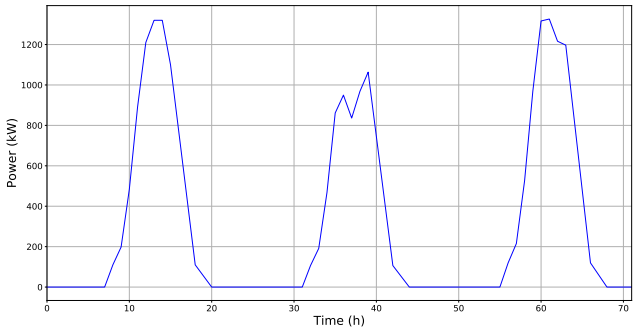

Figure 6.23: Overall photovoltaic generation.

bution with a support of 4 hours.

For all buses, the nominal voltage magnitude is set to $230\,V$, and the safety limits are given by $\pm 10\%$ of the nominal value. The slack bus is constrained to draw at most 6500 kW of active power from the grid and the constraints on the reactive power are set to $\overline{Q_i} = -\underline{Q_i} = 3150\ kVAR$. All the other buses of the network are treated as load buses.

Electricity and gas prices have been taken from the Italian electricity market [109] and they are depicted in Fig. 6.24. Notice that, electricity price changes every hour while gas price is updated once a day.

6.3.2 Simulation Results

The results obtained by simulating the considered IMG show that the proposed control strategy is able to efficiently manage all the grid components. From the electrical point of view, in Fig. 6.25 (top), one may observe the relationship among CHP production, PV generation and main grid power consumption. As expected, when the electricity price is low, the IMG power is mostly drawn from the main grid. In Fig. 6.25 (bottom), the total FU electrical demand

Vehicle Type	Charging cycles					
	1			2		
	$\underline{t_a}$	$\overline{t_a}$	t_d	$\underline{t_a}$	$\overline{t_a}$	t_d
Light Service 1	16:00	20:00	6:00	-	-	-
Light Service 2	16:00	20:00	6:00	-	-	-
Heavy Service 1	17:00	21:00	5:00	-	-	-
Heavy Service 2	16:00	20:00	6:00	-	-	-
Large Industrial 1	9:00	13:00	15:00	18:00	22:00	6:00
Large Industrial 2	10:00	14:00	16:00	20:00	0:00	5:00

Table 6.8: Arrival and departure time of vehicles.

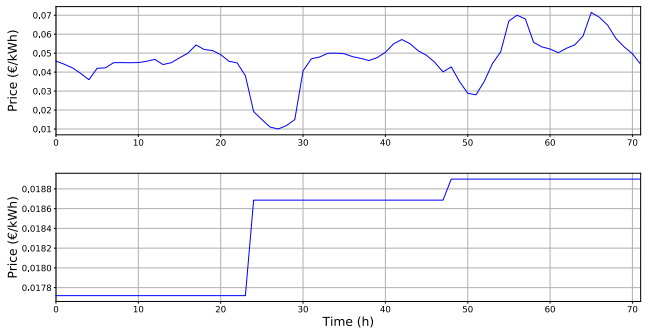

Figure 6.24: Top: electricity price. Bottom: gas price.

is reported, as well as the overall EV charging profile, while in Fig. 6.26, the state of charge of the storages related to FU_1 and FU_2 is depicted.

Moving the attention on the heat demand reported in Fig. 6.27, CHP systems and boilers are employed to satisfy such constraint. In particular, boilers are mainly used both when CHP systems saturate and when producing electrical power through them is not convenient, e.g., around time 25. Concerning the overall heat generation, it can be noticed that the total produced heat always coincides with the requirement except around time 57, when the heat produced by CHP systems exceeds the overall requirement.

In Fig. 6.28, voltage magnitudes of buses 4, 6 and 8 are depicted. It can be observed that voltage magnitudes remain in the working range at all times. The largest fluctuations can be observed at bus 8 (red), which is connected to the most demanding FU, i.e. FU_1.

In order to evaluate the performance of the proposed approach, a benchmark consisting in Algorithm 4.1 without chance constraints (i.e., without lines 9-12) is considered. The two algorithms have been compared over a three-day

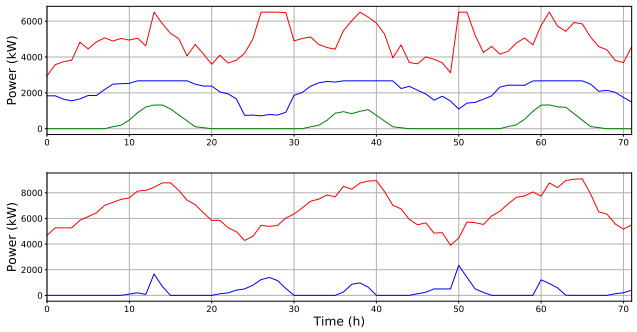

Figure 6.25: Electrical power side of the grid. Top: overall electrical power supply. Overall CHP generation (blue), PV production (green), main grid power consumption (red). Bottom: overall electrical power demand. Overall FU load (red) and EV demand (blue).

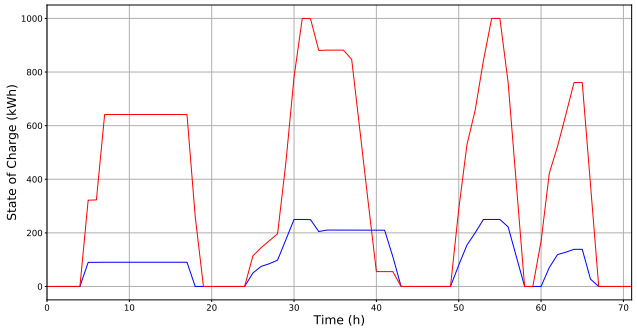

Figure 6.26: State of charge of ESS at FU_1 (red) and FU_2 (blue).

simulation, showing similar overall costs, as reported in Table 6.9. On the other hand, to assess the robustness of the two procedures, an increased EV penetration has been considered. Under this new setting, the benchmark is no more capable to satisfy grid constraints when the number of vehicles increases of about 30%, while the proposed chance constraint approach is able to guarantee an optimal grid operation even for a number of vehicles more than doubled. Hence, thanks to the adopted chance constraint control strategy, the optimization procedure can suitably manage the incoming vehicles with a consequent improvement of the grid security.

	Day 1	Day 2	Day 3	Total
Proposed procedure	8643.56	8457.12	9953.39	27054.07
Benchmark	8644.99	8461.27	9956.88	27063.13

Table 6.9: Grid operation costs [€] over three days.

In Fig. 6.29, the electrical power side of the IMG under double penetration of

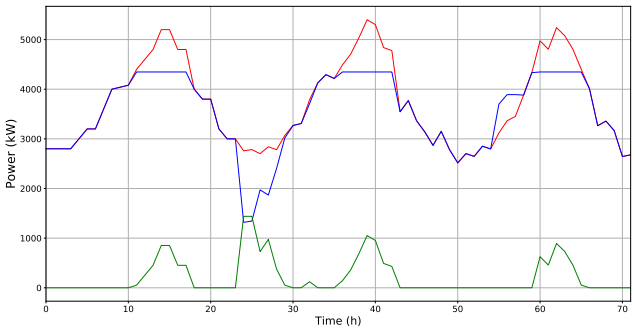

Figure 6.27: MG heat requirement (red), overall CHP thermal generation (blue) and boiler heat production (green).

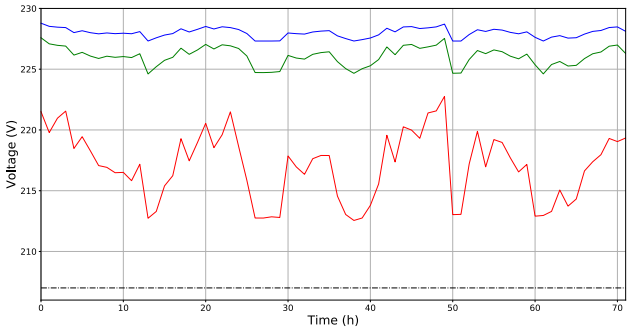

Figure 6.28: Voltages at buses 4 (blue), 6 (green) and 8 (red).

vehicles is depicted. In this setup, the grid is highly stressed. Indeed, the slack bus and the CHP systems reach often their saturation limits due to the heavy demand of EVs. However, the proposed algorithm enforces the feasibility of the IMG network by spreading the EV charging process over the whole plug-in time.

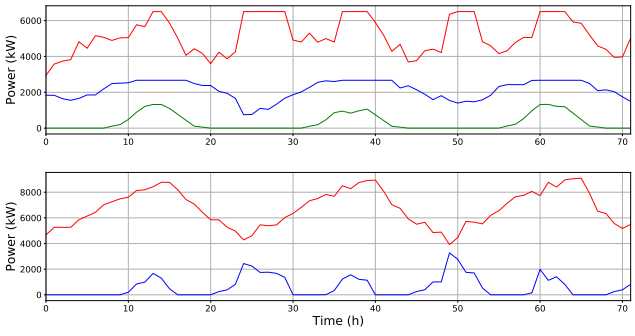

Figure 6.29: Electrical power side of the grid with double penetration of vehicles. Top: overall electrical power supply. Overall CHP generation (blue), PV production (green), main grid power consumption (red). Bottom: overall electrical power demand. Overall FU load (red) and EV demand (blue).

Regarding computational aspects, the proposed algorithm results to be largely tractable. In fact, the time needed by an iteration amounts to about 7 seconds. Simulations have been carried out using CVXPY [110] to model the problem and MOSEK [72] to solve it on a Intel(R) Core(TM) i7-7700 CPU @3.60 GHz with 32 GB of RAM.

6.4 Building Energy Management

In this section, results about the control techniques presented in Chapter 5 are discussed. Heating and cooling operations are considered in Sections 6.4.2 and 6.4.3, respectively, while Section 6.4.4 is devoted to analyzing the performance of the proposed method when inaccurate forecasts of exogenous variable are available. A discussion of the results is given in Section 6.4.5.

6.4.1 Simulation Setup

The simulated test structure is an 8-floor building divided in 126 zones (Fig. 6.30) located in Turin, Italy. The first two floors are devoted to commercial and office activities, respectively, while the remaining floors are assigned to residential apartments. Plans of the three types of floors are reported in Fig. 6.31.

The building is equipped with a PV plant, an electrical storage system and two heat pumps used for heating and cooling purposes, respectively. The heating system is also equipped with a TES to enable hot water storage. Heating and cooling circuit schemes are shown in Fig. 6.32 and 6.33. The building has been designed using DesignBuilder [111] while simulations have been performed via EnergyPlus [101] connected to Matlab through the Building Controls Virtual Test Bed (BCVTB) [112]. Building features are reported in Table 6.10, while materials are summarized in Table 6.11. The energy price time series $p(k)$ has been taken from the Italian electricity market [109]. The EnergyPlus simulation model is assumed as the real building. The sampling time Δ is set to 10 minutes, while the horizon length used by the MPC is fixed to 12 hours, corresponding to 72 samples, i.e., $\lambda = 72$ in Algorithm 5.1.

Figure 6.30: Rendering of the building used in test cases.

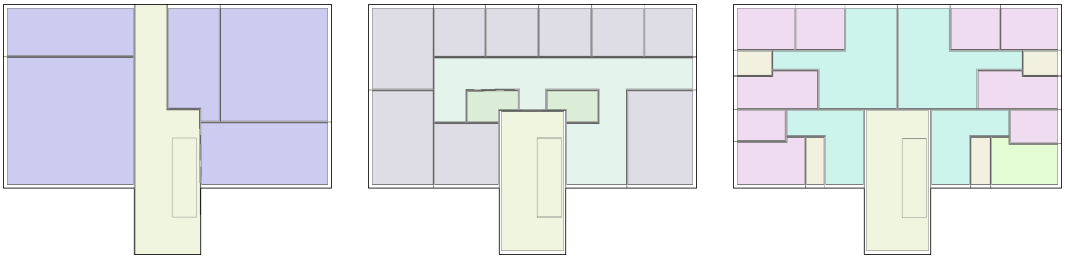

Figure 6.31: Plans of the building floors: commercial (left), office (middle), residential (right).

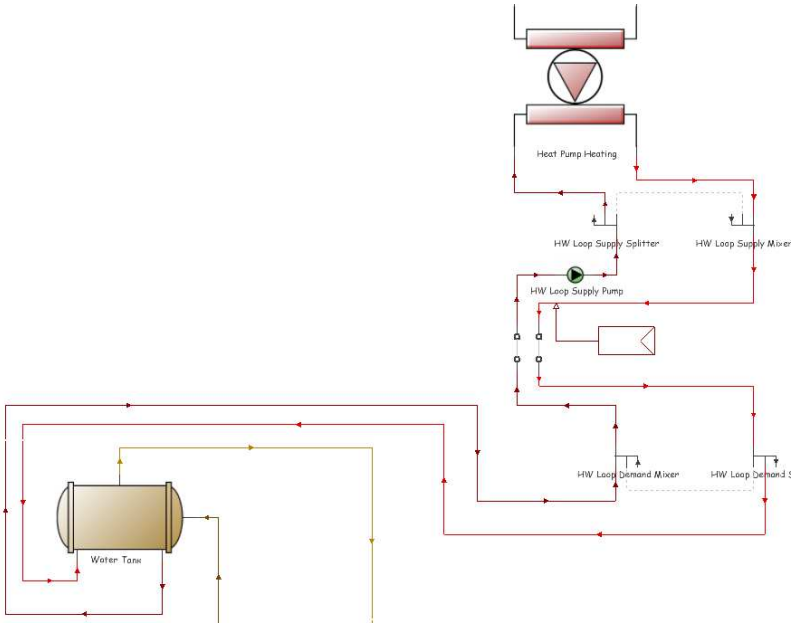

Figure 6.32: Scheme of the heating circuit.

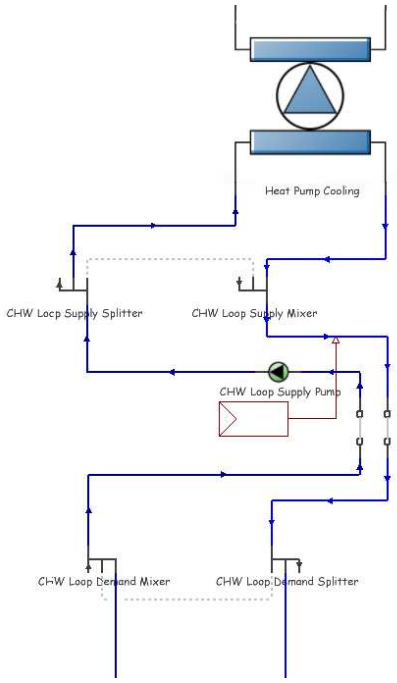

Figure 6.33: Scheme of the cooling circuit.

6.4.2 Winter Season Simulation - Heating Operation Results

The thermal behavior of the building has been modeled as in Section 5.3.1 by means of the autoregressive model (5.1)-(5.2). To this purpose, it is appropriate to define the exogenous input vector $\mathbf{e}(k)$ as

$$\mathbf{e}(k) = [T^A(k) \;\; I(k) \;\; I^2(k) \;\; I(k)T^A(k) \;\; \mathbf{G}'(k)]'$$

where $T^A(k)$ is the outside air temperature, $I(k)$ is the solar irradiance and $\mathbf{G}(k)$ denotes the vector of internal heat gains of the building zones due to human occupancy, lighting and equipments.

For this model, an identification experiment has been performed over a time horizon of 18 days, which have been split in 14 days for estimation and 4 for validation. For each building zone, a coupled model involving all neighboring zones has been employed. The standard *Best FIT index* (FIT) defined in [113, 114] has been used to assess the quality of the estimated model. The average value of the FIT index for all the identified building zones is 75%, 68% and 66%, for 1, 6 and 12-hour ahead predictions, respectively. For a qualitative evaluation, in Fig. 6.34, the 6-hour ahead prediction of the internal temperature of an office zone is compared with the real behavior during the

Building Component		Value
Weather and Location		Turin (Italy)
Floor Area $[m^2]$		375
Floor [#]		8
Zone [#]		126
Window to Wall Ratio [%]		20
Solar Transmittance [%]		30
Internal Loads	Occupants [#]	120
	Lighting $[W/m^2]$	4.00
	Equipment $[W/m^2]$	3.25
Heating: Heat Pump	Heating Capacity $[kW]$	389
	Heating Power Consumption $[kW]$	82
	TES Volume $[m^3]$	8
Cooling: Heat Pump	Cooling Capacity $[kW]$	389
	Cooling Power Consumption $[kW]$	82
Electric Energy Storage	Capacity $[kWh]$	28
	Max Charging Rate $[kW]$	24
	Max Discharging Rate $[kW]$	24
PV Plant	Panels [#]	5
	Plant Surface Area $[m^2]$	100
	Plant Peak Power $[kW]$	10

Table 6.10: Test building characteristics

	External Walls	Internal Walls
Outside Layer	Brickwork/100	Gypsum plaster/13
Layer 2	Extruded polystyrene/80	Brickwork/10
Layer 3	Concrete block/100	Gypsum plaster/13
Layer 4	Gypsum plaster/15	

	Floor	Roof	Windows
Outside Layer	Extruded polystyrene/30	Plywood/10	Generic LoE/6
Layer 2	Cast concrete/300	Glass wool/100	Air/6
Layer 3		Cast concrete/10	Generic Clear/6
Layer 4		Gypsum board/13	

Table 6.11: Test building construction materials (name/thickness [mm])

model validation phase.

Concerning the TES, model (5.12)-(5.13) has been identified, and the associated FIT index turns out to be over 90% even for 12-hour ahead prediction. The PV plant has been identified by employing model (5.25).

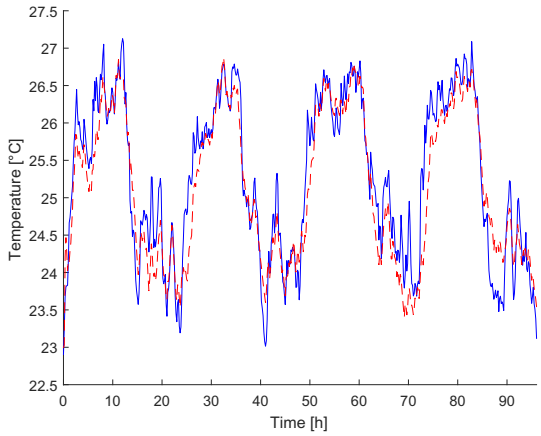

Figure 6.34: Thermal model identification. Comparison between real zone temperature (blue) and 6-hour ahead prediction (red) over the four-day validation period.

	h_j	q_j	S_j $[kWh]$	R_j [€]
$\mathcal{R}_1$	107	5	37	3.6
$\mathcal{R}_2$	178	6	40	4.4
$\mathcal{R}3$	325	3	6	2.8

Table 6.12: Winter season - DR program

Depending on the type of zone (commercial, office, residential), different comfort constraints are enforced. For commercial and office zones, temperature bounds are set to 20-24°C from 8:00 to 18:00, and 15-24°C elsewhen. Bounds for residential zones are 20-24°C from 7:00 to 9:00 and from 19:00 to 01:00, and 15-24°C otherwise. It is worthwhile to note that such bounds can be freely adjusted for each zone to adapt to real scenarios.

A 3-day simulation has been performed to evaluate the proposed control strategy. The price/volume DR requests in the considered period are assumed to be known one day in advance [89] and are reported in Table 6.12. The identified model has been used by the MPC to generate fan input signals, HP setpoints and ESS charging/discharging commands, while real measured data have been generated by the EnergyPlus simulation of the designed building.

At this stage, perfect knowledge of exogenous inputs is assumed. Such an assumption, although not realistic, has been enforced to better assess the quality of the proposed technique. Simulations in presence of uncertain forecasts will be analyzed in detail in Section 6.4.4.

In Fig. 6.35, outdoor temperature T^A and solar irradiance I for the considered

days are reported, while in Fig. 6.36, TES temperature T^{TES}, HP setpoint $T_0^{HP_H}$, ESS state of charge E^{ESS}, energy drawn from the PV plant $\widehat{E}^{PV}$, unit energy price p and total energy drawn from the grid E^G are shown. In Fig. 6.37, the temperature profiles $T_i(k)$ of three different sample zones are depicted along with the required comfort bounds $[\underline{T}_i, \overline{T}_i]$ and fan actuation v_i. It can be noted that the zone temperatures lie within the comfort bounds with small deviations. Indeed, the average bound violation of the worst performing zone over three days is about 0.13°C, see Table 6.13. Notice that, since exact input forecasts are assumed, such infringements are due to modeling errors. This demonstrates the ability of the bound relaxation technique in Section 5.4.3 to manage unpredictable bound violations by pushing the zone temperatures back within the prescribed bounds in a short time after the violations occur. It is worthwhile to recall that keeping air temperature within hard comfort bounds at all times is unfeasible for any conceivable control strategy due to modeling errors and/or unpredictable disturbances. In Table 6.13, numerical values of total cost, DR rewards, and comfort bound violations are reported.

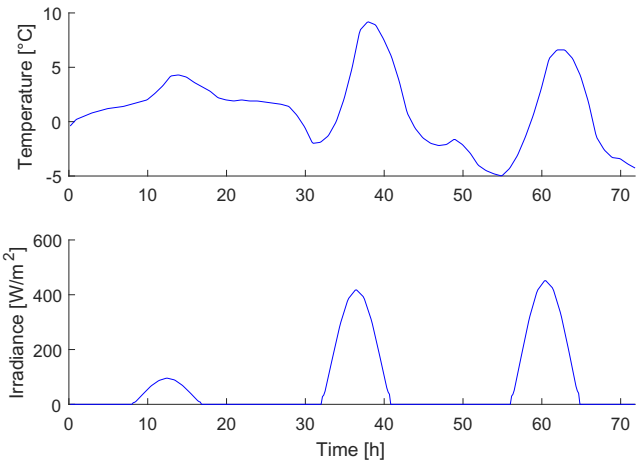

Figure 6.35: Heating operation mode simulation. Meteorological inputs. Top: Outdoor temperature. Bottom: Solar irradiance.

Cost without DR [€]	136.14
No. of fulfilled DR requests	2
DR reward [€]	8.00
Overall cost with DR [€]	128.14
Worst zone average bound violation [°C]	0.139

Table 6.13: Heating operation mode - Simulation results over 3 days

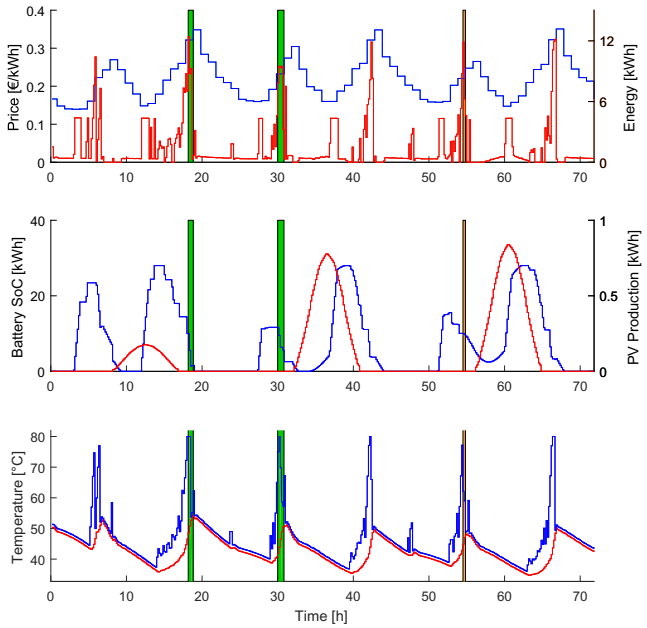

Figure 6.36: Heating operation mode simulation. DR requests are depicted in green if fulfilled, in orange otherwise. Top: energy price (blue) and building energy consumption per time step (red). Middle: ESS state of charge (blue) and energy provided by the PV plant (red). Bottom: TES internal temperature (red) and HP setpoint (blue).

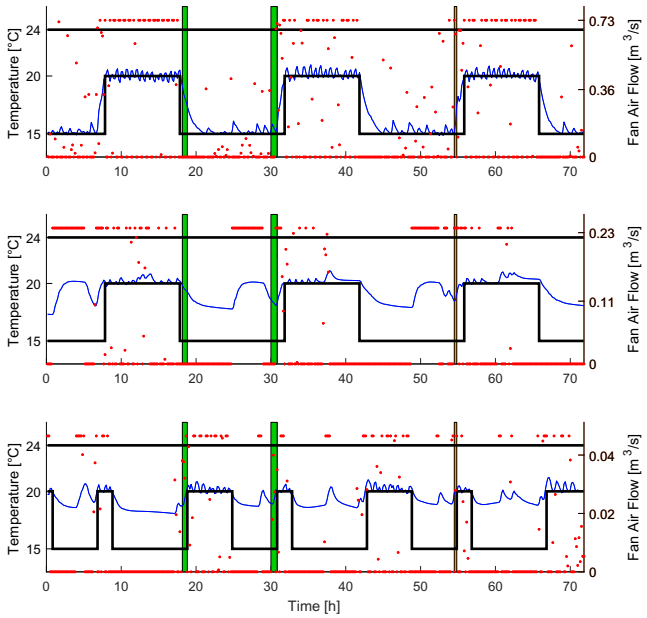

Figure 6.37: Heating operation mode simulation. DR requests are depicted in green if fulfilled, in orange otherwise. Zone internal temperature (blue), comfort bounds (black), fan speed (red dots). Top: commercial zone. Middle: office zone. Bottom: residential zone.

To further assess the performance of the proposed procedure, a standard thermostatic controller with 0.5°C hysteresis has been used as a benchmark. Since thermostatic control is clearly unable to track step variations of the comfort constraints, preheating/precooling is performed with suitable advance in order to provide a fair comparison. Moreover, when thermostatic control is in place, the ESS is operated in the following fashion: if the power currently produced by the PV panels exceeds that needed by the HP, the surplus is stored in the battery, otherwise the controller draws power from the battery in the first place, and then from the grid. Since DR requests cannot be handled by thermostatic control, simulations in absence of DR programs have been performed for the sake of fairness.

In Table 6.14, the total cost is summarized for both strategies along with the average bound violation of the worst performing zone. In the considered days, the total cost achieved by adopting the proposed control technique turns out to be 25.49% less than that obtained by the benchmark.

	Proposed MPC	Thermostatic Control
Overall cost [€]	136.64	183.39
Worst zone average bound violation [°C]	0.139	0.142

Table 6.14: Heating operation mode simulation - Comparison with thermostatic control (without DR)

6.4.3 Summer Season Simulation - Cooling Operation Results

As described in Section 5.3.2, the problem structure for cooling mode is similar to the heating case, with the exception that no TES is assumed to be present. The identified models used under this condition have been obtained in a similar manner. A model for the dynamics of the fluid temperature at the HP inlet ($T_{in}^{HP_C}$) is identified according to (5.17)-(5.18), and the resulting FIT index turns out to be over 80% for 12-hour ahead predictions. This step is not explicitly needed for the heating case since, according to (5.8), the fluid temperature at HP inlet is the same as the TES temperature T^{TES}.

For commercial and office zones, comfort bounds are set to 22-24°C from 8:00 to 18:00, and 22-28°C elsewhen. Bounds for residential zones are 22-24°C from 7:00 to 9:00 and from 19:00 to 01:00, and 22-28°C otherwise.

In Table 6.15 and Fig. 6.38-6.39, the results of a three-day simulation are summarized. In Table 6.16, the comparison with the thermostatic controller is shown. As for the winter season, the proposed MPC reduces the cost by 35.67% with respect to the benchmark, still maintaining similar zone comfort.

Cost without DR [€]	79.68
No. of fulfilled DR requests	3
DR reward [€]	6.40
Overall cost with DR [€]	73.28
Worst zone average bound violation [°C]	0.145

Table 6.15: Cooling operation mode - Simulation results over 3 days

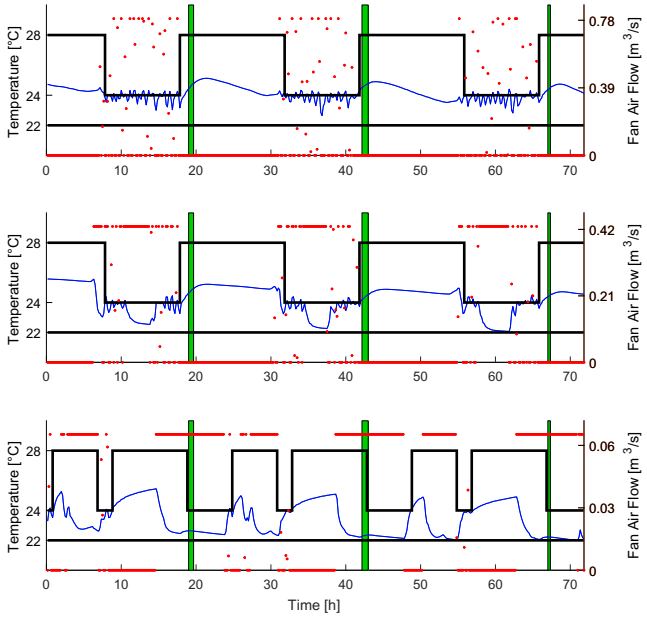

Figure 6.38: Cooling operation mode simulation. Zone internal temperature (blue), comfort bounds (black), fan speed (red dots) and fulfilled DR requests (green). Top: commercial zone. Middle: office zone. Bottom: residential zone.

	Proposed MPC	Thermostatic Control
Overall cost [€]	76.74	119.29
Worst zone average bound violation [°C]	0.156	0.169

Table 6.16: Cooling operation mode simulation - Comparison with thermostatic control (without DR)

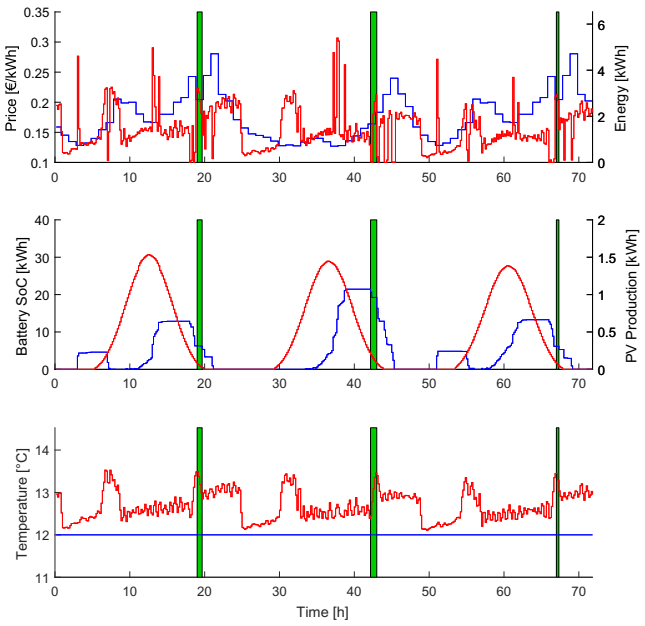

Figure 6.39: Cooling operation mode simulation. DR requests are depicted in green if fulfilled, in orange otherwise. Top: energy price (blue) and building energy consumption per time step (red). Middle: ESS state of charge (blue) and energy provided by the PV plant (red). Bottom: HP setpoint (blue) and fluid temperature at HP inlet (red).

6.4.4 Performance Analysis Under Uncertainties

Up to this point, exact forecasts of the exogenous inputs $\mathbf{e}$ have been considered. Such an assumption is not acceptable in a realistic scenario for weather variables and zone internal gains. On the contrary, it is reasonable to assume that energy price is exactly known one day in advance, as well as the daily DR program [89]. For these reasons, simulations have been performed to evaluate how the proposed technique is sensitive to forecasting errors in outdoor temperature, solar irradiance and internal gains.

In a real scenario, predictions of external temperature are provided by national weather forecast services. Outdoor temperature forecasting errors have been simulated as follows. First, a second-order autoregressive model has been used to compute the noise signal

$$d(k) = a_1\, d(k-1) + a_2\, d(k-2) + \varepsilon(k), \quad k = 0, \dots \tag{6.1}$$

where a_1 and a_2 are the model coefficients and ε is a zero-mean Gaussian distributed random variable. Notice that it is quite common to use autoregressive systems to model temperature uncertainty, see e.g., [115]. Then, denoting by

T^A_{true} the real temperature profile, the temperature forecast $\widehat{T}^A$ to be used by the MPC has been obtained as

$$\widehat{T}^A(k) = T^A_{true}(k) + d(k)\,\frac{k-t}{\lambda}, \quad k = t, \ldots, t+\lambda\ . \tag{6.2}$$

Notice that $\widehat{T}^A(t) = T^A_{true}(t)$, since the outdoor temperature is measured. On the other hand, the term $\frac{k-t}{\lambda}$ takes into account the fact that forecasting accuracy decreases with time. State-of-the-art models for temperature forecasting are able to generate day-ahead estimates with an error of about 2°C [116]. Hence, the coefficients in (6.1) have been chosen conservatively in order obtain a maximum error of 3°C over a 12-hour ahead prediction.

To test the behavior of the proposed control law, a number of uncertain input profiles have been generated and used in simulations. In Fig. 6.40, five different 12-hour ahead forecasts are reported, along with the true temperature profile.

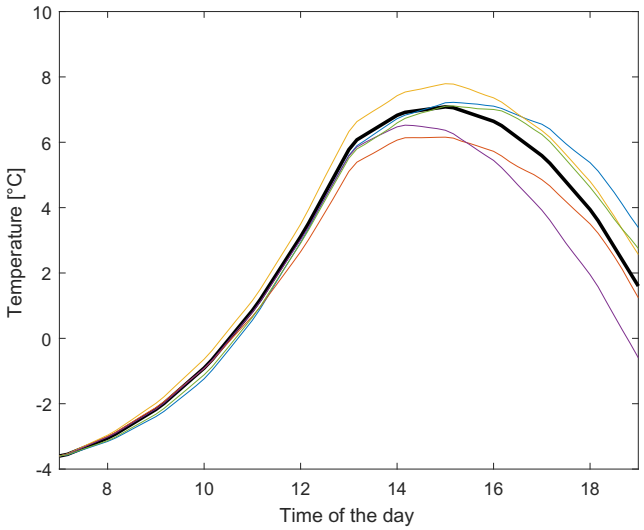

Figure 6.40: Real outdoor temperature (black thick line) and five simulated forecasts (colored thin lines) at a given time.

Predictions of solar irradiance have been obtained by multiplying the real irradiance by a signal generated as in (6.1). In Fig. 6.41, different profiles of solar irradiance predictions are reported along with the actual signal.

To obtain forecasts on zone internal gains, a noise signal as in (6.1) has been added to the real internal gain, by saturating the perturbed signal to 0. In Fig. 6.42, the true internal gain is depicted for each zone type along with five forecasts.

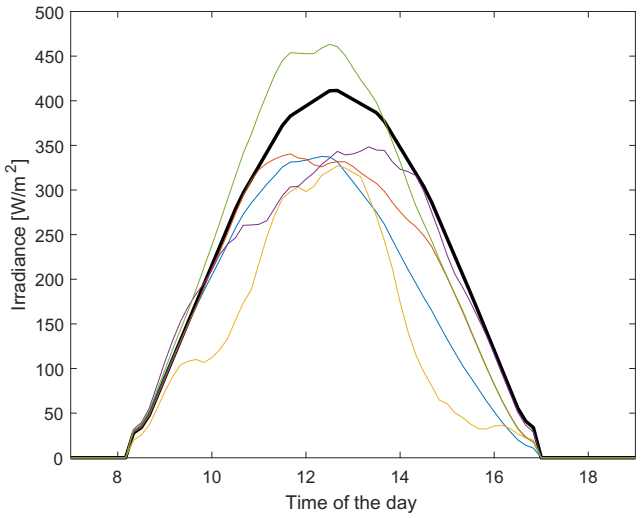

Figure 6.41: Real solar irradiance (black thick line) and five simulated forecasts (colored thin lines) at a given time.

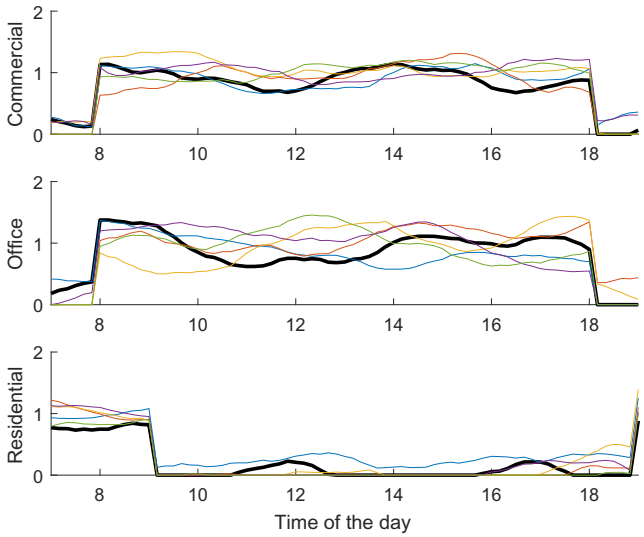

Figure 6.42: Real internal gains (black thick line) and five simulated forecasts (colored thin lines) at a given time. Top: Commercial zone. Middle: Office zone. Bottom: Residential zone.

Twenty simulations in heating mode have been generated for each uncertain input. In Table 6.17, the worst-case value of the total cost and of the average comfort bound violation of the worst performing zone are reported. Inaccurate forecasts are considered both individually and combined. The box plots related to the overall cost for the considered scenarios are shown in Fig. 6.43.

It can be noticed that the presence of inaccurate forecasts may raise the overall cost up to 7.79% with respect to the nominal case, while the difference on

comfort is negligible. The latter fact shows the ability of the control algorithm to minimize the thermal discomfort when unexpected situations occur.

	Overall cost [€]	Worst zone average bound violation [°C]
Exact forecast	136.64	0.139
Uncertain forecast on external temperature	144.82	0.141
Uncertain forecast on solar irradiance	144.98	0.144
Uncertain forecast on zone internal gains	143.90	0.144
Uncertain forecast on all three inputs	147.28	0.146

Table 6.17: Simulation results for exact and inaccurate forecasts (worst-case over 20 realizations)

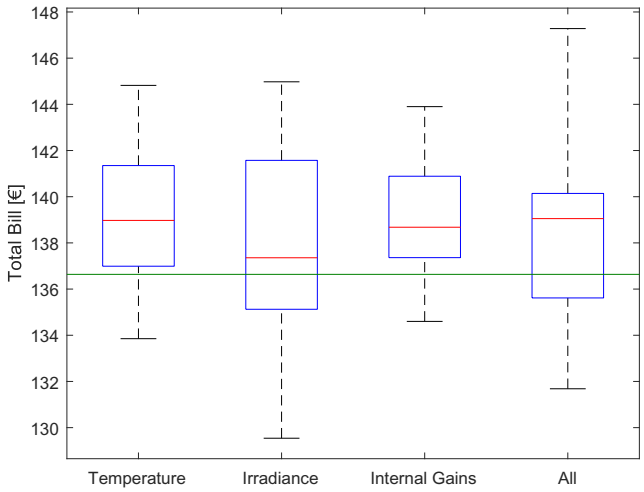

Figure 6.43: Box plot of the total cost in presence of uncertain forecasts over 20 simulations. The three sources of uncertainty are considered once at a time and at the same time. The green line refers to the result for exact forecasts.

6.4.5 Discussion

In this section, the results of the simulation experiments are analyzed and discussed.

Let us first consider the simulation reported in Section 6.4.2, corresponding to winter season and perfect knowledge of exogenous inputs. The identified models are able to predict the system dynamics accurately. As expected, the performance indexes decrease as the prediction horizon grows, yet they remain on acceptable values. Moreover, it is worth remembering that in a receding horizon approach, predictions are updated at each time step, thus making it possible for the control algorithm to adapt against inaccuracies on long-term forecasts.

Concerning the control system simulation in Fig. 6.36, it can be observed that the ESS and the TES are charged and discharged twice a day in order to take advantage of electricity price fluctuations. Moreover, it is apparent that both the ESS and the TES play an important role in order to satisfy DR requests. From Fig. 6.36 and 6.37, it is apparent that the last DR request is not fulfilled, meaning that consumption reduction during the DR interval is not deemed profitable by the controller. In Fig. 6.37, one can see that the comfort bounds are mostly satisfied. In this case, since exact forecasts are assumed, bound violations are only due to discrepancies between the real system and the identified model. However, the magnitude of such bound violations is almost negligible. In fact, as reported in Table 6.13, the average bound violation for the worst zone is less than 0.14°C. The proposed control technique leads to a total cost which is 25.49% less than that obtained by standard thermostatic rules, as reported in Table 6.14. Since the benchmark cannot exploit the knowledge of DR requests, no DR program has been assumed in this case to ensure a fair comparison. Of course, the gap between the two strategies in the presence of DR programs is larger.

Since the assumption of exact forecasts is unrealistic, the cost associated to the benchmark controller is also compared with that obtained by the MPC under inaccurate input predictions. To this purpose, Table 6.17 and Fig. 6.43 show that the MPC cost under uncertain forecasts does not change significantly w.r.t. the nominal one. In fact, the maximum cost under inaccurate forecasts is less than 8% greater than that obtained for exact forecasts. This is a consequence of the receding horizon strategy, which implies that only the prediction errors occurring in the near future significantly affect the perfor-

mance. This makes the proposed approach intrinsically robust to uncertainty, since short-term forecasts are usually quite accurate. In addition to affecting the total cost, uncertainty also plays a role in the preservation of zone temperature comfort bounds. However, this effect is mitigated by the MPC implementation described in Section 5.4.3, as it is clear from Table 6.17, which shows that only a slight increment of discomfort occurs in the presence of unreliable forecasts. Similar considerations can be made for the results obtained in cooling operation, i.e., in summer season.

A final remark concerns the computational burden associated with the controller implementation. For the considered 126-zone building, the time required for computations at each step (i.e., every 10 minutes) is about 15 seconds showing that the proposed algorithm can be efficiently adopted in large-scale applications. Computations have been performed using CPLEX [108] to solve the LPs, on an Intel(R) Core(TM) i7-7700 CPU @3.60 GHz with 32 GB of RAM.

Chapter 7

Conclusions

In this thesis, uncertainties affecting EVs and smart buildings have been handled through optimization techniques providing cost reduction and feasible grid operation. Concerning EVs, optimization problems are mostly based on chance constrained programs. Regarding buildings, an optimization problem based on receding horizon approach has been formulated to guarantee robust performance against environmental uncertainties.

In Chapter 2, three algorithms aimed at the daily peak power minimization of an EV charging station have been proposed. The first algorithm does not assume any available information on uncertain variables, while the second one exploits some statistical knowledge on vehicle arrivals, departures and desired energy to charge. Lastly, in the third algorithm the typical constraint on customer satisfaction is relaxed through a chance constraint approach. All procedures have been formulated in a receding horizon framework and rely on the solution of a linear programming/MILP problem, which provides the optimal charging power for each connected vehicle at each time step. Numerical simulations and comparisons show the effectiveness of the devised techniques, as well as the computational feasibility for implementation in real applications. Further studies will address the problem of peak power reduction in EV charging stations coupled with distributed generation or in the presence of demand response, and refinements on load forecasting possibly through optimization techniques.

To derive a proper energy pricing strategy under uncertain EV demand, in Chapter 3 a chance constrained optimization problem has been formulated. The resulting chance constraint is based on probability distributions that characterize the EV daily behavior. A tractable formulation of the original problem

has been derived, and a procedure to compute the optimal selling price has been devised. While the selling price is computed at the beginning of the day, during the day a receding horizon strategy to operate the ESS exploiting the realizations of the EV random processes has been designed. Results show that such approach is fairly tight. In fact, on average, the daily profit is reasonably close to the required value, while the chance constraint is tightly satisfied. Concerning the receding horizon strategy, the adapted schedule leads to better performance, in general. Moreover, the amount of chance constraint violations is reduced. Future developments will address more complex scenarios, where uncertainty on renewable forecasts and on electricity price are explicitly taken into account. Moreover, charging stations equipped with vehicle-to-grid facilities can be considered, as well as the participation of the parking lot in demand response programs. One more research direction is related to competitive environments, where the energy pricing problem will be analyzed by considering the presence of other players involved in the charging service.

In Chapter 4, a receding horizon approach to the optimal control of an IMG in presence of EVs has been presented. To deal with the uncertainty affecting the arrival times of EVs, a chance constraint approach has been developed and a suitable relaxation technique has been adopted. Simulations involving a 10-bus industrial microgrid have been performed. The proposed approach has been compared with a deterministic method which does not employ chance constraints. Results show that the overall energy bill is similar for both approaches. However, the proposed method outperforms the benchmark when looking at robustness in the presence of high EV penetration. In fact, the benchmark is able to handle EV increase of about 30%; after that network stability is no more guaranteed, while the algorithm based on chance constraints can manage EV growth of more than 100%, thus showing better robustness features. Future developments may involve the use of different kind of techniques for dealing with uncertainty, like for instance, scenario-based approaches. Moreover, uncertainties on vehicle departure times and on other aspects of the IMG (e.g., uncertain FU load profile and uncertain PV generation forecasts) can be considered as well.

Finally, in Chapter 5 the problem of optimizing the electrical energy bill of a building integrating a centralized HVAC, thermal and electrical storage facilities, and PV generation has been addressed. Participation in a DR program has also been considered. The proposed approach exploits a receding horizon MPC strategy involving at each step the solution of an LP and of a MILP

with a number of integer variables equal to the number of DR requests included in the prediction horizon. The procedure can be fruitfully applied to large-size buildings. Experimental validation using a realistic simulation framework has been carried out. Further studies may address more complex setups in which the building is considered as a microgrid in its own right, including electric vehicles, appliances and other kinds of loads. Special attention to active/reactive power flow should be paid in this case in order to guarantee the satisfaction of electrical constraints. More general DR scenarios may also be addressed, such as the presence of incentives for keeping energy consumption above a minimum, which can be efficiently achieved using storage facilities. Finally, different methods for handling uncertainty, like chance constraints or scenario-based approaches, will be investigated and compared with the method proposed in this chapter. To this purpose, suitable problem formulations and related relaxations will be studied to enable such techniques to manage large-scale buildings.

Bibliography

[1] E. Horizon, "The framework programme for research and innovation," Technical Report, Tech. Rep., 2020.

[2] "IEA, electric vehicles," *IEA, Paris*, 2020. [Online]. Available: https://www.iea.org/reports/electric-vehicles

[3] "Global renewables outlook: Energy transformation 2050," *IRENA*, 2020. [Online]. Available: https://irena.org/publications/2020/Apr/Global-Renewables-Outlook-2020

[4] A. Losi, P. Mancarella, and A. Vicino, *Integration of demand response into the electricity chain: challenges, opportunities, and Smart Grid solutions*. John Wiley & Sons, 2015.

[5] X. Cao, X. Dai, and J. Liu, "Building energy-consumption status worldwide and the state-of-the-art technologies for zero-energy buildings during the past decade," *Energy and Buildings*, vol. 128, pp. 198 – 213, 2016. [Online]. Available: http://www.sciencedirect.com/science/article/pii/S0378778816305783

[6] X. Zhang and X. Bai, "Incentive policies from 2006 to 2016 and new energy vehicle adoption in 2010–2020 in China," *Renewable and Sustainable Energy Reviews*, vol. 70, pp. 24–43, 2017.

[7] G. E. IEA, "Outlook 2017," *Two Million and Counting, International Energy Agency*, 2017.

[8] X. Tan, G. Qu, B. Sun, N. Li, and D. H. K. Tsang, "Optimal scheduling of battery charging station serving electric vehicles based on battery swapping," *IEEE Transactions on Smart Grid*, vol. 10, no. 2, pp. 1372–1384, 2019.

[9] M. R. Sarker, H. Pandžić, and M. A. Ortega-Vazquez, "Optimal operation and services scheduling for an electric vehicle battery swapping station," *IEEE Transactions on Power Systems*, vol. 30, no. 2, pp. 901–910, 2015.

[10] Q. Kang, J. Wang, M. Zhou, and A. C. Ammari, "Centralized charging strategy and scheduling algorithm for electric vehicles under a battery swapping scenario," *IEEE Transactions on Intelligent Transportation Systems*, vol. 17, no. 3, pp. 659–669, 2016.

[11] Z. Moghaddam, I. Ahmad, D. Habibi, and Q. V. Phung, "Smart charging strategy for electric vehicle charging stations," *IEEE Transactions on Transportation Electrification*, vol. 4, no. 1, pp. 76–88, 2018.

[12] W. Lee, L. Xiang, R. Schober, and V. Wong, "Electric vehicle charging stations with renewable power generators: A game theoretical analysis," *IEEE Transactions on Smart Grid*, vol. 6, no. 2, pp. 608–617, 2015.

[13] R. Leou, C. Su, and C. Lu, "Stochastic analyses of electric vehicle charging impacts on distribution network," *IEEE Transactions on Power Systems*, vol. 29, no. 3, pp. 1055–1063, 2014.

[14] M. Casini, G. G. Zanvettor, M. Kovjanic, and A. Vicino, "Optimal energy management and control of an industrial microgrid with plug-in electric vehicles," *IEEE Access*, vol. 7, pp. 101 729–101 740, 2019.

[15] O. Erdinç, A. Taşcıkaraoğlu, N. G. Paterakis, İ. Dursun, M. C. Sinim, and J. Catalão, "Comprehensive optimization model for sizing and siting of DG units, EV charging stations, and energy storage systems," *IEEE Transactions on Smart Grid*, vol. 9, no. 4, pp. 3871–3882, 2018.

[16] M. R. Mozafar, M. H. Moradi, and M. H. Amini, "A simultaneous approach for optimal allocation of renewable energy sources and electric vehicle charging stations in smart grids based on improved GA-PSO algorithm," *Sustainable Cities and Society*, vol. 32, pp. 627–637, 2017.

[17] Y. Xiong, J. Gan, B. An, C. Miao, and A. L. C. Bazzan, "Optimal electric vehicle fast charging station placement based on game theoretical framework," *IEEE Transactions on Intelligent Transportation Systems*, vol. 19, no. 8, pp. 2493–2504, 2018.

[18] M. M. Islam, H. Shareef, and A. Mohamed, "Optimal location and sizing of fast charging stations for electric vehicles by incorporating traffic and power networks," *IET Intelligent Transport Systems*, vol. 12, no. 8, pp. 947–957, 2018.

[19] T. Zhang, W. Chen, Z. Han, and Z. Cao, "Charging scheduling of electric vehicles with local renewable energy under uncertain electric vehicle arrival and grid power price," *IEEE Transactions on Vehicular Technology*, vol. 63, no. 6, pp. 2600–2612, 2014.

[20] M. Casini, A. Vicino, and G. G. Zanvettor, "A distributionally robust joint chance constraint approach to smart charging of plug-in electric vehicles," in *Proc. 58th IEEE Conf. on Decision and Control*, Nice, December 2019, pp. 4222–4227.

[21] M. H. K. Tushar, C. Assi, M. Maier, and M. F. Uddin, "Smart microgrids: Optimal joint scheduling for electric vehicles and home appliances," *IEEE Transactions on Smart Grid*, vol. 5, no. 1, pp. 239–250, 2014.

[22] L. Zhang and Y. Li, "A game-theoretic approach to optimal scheduling of parking-lot electric vehicle charging," *IEEE Transactions on Vehicular Technology*, vol. 65, no. 6, pp. 4068–4078, 2015.

[23] M. Ş. Kuran, A. C. Viana, L. Iannone, D. Kofman, G. Mermoud, and J. P. Vasseur, "A smart parking lot management system for scheduling the recharging of electric vehicles," *IEEE Transactions on Smart Grid*, vol. 6, no. 6, pp. 2942–2953, 2015.

[24] M. Maigha and M. L. Crow, "A transactive operating model for smart airport parking lots," *IEEE Power and Energy Technology Systems Journal*, vol. 5, no. 4, pp. 157–166, 2018.

[25] W. Jiang and Y. Zhen, "A real-time EV charging scheduling for parking lots with PV system and energy store system," *IEEE Access*, vol. 7, pp. 86 184–86 193, 2019.

[26] L. Gan, U. Topcu, and S. H. Low, "Optimal decentralized protocol for electric vehicle charging," *IEEE Transactions on Power Systems*, vol. 28, no. 2, pp. 940–951, 2013.

[27] Z. Li, Q. Guo, H. Sun, S. Xin, and J. Wang, "A new real-time smart-charging method considering expected electric vehicle fleet connections," *IEEE Transactions on Power Systems*, vol. 29, no. 6, pp. 3114–3115, 2014.

[28] K. Mahmud, M. J. Hossain, and G. E. Town, "Peak-load reduction by coordinated response of photovoltaics, battery storage, and electric vehicles," *IEEE Access*, vol. 6, pp. 29 353–29 365, 2018.

[29] M. J. E. Alam, K. M. Muttaqi, and D. Sutanto, "A controllable local peak-shaving strategy for effective utilization of PEV battery capacity for distribution network support," *IEEE Transactions on Industry Applications*, vol. 51, no. 3, pp. 2030–2037, 2015.

[30] İ. Şengör, O. Erdinç, B. Yener, A. Taşcıkaraoğlu, and J. P. Catalão, "Optimal energy management of EV parking lots under peak load reduction based DR programs considering uncertainty," *IEEE Transactions on Sustainable Energy*, vol. 10, no. 3, pp. 1034–1043, 2018.

[31] Z. Pan, T. Yu, L. Chen, B. Yang, B. Wang, and W. Guo, "Real-time stochastic optimal scheduling of large-scale electric vehicles: A multidimensional approximate dynamic programming approach," *International Journal of Electrical Power & Energy Systems*, vol. 116, p. 105542, 2020.

[32] G. Zhang, S. T. Tan, and G. G. Wang, "Real-time smart charging of electric vehicles for demand charge reduction at non-residential sites," *IEEE Transactions on Smart Grid*, vol. 9, no. 5, pp. 4027–4037, 2018.

[33] L. Jian, Y. Zheng, X. Xiao, and C. Chan, "Optimal scheduling for vehicle-to-grid operation with stochastic connection of plug-in electric vehicles to smart grid," *Applied Energy*, vol. 146, pp. 150–161, 2015.

[34] W. Tang and Y. J. A. Zhang, "A model predictive control approach for low-complexity electric vehicle charging scheduling: Optimality and scalability," *IEEE transactions on power systems*, vol. 32, no. 2, pp. 1050–1063, 2016.

[35] L. Zhang and Y. Li, "Optimal management for parking-lot electric vehicle charging by two-stage approximate dynamic programming," *IEEE Transactions on Smart Grid*, vol. 8, no. 4, pp. 1722–1730, 2017.

[36] R. Ghotge, Y. Snow, S. Farahani, Z. Lukszo, and A. van Wijk, "Optimized scheduling of EV charging in solar parking lots for local peak reduction under EV demand uncertainty," *Energies*, vol. 13, no. 5, p. 1275, 2020.

[37] V.-L. Nguyen, T. Tran-Quoc, S. Bacha, and B. Nguyen, "Charging strategies to minimize the peak load for an electric vehicle fleet," in *IECON 2014-40th Annual Conference of the IEEE Industrial Electronics Society*, 2014, pp. 3522–3528.

[38] G. S. Aujla, N. Kumar, M. Singh, and A. Y. Zomaya, "Energy trading with dynamic pricing for electric vehicles in a smart city environment," *Journal of Parallel and Distributed Computing*, vol. 127, pp. 169 – 183, 2019. [Online]. Available: http://www.sciencedirect.com/science/article/pii/S0743731518304416

[39] M. Alizadeh, H. Wai, M. Chowdhury, A. Goldsmith, A. Scaglione, and T. Javidi, "Optimal pricing to manage electric vehicles in coupled power and transportation networks," *IEEE Transactions on Control of Network Systems*, vol. 4, no. 4, pp. 863–875, 2017.

[40] V. Subramanian and T. K. Das, "A two-layer model for dynamic pricing of electricity and optimal charging of electric vehicles under price spikes," *Energy*, vol. 167, pp. 1266 – 1277, 2019. [Online]. Available: http://www.sciencedirect.com/science/article/pii/S0360544218321686

[41] S. Limmer and T. Rodemann, "Peak load reduction through dynamic pricing for electric vehicle charging," *International Journal of Electrical Power & Energy Systems*, vol. 113, pp. 117 – 128, 2019. [Online]. Available: http://www.sciencedirect.com/science/article/pii/S0142061518327753

[42] J. Soares, M. A. F. Ghazvini, N. Borges, and Z. Vale, "Dynamic electricity pricing for electric vehicles using stochastic programming," *Energy*, vol. 122, pp. 111 – 127, 2017. [Online]. Available: http://www.sciencedirect.com/science/article/pii/S0360544216319132

[43] A. Ghosh and V. Aggarwal, "Menu-based pricing for profitable electric vehicle charging with vehicle-to-grid service," in *2018 International Conference on Signal Processing and Communications (SPCOM)*, July 2018, pp. 237–241.

[44] T. Aljohani, A. Ebrahim, and O. Mohammed, "Dynamic real-time pricing structure for electric vehicle charging considering stochastic microgrids energy management system," in *2020 IEEE International Conference on Environment and Electrical Engineering and 2020 IEEE Industrial and Commercial Power Systems Europe (EEEIC / I CPS Europe)*, June 2020, pp. 1–8.

[45] C. Luo, Y. Huang, and V. Gupta, "Stochastic dynamic pricing for ev charging stations with renewable integration and energy storage," *IEEE Transactions on Smart Grid*, vol. 9, no. 2, pp. 1494–1505, March 2018.

[46] W. Xie, S. Ahmed, and R. Jiang, "Optimized bonferroni approximations of distributionally robust joint chance constraints," *Mathematical Programming*, pp. 1–34, 2019.

[47] A. Hirsch, Y. Parag, and J. Guerrero, "Microgrids: A review of technologies, key drivers, and outstanding issues," *Renewable and Sustainable Energy Reviews*, vol. 90, pp. 402 – 411, 2018. [Online]. Available: http://www.sciencedirect.com/science/article/pii/S136403211830128X

[48] Z. Shuai, Y. Sun, Z. J. Shen, W. Tian, C. Tu, Y. Li, and X. Yin, "Microgrid stability: Classification and a review," *Renewable and Sustainable Energy Reviews*, vol. 58, pp. 167 – 179, 2016. [Online]. Available: http://www.sciencedirect.com/science/article/pii/S1364032115015841

[49] S. Parhizi, H. Lotfi, A. Khodaei, and S. Bahramirad, "State of the art in research on microgrids: A review," *IEEE Access*, vol. 3, pp. 890–925, 2015.

[50] M. Zhang and J. Chen, "The energy management and optimized operation of electric vehicles based on microgrid," *IEEE Transactions on Power Delivery*, vol. 29, no. 3, pp. 1427–1435, June 2014.

[51] S. Deilami, "Online coordination of plug-in electric vehicles considering grid congestion and smart grid power quality," *Energies*, vol. 11, no. 9, 2018. [Online]. Available: http://www.mdpi.com/1996-1073/11/9/2187

[52] R. C. Green, L. Wang, and M. Alam, "The impact of plug-in hybrid electric vehicles on distribution networks: a review and outlook," in *IEEE PES General Meeting*, July 2010, pp. 1–8.

[53] M. A. López, S. Martín, J. A. Aguado, and S. de la Torre, "V2G strategies for congestion management in microgrids with high penetration of electric vehicles," *Electric Power Systems Research*, vol. 104, pp. 28–34, 2013.

[54] J. Clairand, J. Rodrìguez-Garcìa, and C. Àlvarez-Bel, "Smart charging for electric vehicle aggregators considering users' preferences," *IEEE Access*, vol. 6, pp. 54 624–54 635, 2018.

[55] I. Alsaidan, A. Khodaei, and Wenzhong Gao, "Distributed energy storage sizing for microgrid applications," in *2016 IEEE/PES Transmission and Distribution Conference and Exposition (T D)*, May 2016, pp. 1–5.

[56] S. Y. Derakhshandeh, A. S. Masoum, S. Deilami, M. A. S. Masoum, and M. E. Hamedani Golshan, "Coordination of generation scheduling with pevs charging in industrial microgrids," *IEEE Transactions on Power Systems*, vol. 28, no. 3, pp. 3451–3461, 2013.

[57] M. Naderi, S. Bahramara, Y. Khayat, and H. Bevrani, "Optimal planning in a developing industrial microgrid with sensitive loads," *Energy Reports*, vol. 3, pp. 124 – 134, 2017. [Online]. Available: http://www.sciencedirect.com/science/article/pii/S2352484716301020

[58] M. Choobineh and S. Mohagheghi, "A multi-objective optimization framework for energy and asset management in an industrial microgrid," *Journal of Cleaner Production*, vol. 139, pp. 1326 – 1338, 2016. [Online]. Available: http://www.sciencedirect.com/science/article/pii/S0959652616313026

[59] A. Ben-Tal, L. El Ghaoui, and A. Nemirovski, *Robust optimization*. Princeton University Press, 2009, vol. 28.

[60] J. R. Birge and F. Louveaux, *Introduction to stochastic programming*. Springer Science & Business Media, 2011.

[61] G. C. Calafiore and M. C. Campi, "The scenario approach to robust control design," *IEEE Transactions on Automatic Control*, vol. 51, no. 5, pp. 742–753, May 2006.

[62] S. Zymler, D. Kuhn, and B. Rustem, "Distributionally robust joint chance constraints with second-order moment information," *Mathematical Programming*, vol. 137, no. 1, pp. 167–198, 2013.

[63] M. Honarmand, A. Zakariazadeh, and S. Jadid, "Self-scheduling of electric vehicles in an intelligent parking lot using stochastic optimization," *Journal of the Franklin Institute*, vol. 352, no. 2, pp. 449 – 467, 2015.

[64] W. H. Kwon and S. H. Han, *Receding horizon control: model predictive control for state models*. Springer Science & Business Media, 2006.

[65] J. H. Lee, "Model predictive control: Review of the three decades of development," *International Journal of Control, Automation and Systems*, vol. 9, no. 3, p. 415, 2011.

[66] D. Kothari and I. Nagrath, *Modern Power System Analysis*. Tata McGraw-Hill Publishing Company, 2003. [Online]. Available: https://books.google.it/books?id=zfxQFM3RkkEC

[67] A. Wood, B. Wollenberg, and G. Sheblé, *Power Generation, Operation, and Control*. Wiley, 2013.

[68] S. H. Low, "Convex relaxation of optimal power flow-part i: Formulations and equivalence," *IEEE Transactions on Control of Network Systems*, vol. 1, no. 1, pp. 15–27, March 2014.

[69] J. Grainger and W. Stevenson, *Power system analysis*, ser. McGraw-Hill series in electrical and computer engineering: Power and energy. McGraw-Hill, 1994. [Online]. Available: https://books.google.it/books?id=NBIoAQAAMAAJ

[70] A. Giannitrapani, S. Paoletti, A. Vicino, and D. Zarrilli, "Optimal allocation of energy storage systems for voltage control in LV distribution networks," *IEEE Transactions on Smart Grid*, vol. 8, no. 6, pp. 2859–2870, Nov 2017.

[71] J. Luedtke and S. Ahmed, "A sample approximation approach for optimization with probabilistic constraints," *SIAM Journal on Optimization*, vol. 19, no. 2, pp. 674–699, 2008.

[72] MOSEK ApS, *The MOSEK optimization toolbox for MATLAB manual. Version 8.1.*, 2017. [Online]. Available: http://docs.mosek.com/8.1/toolbox/index.html

[73] J. Sturm, "Using SeDuMi 1.02, a Matlab toolbox for optimization over symmetric cones," *Optimization Methods and Software*, vol. 11–12, pp. 625–653, 1999.

[74] K. C. Toh, M. J. Todd, and R. H. Tütüncü, "SDPT3 - a Matlab software package for semidefinite programming, version 1.3," *Optimization Methods and Software*, vol. 11, no. 1-4, pp. 545–581, 1999.

[75] A. Afram and F. Janabi-Sharifi, "Review of modeling methods for HVAC systems," *Applied Thermal Engineering*, vol. 67, no. 1, pp. 507 – 519, 2014. [Online]. Available: http://www.sciencedirect.com/science/article/pii/S1359431114002348

[76] D. Lee and C.-C. Cheng, "Energy savings by energy management systems: A review," *Renewable and Sustainable Energy Reviews*, vol. 56, pp. 760 – 777, 2016. [Online]. Available: http://www.sciencedirect.com/science/article/pii/S1364032115013349

[77] A. Afram and F. Janabi-Sharifi, "Theory and applications of HVAC control systems - a review of model predictive control (MPC)," *Building and Environment*, vol. 72, pp. 343 – 355, 2014. [Online]. Available: http://www.sciencedirect.com/science/article/pii/S0360132313003363

[78] W. Cole, E. Hale, and T. Edgar, "Building energy model reduction for model predictive control using openstudio," in *American Control Conference (ACC)*, June 2013, pp. 449–454.

[79] Y. Ma, F. Borrelli, B. Hencey, B. Coffey, S. Bengea, and P. Haves, "Model predictive control for the operation of building cooling systems," *IEEE Transactions on Control Systems Technology*, vol. 20, no. 3, pp. 796–803, May 2012.

[80] Y. Kwak, J.-H. Huh, and C. Jang, "Development of a model predictive control framework through real-time building energy management system data," *Applied Energy*, vol. 155, pp. 1 – 13, 2015.

[81] F. Oldewurtel, A. Parisio, C. N. Jones, D. Gyalistras, M. Gwerder, V. Stauch, B. Lehmann, and M. Morari, "Use of model predictive control and weather forecasts for energy efficient building climate control," *Energy and Buildings*, vol. 45, pp. 15 – 27, 2012.

[82] F. Oldewurtel, C. N. Jones, A. Parisio, and M. Morari, "Stochastic model predictive control for building climate control," *IEEE Transactions on Control Systems Technology*, vol. 22, no. 3, pp. 1198–1205, 2014.

[83] Y. Ma, J. Matuško, and F. Borrelli, "Stochastic model predictive control for building HVAC systems: Complexity and conservatism," *IEEE Transactions on Control Systems Technology*, vol. 23, no. 1, pp. 101–116, 2015.

[84] J. Drgoňa, D. Picard, M. Kvasnica, and L. Helsen, "Approximate model predictive building control via machine learning," *Applied Energy*, vol. 218, pp. 199 – 216, 2018.

[85] M. Killian and M. Kozek, "Implementation of cooperative fuzzy model predictive control for an energy-efficient office building," *Energy and Buildings*, vol. 158, pp. 1404 – 1416, 2018.

[86] M. H. Albadi and E. El-Saadany, "Demand response in electricity markets: An overview," in *Power Engineering Society General Meeting, 2007. IEEE*, June 2007, pp. 1–5.

[87] P. Baboli, M. Moghaddam, and M. Eghbal, "Present status and future trends in enabling demand response programs," in *Power and Energy Society General Meeting, 2011 IEEE*, July 2011, pp. 1–6.

[88] V. Balijepalli, V. Pradhan, S. Khaparde, and R. M. Shereef, "Review of demand response under smart grid paradigm," in *Innovative Smart Grid Technologies - India (ISGT India), 2011 IEEE PES*, Dec 2011, pp. 236–243.

[89] R. Belhomme, R. Cerero, G. Valtorta, and P. Eyrolles, "The ADDRESS project: Developing active demand in smart power systems integrating renewables," in *2011 IEEE Power and Energy Society General Meeting*, July 2011, pp. 1–8.

[90] D. P. Chassin, J. Stoustrup, P. Agathoklis, and N. Djilali, "A new thermostat for real-time price demand response: Cost, comfort and energy impacts of discrete-time control without deadband," *Applied Energy*, vol. 155, no. 0, pp. 816–825, 2015.

[91] D. Patteeuw, K. Bruninx, A. Arteconi, E. Delarue, W. D'haeseleer, and L. Helsen, "Integrated modeling of active demand response with electric heating systems coupled to thermal energy storage systems," *Applied Energy*, vol. 151, pp. 306 – 319, 2015.

[92] F. Oldewurtel, D. Sturzenegger, G. Andersson, M. Morari, and R. S. Smith, "Towards a standardized building assessment for demand response," in *52nd IEEE Conference on Decision and Control*, 2013, pp. 7083–7088.

[93] S. Behboodi, D. P. Chassin, N. Djilali, and C. Crawford, "Transactive control of fast-acting demand response based on thermostatic loads in real-time retail electricity markets," *Applied Energy*, vol. 210, pp. 1310 – 1320, 2018.

[94] P. Loevenbruck, "Residential storage to improve system resilience: Technical design and cost estimation," in *CIRED Workshop 2016*, June 2016, pp. 1–4.

[95] C. J. C. Williams, J. O. Binder, and T. Kelm, "Demand side management through heat pumps, thermal storage and battery storage to increase local self-consumption and grid compatibility of PV systems," in *2012 3rd IEEE PES Innovative Smart Grid Technologies Europe (ISGT Europe)*, Oct 2012, pp. 1–6.

[96] X. Wu, X. Hu, X. Yin, C. Zhang, and S. Qian, "Optimal battery sizing of smart home via convex programming," *Energy*, vol. 140, pp. 444 – 453, 2017. [Online]. Available: http://www.sciencedirect.com/science/article/pii/S036054421731472X

[97] X. Wu, X. Hu, Y. Teng, S. Qian, and R. Cheng, "Optimal integration of a hybrid solar-battery power source into smart home nanogrid with plug-in electric vehicle," *Journal of Power Sources*, vol. 363, pp. 277 – 283, 2017. [Online]. Available: http://www.sciencedirect.com/science/article/pii/S0378775317309771

[98] P. Koponen, J. Ikaheimo, A. Vicino, A. Agnetis, G. De Pascale, N. Ruiz Carames, J. Jimeno, E. Sanchez-Ubeda, P. Garcia-Gonzalez, and R. Cossent, "Toolbox for aggregator of flexible demand," in *Energy Conference and Exhibition (ENERGYCON), 2012 IEEE International*, Sept 2012, pp. 623–628.

[99] G. Bianchini, M. Casini, A. Vicino, and D. Zarrilli, "Demand-response in building heating systems: A model predictive control approach," *Applied Energy*, vol. 168, pp. 159 – 170, 2016.

[100] S. Boyd and L. Vandenberghe, *Convex Optimization*. Cambridge (UK): Cambridge University Press, 2004.

[101] "EnergyPlus engineering reference," online: http://apps1.eere.energy.gov/buildings/energyplus/.

[102] E. Hittinger, T. Wiley, J. Kluza, and J. Whitacre, "Evaluating the value of batteries in microgrid electricity systems using an improved energy systems model," *Energy Conversion and Management*, vol. 89, pp. 458 – 472, 2015. [Online]. Available: http://www.sciencedirect.com/science/article/pii/S0196890414008929

[103] R. Dows and E. Gough, "PVUSA procurement, acceptance, and rating practices for photovoltaic power plants," Pacific Gas and Electric Company, San Ramon, CA, Tech. Rep., 1995.

[104] D. Pepe, G. Bianchini, and A. Vicino, "Model estimation for solar generation forecasting using cloud cover data," *Solar Energy*, vol. 157, pp. 1032–1046, 2017.

[105] ——, "Estimating PV forecasting models from power data," in *IEEE EnergyCon 2018*. IEEE, 2018, pp. 1–6.

[106] G. Bianchini, S. Paoletti, A. Vicino, F. Corti, and F. Nebiacolombo, "Model estimation of photovoltaic power generation using partial information," in *Innovative Smart Grid Technologies Europe (ISGT EUROPE), 2013 4th IEEE/PES*. IEEE, 2013, pp. 1–5.

[107] J. Löfberg, "Yalmip : A toolbox for modeling and optimization in Matlab," in *In Proc. of the CACSD Conference*, Taipei, Taiwan, 2004.

[108] IBM, "IBM ILOG Cplex Optimizer," online: http://www-01.ibm.com/software/integration/optimization/cplex-optimizer/.

[109] Gestore Mercati Energetici, "Andamento dei prezzi e dei volumi," 2018, online: http://www.mercatoelettrico.org.

[110] S. Diamond and S. Boyd, "CVXPY: A Python-embedded modeling language for convex optimization," *Journal of Machine Learning Research*, vol. 17, no. 83, pp. 1–5, 2016.

[111] "DesignBuilder software tool," online: https://www.designbuilder.co.uk/software/product-overview.

[112] M. Wetter, "Co-simulation of building energy and control systems with the Building Controls Virtual Test Bed," *Journal of Building Performance Simulation*, vol. 4, no. 3, pp. 185–203, 2011.

[113] L. Ljung, *System Identification: Theory for the User (Second Edition)*. Upper Saddle River, NJ, USA: Prentice Hall PTR, 1999.

[114] ——, "System identification toolbox for use with MATLAB : user's guide," Natick, MA, 2007.

[115] G. Darivianakis, A. Georghiou, R. S. Smith, and J. Lygeros, "The power of diversity: Data-driven robust predictive control for energy-efficient buildings and districts," *IEEE Transactions on Control Systems Technology*, vol. PP, no. 99, pp. 1–14, 2017.

[116] K. Feldmann, M. Scheuerer, and T. L. Thorarinsdottir, "Spatial postprocessing of ensemble forecasts for temperature using nonhomogeneous gaussian regression," *Monthly Weather Review*, vol. 143, no. 3, pp. 955–971, 2015.